2016

Graphene encapsulating process: A road map for manufacturing aluminium matrix composites with superior mechanical properties

Alireza Fadavi Boostani
University of Wollongong

UNIVERSITY OF WOLLONGONG

School of Mechanical, Materials & Mechatronic Engineering

Graphene encapsulating process: A road map for manufacturing aluminium matrix composites with superior mechanical properties

Alireza Fadavi Boostani

"This thesis is presented as part of the requirements for the award of the Degree of Doctor of Philosophy of the University of Wollongong"

June 2016

Abstract

Manufacturing aluminium matrix composites with a uniform distribution of the nanoparticles using liquid fabrication methods is a rigorous task, attributed to the high propensity of these nanoparticles to agglomerate.

A novel method was proposed in this study for the first time to diminish the agglomeration propensity of SiC nanoparticles using graphene encapsulation process (Chapters 3 and 4). This method was invented based upon two different processing routes, encompassing ball milling and solvo-thermal assisted methods (Chapter 5) to wrap graphene sheets around SiC nanoparticles. As-received and graphene encapsulated SiC nanoparticles were then incorporated into A357 aluminium alloy using semi-solid stir-casting method under high purity (99.999%) argon gas.

To delineate the mechanism by which graphene encapsulating method diminishes the agglomeration of SiC nanoparticles during the liquid processing, a novel theoretical approach based on the van der Waals-Casimir interaction free energy (Chapter 6) was implemented to show the unprecedented capacity of graphene sheets in manipulating the Hamaker constant of SiC nanoparticles. This manipulated Hamaker constant, in turn, stimulates deagglomeration and engulfment of these particles within solidifying matrix.

Intensive attention has been given to microscopical investigation of the microstructure using high resolution transmission electron microscopy (HR-TEM) and field emission scanning electron microscopy (FE-SEM), revealing that graphene sheets were dispersed within aluminium matrix with two different architectures, encompassing onion-like graphene shells encapsulating SiC nanoparticles and disk-shaped graphene nanosheets.

Additionally, a novel solidification model was suggested (Chapter 4) to show how graphene sheets can affect the distribution of SiC nanoparticles to be dispersed uniformly within grains rather than agglomerated at grain boundaries, deteriorating the tensile properties of the produced composites. This model takes into account the alteration of the solidification mechanism of SiC nanoparticles from pushing to engulfment. This nanostructure manipulation brought about 350% and 258% augmentation in yield strength and elongation, respectively, compared to that of unreinforced aluminum alloy.

To differentiate the actual capacity of the invented graphene encapsulation method on the mechanical and microstructural properties of the produced composites from other conventional manufacturing routes, such as semi-solid and squeeze casting, different fabrication routes including stir casting (Chapter 4), pressure assisted stir-casting (Chapters 5), semi-solid powder forming process (Chapter 6) and thixoforming (Chapter 7) were employed. Achieved results have demonstrated that the graphene encapsulating method has a significant effect on enhancing the mechanical properties of the composites produced using these manufacturing processes.

To delineate the mechanism by which graphene sheets participate in strengthening of the aluminium matrix composites, a new strengthening analytical model was devised (Chapter 7), making use of Orowan, thermal-activated dislocation, fiber pull-out, shear lag and geometrically necessary strengthening mechanisms. The devised strengthening model has shown the significant effect of thermally activated dislocation strengthening mechanism in fortifying the aluminium matrix, ascribed to the exceptional negative thermal expansion coefficient of graphene sheets.

Acknowledgements

I really would like to appreciate all supports that I have received from my supervisor, Professor Zhengyi Jiang. He taught me the way that I can approach scientific research. He has provided me with a different look of the world and guided me through the difficulties that I encountered during my PhD study. He is my model not only as an academic, but as a patient person which is crucial during research projects. He has also supported me during PhD study many times and never left me alone.

I would like to express my gratitude to my co-supervisor Dr. Dongbin Wei for his invaluable guidance and comprehension through the completion of this work. I want to thank Dr. Gilberto Casillas for the incredible help in my TEM experiments and for the additional value that his experience has provided to my work.

My greatest appreciation goes to my parents and especially my mother. They provided me the freedom to ascertain my dreams by sacrificing their life and time to support me emotionally during the harsh time of my PhD research and I have this commitment to compensate all of their efforts by being a successful person. Without their initial motivation and continuous support, it would have been difficult for me to reach where I am today. I would like to offer my great appreciation to my brother Sasan Boostani who has supported me during this difficult journey. Despite of a large distance between me and my family, Sasan always has stayed close to my parents and supported them not to feel bad about my absence.

Thesis Style

This thesis has been prepared in journal article compilation style format based on the accepted papers extracted from my PhD study and published in Elsevier ISI journals. The compilation style of writing was used for this thesis due to the complimentary relationship of the work introduced in each paper from the introduction of the graphene encapsulating process as a new manufacturing route (Chapter 3). Following the enhanced mechanical properties brought about by the invented graphene encapsulating method (Chapter 3), it has been demonstrated (Chapter 4) that this is accomplished by manipulating the solidification mechanism of SiC nanoparticles from pushing to engulfment within aluminium matrix. This is resulted in uniform dispersion of SiC nanoparticles encapsulated by graphene sheets within aluminium matrix (Chapter 4). The solvothermal-assisted graphene encapsulation, however, was introduced (Chapter 5) to alleviate the inhomogeneity found in the number of graphene sheets covering SiC nanoparticles in ball milling assisted process. The mechanism resulted in engulfment of SiC nanoparticles is introduced in Chapter 6 by demonstrating the effect of graphene sheets on manipulating the Hamaker constant of SiC nanoparticles. Following the incorporation of graphene sheets within aluminium matrix, Chapter 7 represents the effect of graphene sheets in enhancing the effect of thermally activated dislocations and Orowan strengthening in strengthening the produced composites.

List of Publications

The following published papers are used in generating different Chapters 3 - 7 of this PhD thesis respectively. In additional, the papers published outside the scope of my PhD thesis, but as a result of the cooperation between our group and our international colleagues, have also been listed. It should be noted that permission regarding the copyrights of using these papers in this thesis has been obtained from the Elsevier according to the authors' right of the Elsevier that can be seen in Table 1-1.

Chapter 3

1- A. Fadavi Boostani, S. Tahamtan, Z.Y. Jiang, D. Wei, S. Yazdani, R. Azari Khosroshahi, R. Taherzadeh Mousavian, J. Xu, X. Zhang, D. Gong,

Enhanced tensile properties of aluminium matrix composites reinforced with graphene encapsulated SiC nanoparticles
Composites Part A, 68 (2015) 155-163.

Chapter 4

2- A. Fadavi Boostani, R.T. Mousavian, S. Tahamtan, S. Yazdani, R.A. Khosroshahi, D. Wei, J.Z. Xu, D. Gong, X.M. Zhang, Z.Y. Jiang,

Graphene sheets encapsulating SiC nanoparticles: A roadmap towards enhancing tensile ductility of metal matrix composites

Materials Science and Engineering A, 648 (2015) 92-103.

Chapter 5

3- A. Fadavi Boostani, R.T. Mousavian, S. Tahamtan, S. Yazdani, R.A. Khosroshahi, D. Wei, J.Z. Xu, D. Gong, X.M. Zhang, Z.Y. Jiang,

Solvothermal-assisted graphene encapsulation of SiC nanoparticles: A new horizon toward toughening aluminium
Materials Science and Engineering A, 653 (2016) 99-107.

Chapter 6

4- A. Fadavi Boostani, S. Tahamtan, S. Yazdani, R. Azari Khosroshahi, D. Wei, H. Sahamirad, X.M. Zhang, Z.Y. Jiang

Graphene tweaking Hamaker constant of SiC nanoparticles: A new horizon to solve the conflict between strengthening and toughening

Accepted manuscript, Scripta Materialia, 118 (2016) 65-69

Chapter 7

5- A. Fadavi Boostani, S. Yazdani, R. Taherzadeh Mousavian, S. Tahamtan, R. Azari Khosroshahi, D. Wei, D. Brabazon, J.Z. Xu, X.M. Zhang, Z.Y.

Strengthening mechanisms of graphene sheets in aluminium matrix nanocomposites

Materials & Design, 88 (2015) 983-989

During my PhD study, I have also participated in publications of the following papers in the field of metal matrix composites.

1- S. Tahamtan, A. Halvaee, M. Emamy, Z.Y. Jiang, A. Fadavi Boostani

Exploiting superior tensile properties of a novel network-structure AlA206 matrix composite by hybridizing micron-sized Al_3Ti with Al_2O_3 nano particulates

Materials Science and Engineering A, 619 (2014) 190-198.

2- S. Soltani, R. Azari Khosroshahi, R. Taherzadeh Mousavian, Z.Y. Jiang, A. Fadavi Boostani, Dermot Brabazon

Stir casting process for manufacture of Al–SiC composites

Rare Metals, (2015) 1-10

3- R. Taherzadeh Mousavian, N. Azizi, Z.Y. Jiang, A. Fadavi Boostani

Effect of Fe_2O_3 as an accelerator on the reaction mechanism of Al–TiO_2 nanothermite system

Journal of Thermal Analysis and Calorimetry, 117(2014) 711-719.

Table 1-1: The authors' right for including the published papers in the thesis.

Table of Author's Right			
	Preprint version (with a few exceptions- see below*)	**Accepted Author Manuscript**	**Published Journal Articles**
Use for classroom teaching by author or author's institution and presentation at a meeting or conference and distributing copies to attendees	Yes	Yes	Yes
Use for internal training by author's company	Yes	Yes	Yes
Distribution to colleagues for their research use	Yes	Yes	Yes
Use in a subsequent compilation of the author's works	Yes	Yes	Yes
Inclusion in a thesis or dissertation	Yes	Yes	Yes
Reuse of portions or extracts from the article in other works	Yes	Yes with full acknowledgement of final article	Yes with full acknowledgement of final article
Preparation of derivative works (other than commercial purposes)	Yes	Yes with full acknowledgement of final article	Yes with full acknowledgement of final article
Preprint servers	Yes	Yes with the specific written permission of Elsevier	No
Voluntary posting on open web sites operated by author or author's institution for scholary purposes	Yes (author may later add an appropriate bibliographic citation, indicating subsequent publication by Elsevier and journal title)	Yes, with appropriate bibliographic citation and a link to the article once published	Only with the specific written permission of Elsevier
Mandated deposit or deposit in or posting to subject-oriented or centralized repositories	Yes under specific agreement between Elsevier and the repository	Yes under specific agreement between Elsevier and the repository **	Yes under specific agreement between Elsevier and the repository
Use or posting for commercial gain or to substitute for services provided directly by journal	Only with the specific written permission of Elsevier	Only with the specific written permission of Elsevier	Only with the specific written permission of Elsevier
** Voluntary posting of Accepted Author Manuscripts in the arXiv subject repository is permitted.			

Declaration of Authorship

I hereby declare that I am the main author of papers used in this PhD thesis. Professor Zhengyi Jiang and Dr. Dongbin Wei have been involved in these papers as a principal supervisor and co-supervisor of my PhD study, respectively. Dr. Saleh Tahamtan has helped us in the project in the case of stir casting process. Professor Dermot Brabazon has assisted us in analysing the microstructural and mechanical properties of the produced composites. Professor Sasan Yazdani and Dr. Rasoul Azari Khosroshahi have participated in interpretation of the TEM pictures. Mr. Reza Taherzadeh Mousavian has helped us in interpreting the results achieved form casting processes. Professors J. Xu, X. Zhang, and D. Gong have worked with our group in analysing the results of mechanical properties. Mr. Hossein Sahamirad has cooperated with us in calculation the Hamaker constants of the nanoparticles used in this study. Finally, I would like to offer my great appreciation regarding all efforts that these academics have done during my PhD study.

Table of Contents

List of Figures

List of Tables

Chapter 1 Introduction

1.1 Background

Metal matrix composites (MMCs), fortified with continuous ceramic fibers, demonstrate high mechanical properties and specific elastic modulus compared to unreinforced metals/alloys [1-4]. The problems restricting the usage of these composites are related to the high price of fortifying fibers and manufacturing processes. MMCs reinforced with nanoparticles, however, are isotropic, easier to produce with lower price compared to those fabricated by the continuous fiber-reinforced composites. The metallic matrices confer high elongation and toughness accompanied by high modulus and strength of the nanoparticles for manufacturing MMCs with superior tensile strength and elongation. The challenging task, however, is uniform distribution of nanoparticles within the metallic matrices during fabrication process [3, 5, 6]. This related to the high propensity of these particles for agglomeration, diminishing acquiring the superior ductility.

Studies implemented on the MMCs have shown that distribution of nanoparticles can significantly affect mechanical properties of these composites [7-12]. This is attributed to the higher possibility of cracks to propagate through agglomerated nanoparticles settled preferentially at the grain boundaries rather than being engulfed within grain interiors. To this end, different manufacturing routes have been invented to tackle this problem using powder metallurgy [13-15], semis-solid casting [11, 16-18], stir casting [19], ultrasonic-assisted casting [20], flake powder metallurgy and semi-solid powder processing [21, 22]. The invented fabrication routes, however, have not been highly successful in providing uniform distribution of nanoparticles within the solidified matrix, thereby restricting achievement of enhanced tensile properties for the produced composites. The reason can be ascribed to the absence of any in-depth study to consider some critical aspects of incorporation of nanoparticles within advancing solid/liquid interface such as thermophysical properties of particles and matrix [23], wettability of particles [24, 25] and most importantly intrinsic characteristic of nanoparticles such Hamaker constant [26].

This study, therefore, combines novel synthesis and fabrication routes, making use of detailed atomic-scale characterizations and quantitative investigations to capture the effect of graphene sheets on manipulating the microstructural characteristics of aluminium based composites reinforced with SiC nanoparticles, thereby conferring superior tensile properties to these composites. Although there are some studies that used graphene sheets as reinforcements in metal matrix composites in recent years [21, 27-29], the effect of graphene on manipulating the intrinsic characteristics of the nanoparticles to tailor the mechanical and physical properties of the metal matrix composites is far from being known. This study, therefore, aims at exploiting the unprecedented characteristic of graphene sheets on manipulating the intrinsic properties of SiC nanoparticles to enhance the engulfment of these particles within the aluminium matrix during solidification to render significant enhancement in tensile properties of the aluminium metal matrix composites.

1.2 Scope of the Thesis and its Objectives

The goal of this study is to investigate the effect of adding graphene sheets as reinforcement on the microstructure and mechanical properties of aluminium based composites reinforced with SiC nanoparticles. A principal objective is to establish a basic understanding of the effect of the graphene sheets on the solidification behaviour of aluminium phase containing SiC nanoparticle, encapsulated by graphene sheets, resulted in micro/nano structural changes in the solidified matrix, thereby affecting the mechanical and physical properties of the produced composites.

We have utilized a novel graphene encapsulating technique to encapsulate SiC nanoparticles, combined with detailed electron microscopy investigation to have a science-based insight into the mechanism behind the graphene encapsulation technique and the evolution of micro/nano structure in the produced composites. Additionally, the interface between nano-size reinforcing blocks, i.e. SiC nanoparticles encapsulated by graphene sheets, and the aluminium matrix, and the fracture surfaces of the fabricated composites were investigated by FE-SEM and TEM. In particular, the fundamentals related to the solidification behaviour of the

SiC nanoparticles, encapsulated by graphene sheets, when they encounter with the advancing solid/liquid interface at the nanoscale regime were investigated. These mechanisms have not been investigated so far, neither in composites fabricated by powder preform nor those produced from raw entities. Strengthening mechanisms of graphene sheets were also studied to make a bridge between nanostructural evolutions brought about due to incorporation of the graphene sheets within the aluminium matrix and the enhanced tensile properties of the produced composites.

Different fabrication routes including the stir-casting, pressure assisted casting in the semi-solid state, semi-solid powder forming and the thixoforming processes were used in this study for manufacturing aluminium based composites reinforced with SiC nanoparticles encapsulated by graphene sheets. To delineate the effect of graphene encapsulation on the microstructural and mechanical properties of the produced composites, two different types of the SiC nanoparticles including as-received and graphene encapsulated ones were used as reinforcements. The graphene encapsulation of SiC nanoparticles was not limited only to the proposed ball milling process, but it was also investigated using a new solvothermal process invented in this study.

1.3 Overview of the Thesis

This chapter has represented a brief background of metal matrix composites as well as a brief discussion regarding the subject areas and objectives which are going to be covered in this thesis. An overview of the individual chapters of the thesis is also given below.

Chapter 2 presents the literature review of metal matrix composites in general and aluminium matrix composites reinforced with nanoparticles in particular. A brief introduction to metal matrix composites encompassing the definition, classification, manufacturing processes and properties has been presented, targeting mainly the processing routes and mechanical properties of metal matrix composites reinforced with nanoparticles and graphene sheets.

Chapter 3 explains the initial results of manufacturing aluminium matrix composites reinforced with SiC nanoparticles using invented graphene encapsulating method. These encompass the fabrication of the composite samples,

preparation of samples for microstructural and mechanical characterizations with emphasis on demonstrating the effect of graphene sheets on alleviating the agglomeration of SiC nanoparticles. This chapter has presented some basic theories and principles to explain the mechanisms by which graphene encapsulation process can disperse SiC nanoparticles uniformly through the solidified aluminium matrix.

Chapter 4 aims at expounding the initiative mechanisms presented in Chapter 3 for the uniform distribution of SiC nanoparticles based on a new solidification model invented in this study. This solidification model demonstrates the effect of graphene sheets on manipulating the thermal conductivity of SiC nanoparticles to enhance the propensity of these nanoparticles for engulfment within grain boundaries rather than agglomerating at grain boundaries. This chapter also ascertains the true potential of graphene sheets in enhancing the tensile properties of the produced composites from other conventional processing routes.

Chapter 5 introduces a new process for graphene encapsulation of SiC nanoparticles by means of solvo-thermal assisted approach to alleviate the inhomogeneity seen in the number of graphene sheets coating SiC nanoparticles to enhance the engulfment propensity of these nanoparticles within aluminium matrix in the subsequent stir-casting process.

Chapter 6 suggests a new theoretical approach about the effect of graphene sheets on manipulating the Hamaker constant of SiC nanoparticles, prompting the engulfment of these particles within advancing solid/liquid interface.

Chapter 7 presents a new strengthening mechanism devised in this study, encompassing the effective strengthening mechanisms coming to practice due to incorporation of graphene sheets within aluminium matrix. The micro/nano structure of the produced composites was investigated using a high resolution TEM to clarify in-details the effect of graphene sheets on producing the thermal-activated dislocations.

At the last part of this thesis (Chapter 8), the results achieved in this study are summarized and the main conclusions are reviewed. Additionally, some suggestions for future studies were presented to delineate some stages that can be

elaborated more to expand the investigation into other critical areas in fabrication of advanced aluminium metal matrix composites.

Chapter 2 Literature Review

2.1 Metal Matrix Composites (MMCs)

Metal-matrix composites (MMCs) are a hybrid material in which rigid ceramic reinforcements are embedded in a ductile metal alloy matrix [4]. They tailor the best properties of two different materials, such as ductility and toughness of the metallic matrix and the high modulus and strength of ceramic reinforcements. Their first application can be traced back to the late 1960s, with the development of a steel-wire reinforced copper alloy [30]. The aerospace industry was the first one to apply the technology of composite materials to spacecraft components. Advanced materials with high mechanical properties are crucial when the working environment is extreme and critical, which is predominant in space missions. It should be considered that the International Space Station will experience about 175,000 thermal cycles ranging from +125 °C to -125 °C as it travels in and out of the Earth's shadow. The usage of the aluminium matrix composites (AMCs) were specifically expanded for aerospace and defence applications [4]. AMCs reinforced with continuous boron fiber were utilized in the Space Shuttle Orbiter as the frame; it has also been reported that other applications such as landing gear drag link results in 45% reduction in the total weight. The AMCs reinforced with graphite was also used as a main part of the antenna boom in the Hubble Space Telescope with total length of the 3.6 m, providing the demanded stiffness to sustain the position of the antenna during space missions.

The application of the MMC has been developed extensively in the last 10 years, attributed to the promising mechanical and physical properties of these composites. Fig. 2-1 represents the world usage of MMCs [31]. It has been reported that the usage rate of the MMCs is around 5.9% and it is predicted that the total consumption of these composites can enhance from 5500 tons related to the 2012 to 8200 tons in 2019. This enhancement in the usage of the MMCs in industries results in inventing the advanced and novel manufacturing processes at a low cost and with high efficiency. It is anticipated that there are more developments in production of the MMCs, but the lack in the stability and reproducibility of the process, and insufficient economic productivity still endanger the production of the advanced MMC for high-tech industries [32]. One

of the most promising features in manufacturing the metal matrix composites is exploiting the advantage of the constituent materials including matrix and reinforcement [15] to meet the specific demands needed for advance applications such as aerospace, automobile and electronic industries. A composite can be defined as a material made from several constituents intimately bonded together. Aluminium is considered as the most common matrix for manufacturing the MMCs, attributed to the low density, precipitation strengthening, good corrosion resistance, and high thermal and electrical conductivity [20]. There are different ceramic particles that can be used as reinforcements in AMCs including TiB_2, B_4C, TiC, WC, BN, ZrO_2, but the most common ceramic reinforcements utilized are SiC or Al_2O_3 [33]. AMCs reinforced with ceramic particles represent enhanced tensile properties over conventional monolithic materials, such as higher strength, stiffness, and weight savings [34, 35].

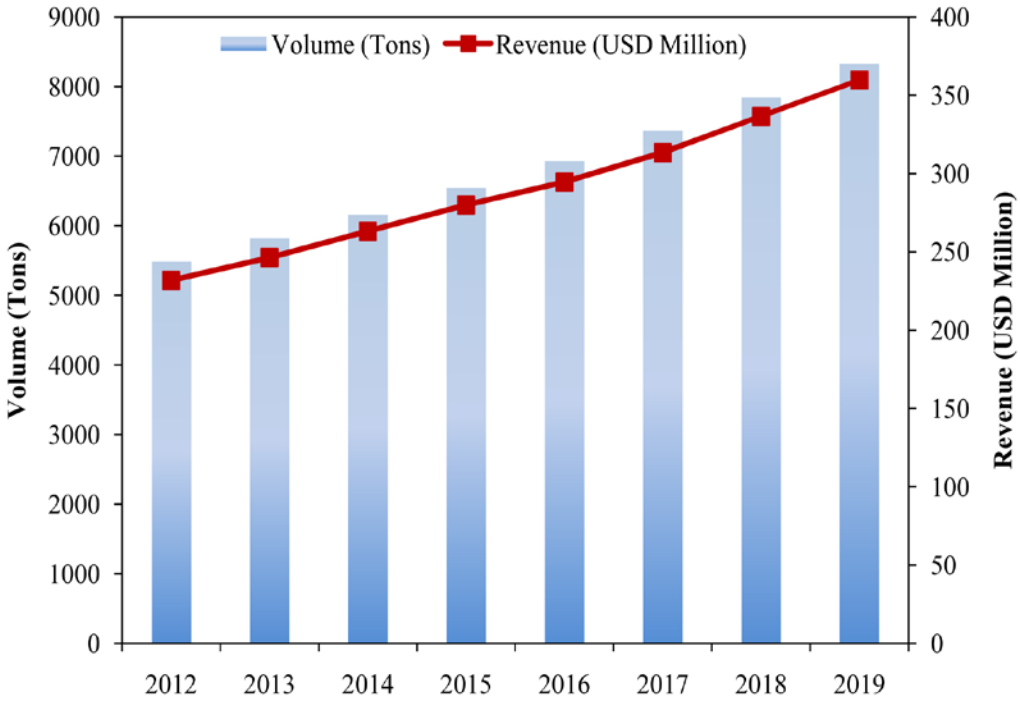

Fig. 2-1: The usage trend of MMC [31].

Despite this enhanced tensile properties of the AMCs reinforced with ceramic particles, these composites suffer significantly from diminished tensile ductility and fracture toughness compared to the unreinforced alloys [19], imparting significant limitation in structural applications.

2.2 MMCs reinforced with nanoparticles

MMCs reinforced with nanoparticles can be considered as promising alternative to prevail over the limitations of MMCs reinforced with micron-sized particles [36]. The manufacturing of the MMCs reinforced with nanoparticles, however, is a challenging task, attributed to the difficulties in dispersing a uniform distribution of the nanoparticles within aluminium matrix [37].

In 2004, the American Ceramic Society explained Nanotechnology as "The creation, processing, characterization, and utilization of materials, devices, and systems with dimensions on the order of 0.1-100 nm, exhibiting novel and significantly enhanced physical, chemical, and biological properties, functions, phenomena, and processes due to their nanoscale size''.

The mechanical, electrical, thermal, optical, electrochemical and catalytic properties of the nanocomposite will differ markedly from that of the component materials. It has been reported [33] that certain size effects govern the property of these materials.

There is a significant tendency to replace the nanoparticles with other discontinuous reinforcing nanofiller such as nano-fibers, nano-wires or nano-platelets. The most important nanoparticles used in the composites as reinforcement are SiC, TiC, WC, TaC, TiB_2, AlN, and Al_2O_3 [33]. MMCs reinforced with nanoparticles have different promising properties as follows.

The significant and unique change of the fracture mode from inter-granular fracture related to the monolithic metal to trans-granular fracture mode applicable for nanocomposites

- Enhanced tensile properties
- Increased fracture toughness
- Profound enhancement in creep, thermal shock, and wear resistance
- High stability of structure at high temperatures.

It has been shown that adding SiC particles to the aluminium matrix can enhance the dimensional stability based on the size of the reinforcement. There is a significant diminution in temperature sensitivity of aluminium reinforced with micro/nano sized SiC particles, but the effect of adding SiC nanoparticles are more predominant than the micron ones [4].

It has been also reported by Ren and Chan [38] that the wear resistance of the 7075 aluminium matrix composites (AMCs) reinforced with SiC nanoparticles can be enhanced significantly compared to the ones reinforced with micron-sized SiC particles. Additionally, the loading content of the reinforcement needed to enhance the mechanical properties of the MMCs reinforced with nanoparticles are significantly lower than the one needed for micron-sized particles. For instance, it has been reported that adding small percentage (1 vol. %) of Si_3N_4 (10 nm) into the aluminium matrix can enhance the tensile strength to the values significantly higher than the ones achieved after incorporation of micron-sized SiC particles (3.5 μm) with 15 vol. % loading content, resulted in enhancing the yield strength of the nanocomposites compared to the microcomposites [39].

It has been approved that there is a threshold size ("critical size") below that the mechanical, electrical, thermal, optical, electrochemical and catalytic properties of the nanocomposite can be improved significantly [33]. It should be noted that the mechanism by which these nanoparticles can augment these properties remains a matter of debate among researchers.

Previous studies have shown that incorporation of nanoparticles within the metallic matrices can bring about a significant enhancement in mechanical properties [40-42] compared to those produced using micron-sized particles, attributed to the strengthening resulted from dispersion of these particles at different load content. For instance, it has been reported that reducing the size of the reinforcement to the nanometric scale can result in augmentation of the elastic modulus, and yield strength of the produced composites [43].

The mechanical properties of composites can be affected principally by the nature of bonding between the nanoreinforcemnt and the surrounding matrix. It has been generally accepted that the reduction of the size of grains and the reinforcements can enhance the mechanical properties such as strength and hardness due to increasing the effective barriers inhibiting the movement of dislocation through the matrix [44]. This strategy, however, has some drawbacks related to the diminution of the ductility and deteriorating high creep rate associated with the reduction of the grain size. It has also been approved that the mechanical properties of nanocrystalline materials are not very authentic. This is

ascribed to the enhancement of the porosity content of these materials due to insertion of the microvoids associated with incorporation of nanoparticles within the matrix [45]. This enhancement in the porosity of the nanodispersed aluminium casting alloys has also been reported by Mahallawi et al.[11].

Different studies have demonstrated that the mechanical characteristics of nanocomposites are significantly related to the uniform distribution of nanoparticulates, properties of the nanosized powders, volume fraction of the nanoparticulates within the matrix, as shown in Fig. 2-2, and at the grain boundaries [32].

Uniform distribution of the nanoparticles within metallic matrices, however, is a challenging task in solid and liquid processing routes. This is related to the high propensity of these particles to the agglomeration and other interactive phenomena, i.e. as electro-repulsion [42, 46], especially at high volume fractions. This, in turn, diminishes the mechanical properties including fracture toughness and the elastic modulus.

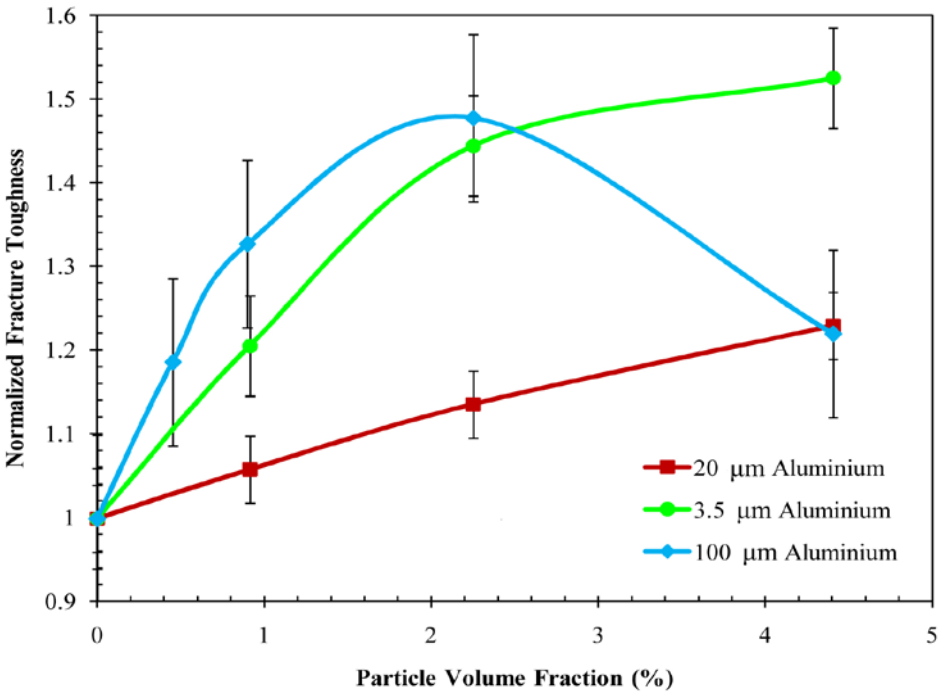

Fig. 2-2: Normalized fracture toughness with respect to volume fraction variation for various nano- size particles [47].

2.3 Aluminium matrix composites (AMCs) reinforced with nanoparticles

Particulate-reinforced nanocomposites have been extensively employed in the automotive industry for their capability to withstand high temperature and pressure conditions [14, 33, 37, 48, 49]. Several manufacturing methods have been used to fabricate them. Nonhomogeneous particle dispersion and a poor interface bonding are the main drawbacks of conventional techniques [3, 50, 51]. Reinforcing aluminium matrix with submicron/nano particles confers profound improvement in mechanical and physical properties on AMCs [11, 19, 52]. Different studies have been concentrated on the manufacturing processes and mechanical properties of AMCs reinforced with nanoparticles such as SiC or Al_2O_3 [53, 54].

Tahamtan et al. [55] have utilized mechanical stir mixing to manufacture A206 nanocomposite reinforced with 5 vol.% Al_2O_{3p}. It has been shown that the contact angle between aluminium and Al_2O_3 is around 100º, bringing about a severe agglomeration for Al_2O_3 nanoparticles [56].

This poor wetting characteristic of Al_2O_3 nanoparticles stimulates clustering of these particles and their floating on the liquid metal surface [57]. To enhance the wettability of alumina nanoparticles (100 nm), these particles were ball-milled with Mg and Al powders accompanied by cold pressing into disc specimens. Ball-milled discs were introduced into molten A206 alloy for forming nanocomposite. This augments the wettability of ball-milled alumina with molten metal significantly, leading to better distribution of nanoparticles in the melt [17]. It was also reported by Mazahery et al. [9] that ball milling of Al_2O_3 nanoparticles (50 nm) with aluminium particles (16 μm) before incorporation within liquid A356 can reduce the agglomeration of these particles.

It has been reported recently [58] that A356 aluminium based nanocomposites can be manufactured using Al_2O_3 nanoparticles by both stir casting and compocasting processes. It has been shown that the Al_2O_3 nanoparticles can have a profound effect for nucleation of aluminium phase, leading to manufacturing nanocomposites with nano-sized grains. The result has also corroborated that compocasting can enhance wettability of particles and liquid aluminium, resulted in refining the grain structure of the produced composites. Compocasting process also brings lower porosity content compared with composites produced using stir-

casting method. The uniform distribution of nanoparticles in A356 aluminium based composites, produced using compocasting, was also confirmed by El-Mahallawi et al. [11].

2.4 AMCs reinforced with graphene sheets

The growing demand for utilizing aluminium in automotive and aerospace applications has made AMCs as an important material to be used in the structural applications. As mentioned in Section 2.3, the mechanical properties of the AMCs can be significantly improved due to implementation of the nanoparticles within the aluminium matrix. Based on this, carbon nanotubes (CNTs) have demonstrated a great promise as reinforcement in AMCs as a conventional material to study in metal carbon composites [22]. Following this, graphene has received significant attention recently as a novel reinforcement in composites [27, 28], attributed to high mechanical properties, Young's modulus, electrical and thermal conductivity of graphene sheets [59]. Although most studied have focused on improving the mechanical properties of the polymer matrixes [60], there are few studies considering utilization of graphene sheets in metal matrixes [29, 61]. This is ascribed to the difficulties in uniform distribution of graphene sheets within metal matrices and potential chemical reactions at the interface of graphene sheets and aluminium [28], deteriorating the mechanical, thermal and electrical properties of the produced composites. Based on this, some studies have shown the profound effect of graphene sheets in improving the mechanical properties [61], while other researches have represented diminished tensile properties as a result of graphene incorporation [27]. These differences are attributed to the quality of dispersion, manufacturing process, and chemical reactions at the interface of graphene sheets and aluminium matrix.

Utilizing graphene sheets in improving the mechanical properties of the metal matrix composites produced by different manufacturing processes requires generating a homogeneous dispersion of the graphene sheets within the metal matrix. It has been shown that the powder metallurgy routes can be an appropriate route for uniform dispersion of nanoparticles [62, 63]. For example, Wang et al. [61] has suggested powder metallurgy route accomplished using flake metallurgy

as an effective route to disperse graphene sheets within aluminium matrix. This is resulted in enhancing the tensile properties of aluminium based composites. The invented fabrication route, however, was not highly successful in imparting enhanced tensile properties to the produced composites, attributed to the nonuniform distribution of the graphene sheets within the matrix.

Regarding chemical reactions at the interface of graphene sheets and aluminium matrix, Bastwros et al. [21] has claimed that the enhancement in the tensile properties of the Al6061 aluminium alloy can be related to the formation of graphene sheets or aluminium carbide within the matrix.

2.5 Uniform distribution of nanoparticles in MMCs

One of the key challenges in manufacturing MMCs is the uniform distribution of nanoparticles in the matrix of the MMCs. It has been established before that the mechanical characteristics of AMCs are mainly related to the distribution of nanoparticles. In fact, nonuniform dispersion of particles, i.e. agglomeration, can significantly deteriorate mechanical properties and especially the ductility and fracture toughness [64]. The main problem encountered in MMCs processing is the agglomeration of the nanoparticles during liquid holding or during casting. This is attributed to the density differences between the nano particles and the matrix alloy melt. The dispersion of nanoparticles can be affected by several stages during liquid processing including (a) dispersion in the liquid due to mixing, (b) distribution in the liquid after mixing, but before solidification, and (c) redispersing as a result of solidification [65].

The mechanical mixer utilized during liquid stirring, the liquid temperature, and the type, amount and nature of the nanoparticles are some of the main parameters. These parameters should be considered when analysing the agglomeration of nanoparticles in manufacturing processes. This is especially important in mechanical mixing methods for dispersion of nanoparticles in the liquid. It has also been approved that the uniform distribution of the nanoparticles in a matrix is also affected by pouring rate, pouring temperature and gating systems [65].

The AMCs can be manufactured by different production methods including liquid processing (such as stir casting) and solid-phase processing (such as powder

metallurgy), which are discussed in details in the next section. It has been approved that liquid processing has some important advantages such as better matrix-particle bonding, ability to tailor the matrix structure, simplicity, low cost of processing and nearer net shape [66, 67] in comparison with solid state processes such as powder metallurgy [68]. The liquid state manufacturing routes, however, suffer from two main problems including diminished wettability of nanoparticles in most liquids, and secondly the nanoparticles are more susceptible to sink or float based on their density. This restricts the achievement of the uniform distribution of these particles within the matrix. This, in contrast, is not the case in the solid state processes such as powder metallurgy [69], representing the significant effect of manufacturing method on the distribution of nanoparticles.

From solidification stand point, particle pushing during solidification can also result in the agglomeration of the particles in the intergranular and interdendritic areas of the matrix [70]. For example, when the matrix alloy follows the dendritic solidification, the dendritic regions in the solidifying matrix will have a significant effect on the particle dispersion after solidification [23]. It has also been found that adding inoculating agents can manipulate the solidification mechanism of Ali-Si alloys to promote the fine grained microstructure. This facilitates uniform dispersion of nanoparticles within the intergranular sections of the dendritic structure [65]. This, in turn, can also improve the dispersion of eutectic, the intermetallic and the shrinkage porosity produced in the last freezing zones of the solidified matrix.

During manufacturing of the cast AMCs, it has been realized that generation of the dendritic structures can promote agglomeration of particles. Developing fine dendrite or regular globular primary phase during solidification, however, can significantly stimulate the engulfment of particles within the solidifying matrix [65]. This demonstrates the importance of novel manufacturing routes to develop formation of the fine grains. This is resulted in diminishing the heterogeneity of the reinforcement dispersion in the solidified matrix to enhance the tensile properties of the AMCs.

2.6 Engulfment or pushing of particles during solidification

The interaction between the particles and the interface is of interest. This is related to its significance on different systems such as determining particle distribution in MMCs reinforced with ceramic particles, growth of monotectics [71], formation of segregated inclusions during casting [72] and emulsion of organic cell suspensions in ice in cryobiology [73].

In particular as mentioned in the last section, dispersion of particles in MMCs is one of the important microstructural aspects of the MMCs. This affects the mechanical and physical properties of the MMCs produced by liquid processing such as stir casting process and solid state processing such as powder metallurgy.

In general, the particles can be uniformly dispersed within solidifying matrix, rendering improved mechanical properties, or agglomerated along grain boundaries. As a result, it causes to diminish mechanical properties especially ductility [64]. This is, therefore, vital to determine the parameters that can stimulate the uniform dispersion of particles, i.e. engulfment, within advancing solid/liquid interface or pushing them to the interdendritic regions, i.e. agglomeration, during solidification. Different studies, therefore, have been concentrated on investigating the interactions between solid/liquid interfaces during solidification [74-76].

It has been proved by the kinetic models that engulfment or pushing of particles can be determined by the critical velocity of the interface [70]. In fact, if the velocity of advancing solid/liquid interface is bigger than the critical velocity, the particles can be engulfed within the matrix. On the other hand, if the velocity of advancing solid/liquid interface is lower than the critical velocity, the particles will be pushed away from moving interface. This results in their agglomeration at grain boundaries.

Thermodynamic models [77] suggest calculation of the thermodynamic free energy change during engulfment of the particle by the advancing solid/liquid interface when the interface velocities are very small. Thermophysical models [78-80] consider the ratio between thermal conductivity of the particles and liquid as an important factor to determine the engulfment or pushing of the particles from advancing solid/liquid interface. According to these models, the interface has this

propensity to have convex shape when it approaches to the particles with a thermal conductivity lower than the melt, prompting pushing or agglomeration of them at grain boundaries [81]. Particles with thermal conductivity higher than the liquid, however, stimulate the concave shape in the advancing solid/liquid interface, resulting in capturing or engulfment of these particles within advancing solid/liquid interface.

2.7 Graphene/nanoparticles interactions: A road map to manufacture composites with exceptional properties

The implementation of nanoparticles in manufacturing nanocomposites with enhanced mechanical properties has been established fully before [52, 82]. The exceptional characteristics of graphene can bring about new frontiers in exploiting the extraordinary properties of nanoparticles. This can be realised by synergistic effects of graphene and nanoparticles on different composites such as metal, ceramic and polymer based composites.

It has been reported that different nanoparticles of metals, metal oxides and semiconducting materials have been decorated on 2-D structure of graphene [83, 84], resulting in superior properties in the produced composite.

It should be also noted that the nanoparticles are directly deposited on the graphene sheets by considering this fact that no molecular bonds are required to connect the nanoparticles and the graphene. This is diminishing the detrimental effect of these particles on the host graphene substrate. This, therefore, results in providing an appropriate room for deposition of nanoparticles on the graphene sheets to render novel functionalities not only to the graphene sheets but also to the deposited nanoparticles for different applications such as catalytic [85], energy storage, photo catalytic, sensor, and optoelectronics applications [59].

As shown in Fig. 2-3, the deposition of nanoparticles, such as TiO_2, on the surface of reduced-graphene oxide (RGO) sheets can be considered as a practical approach to produce composites with synergic properties of nanoparticles and graphene sheets.

The TEM picture shown in Fig. 2-3 represents formation of the composite by combination of similar stacked RGO sheets associated with a higher density of TiO_2 on the RGO sheets. This picture shows the anchoring capacity of reduced-

graphene oxide in deagglomeration of TiO_2 nanoparticles. Investigation of the lattice spacing extracted from the TiO_2/ RGO demonstrated in Fig. 2-3B revealed periodicities of 2.12 Å (Fig. 2-3C) and 2.35 Å (Fig. 2-3D) from different locations on the composite [85].

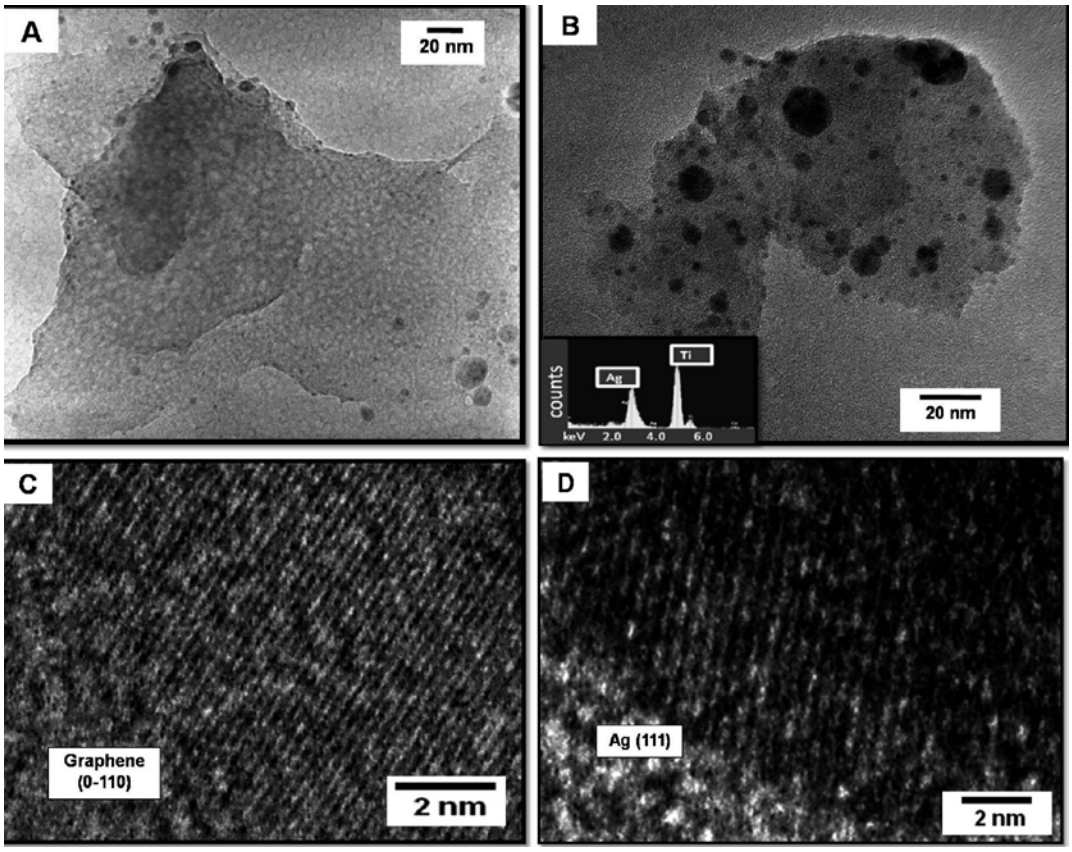

Fig. 2-3: TEM images of the experimental work conducted for production of TiO_2/ RGO composite with synergic effects of metal oxides and RGO [85].

In this case, this approach aims at using mixed properties of graphene and metal oxides as active materials to enhance the ability to store the electrochemical energy, and to diminish or even eliminate the present technical challenges. These challenges generally are generated in each separate component of graphene and metal oxides as active materials to manufacture the electrodes. In fact, the graphene sheets in the produced composite facilitate chemical functionality and compatibility for distributing the metal oxides uniformly within the composite. The metal oxide component, on the other hand, produces high capacity to store the electrochemical energy based on its structure, size and crystallinity.

This unique functionality of graphene sheets in diminishing the agglomeration of metal oxides, however, has not been reported to be used for alleviating the agglomeration of nanoparticles in metal matrix composites so far. Additionally, as mentioned in Section 2.6, nanoparticles with higher thermal conductivity than the liquid matrix have higher propensity to be engulfed within advancing solid/liquid aluminium rather than being agglomerated at grain boundaries.

As mentioned in Sections 2-2 and 2-5, uniform distribution of nanoparticles during manufacturing process of MMCs is a challenging task [5, 7, 20, 29, 36, 37, 50, 53, 54, 74, 86-94], restricting widespread applications of these composites. On the other hand, according to the literature review conducted in Sections 2-4 to 2-7, it has been revealed that production of composites with possible interactions of nanoparticles and graphene sheets can be an excellent strategy for enhancing the propensity of these particles to be engulfed within advancing solid/liquid aluminium. Our studies, however, have shown that there is no research on exploiting the superior thermal conductivity of graphene sheets for improving the uniform distribution of nanoparticles by augmenting the tendency of them for engulfment in MMCs.

2.8 Manufacturing processes of AMCs

As shown in Fig. 2-4, there are different manufacturing routes for production of aluminium matrix composites including: (1) solid state; (2) liquid state and (3) deposition processes [95]. Solid-state processes can be used when the high mechanical properties needed for AMCs, ascribed to diminishing the segregation effects and products formed as a result of brittle reaction which are common in the parts manufactured using liquid state process [35]. The liquid state processing methods are considered due to the lower processing price and flexibility in handling and the ability to manufacture different shapes using the conventional casting methods.

These methods, however, are suffering from rigorous adjustments needed to control the processing parameters and formation of undesirable chemical products at the interface between aluminium and reinforcing materials [35].

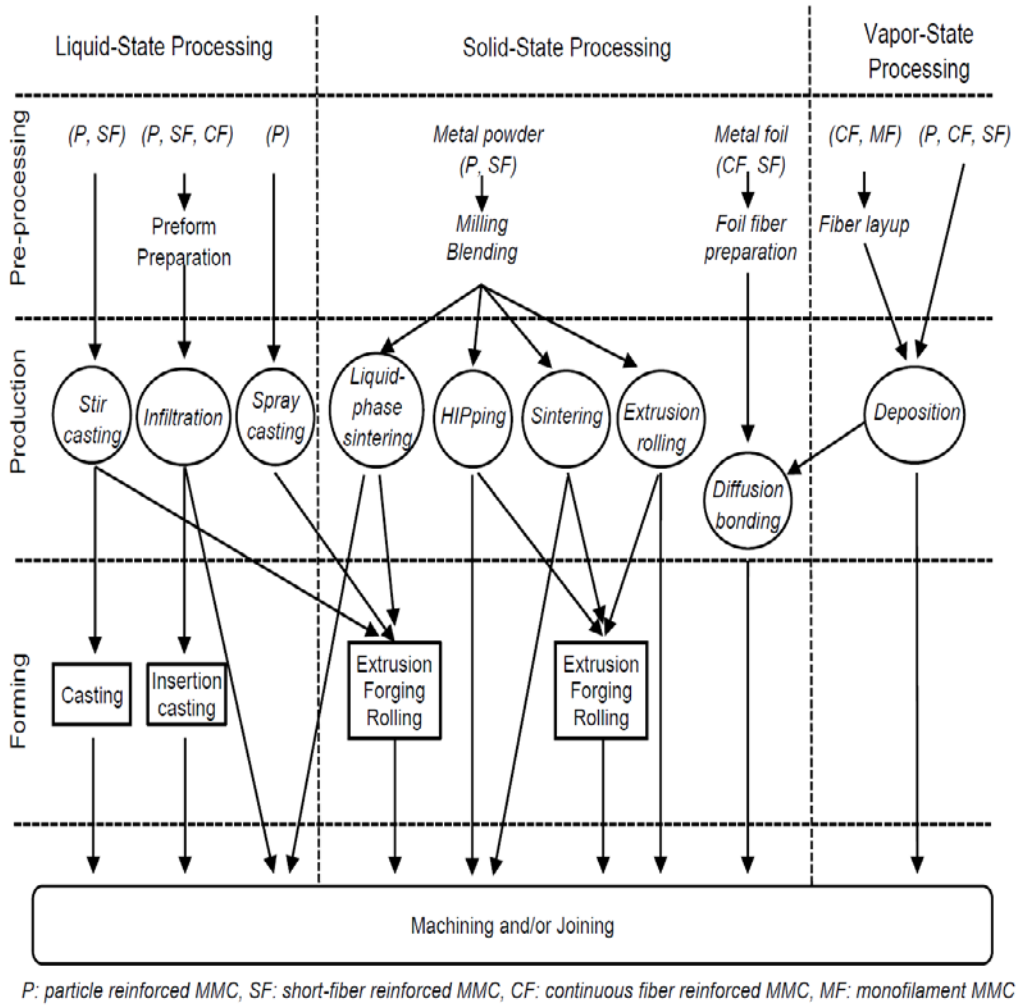

Fig. 2-4: Manufacturing processes of the metal matrix composites [96].

The deposition processes for production of MMCs, however, demonstrate ultra-fine grain size and diminished segregation for the matrix. The disadvantages related to these methods can be classified as high processing cost and limitation in manufacturing the complex parts.

Based on the aforementioned classification for manufacturing processes of the AMCs reinforced with nanoparticles, different producing routes have been introduced encompassing the ultrasonic assisted casting [20], nano-sintering, powder metallurgy [97], high energy ball milling [98], friction stir process [29] where agglomeration of the reinforcing nanoparticles can bring about significant changes in microstructure of produced composites such as enhancing the grain growth and porosity. This can significantly deteriorate the mechanical properties.

Based on this, it is a challenging task to diminish the agglomeration of nanoparticles to retain the augmented mechanical properties during fabrication process [3, 65, 86], necessitating further investigation to control the microstructures under various processing conditions. Table 2-1 shows the advantages and limitations associated with different processing routes used for fabrication of metal matrix composites [91]. Mechanical alloying (MA) invented in 1970s is considered as a processing route for uniform dispersion of reinforcing particulates within another material called matrix. Since then, different studies have been done to use the MA method for preparing numerous advanced engineering materials including amorphous alloys [99], structured metal nitrides [100], and metal hydrides and metal carbides [101]. Ball milling process, however, has demonstrated a good capability in producing metal matrix composites such as Al/SiC composite with a good distribution of SiC nanoparticulates in the aluminium matrix [102].

Kang and Chang [36] has used the MA process for producing the aluminium composite reinforced with micron/nano-sized SiC particles using different load contents of SiC particles varied between 0 to 7%. They have shown that by using SiC nanoparticles as reinforcement, the maximum tensile yield strength (175MPa) can be achieved at loading content close to 4%, while the tensile elongation diminishes from 25% to 7% related to the composites reinforced with 7% volume fraction of these nanoparticles (Fig. 2-5(b)). They came to this conclusion that the maximum enhancement in tensile properties can be achieved at loading content of SiC nanoparticles close to 4%, related to the strengthening effect of SiC nanoparticles in enhancing the dislocation density, as shown in Fig. 2-6(a), but increasing the loading content more than this threshold value can result in deterioration of the tensile properties attributed to the agglomeration of these particles at grain boundaries, as shown in Fig. 2-6(b).

Compared with MA, liquid based processing, encompassing the stirring of ceramic particles into melts, can be considered as a promising manufacturing route in manufacturing metal matrix composites.

Table 2-1: Advantages and limitations of different manufacturing processes for aluminium matrix composites [91].

Powder Metallurgy Process	**Advantages**	1- Homogeneity of mixture is better controlled, component is produced in near net shape dimension, good ductility, low ball to powder charge ratio provides a better blend homogeneity. 2- The gas atomized aluminium particles exhibit a spherical shape with broad size distribution while small satellite particles are attached to the large ones. 3- The most economical method for manufacturing aluminium MMCs, one can avoid the segregation and agglomeration of the reinforcement particles. 4- The high-energy ball milling offers grain size refinement, making the crystals less susceptible to fracture, and hence nano crystallization process of aluminium MMCs has been the subject of intensive research in recent years.
	Limitations	1-In processing of Aluminium, the oxide and hydroxide films coating the powder. 2-Metal powders do not act as perfect liquids under pressure and a difference in pressure is established both parallel and perpendicular to the direction of pressing.
Casting Process	**Advantages**	Better matrix–particle bonding, easier control of matrix structure, simplicity, low cost of processing, and nearer net shape.
	Limitations	Extremely difficult for the mechanical stirring method to distribute and disperse nano-scale particles uniformly in metal melts due to their large surface- to-volume ratio and their low wettability in metal.
Pressure Infiltration Process	**Advantages**	This method allows the powder particles to be kept in a liquid
	Limitations	Abnormal grain growth was noted for samples containing the larger particle size, since the number of particles reduces with increasing particle size. This lowers the potential for grain boundary pinning during sintering, and hence, for limiting grain growth.
Wet Chemical Method	**Advantages**	1- The phase of such obtained powder is more uniform, the surface bonding between metal and ceramic was enhanced, and the green density is improved greatly 2- Cost less process for preparing high quality nano-size alumina powders
	Limitations	Problem in diminishing the porosity content of the produced powders
Friction Stir Process	**Advantages**	1- To form ultrafine-grained structure in Al and Mg alloys 2- To produce fine-grained microstructure, which exhibits superior plasticity 3- To homogenize microstructure of nanocomposites 4- To refine the microstructure of cast aluminium alloys
	Limitations	Limitation in the size of the composites produced by this method

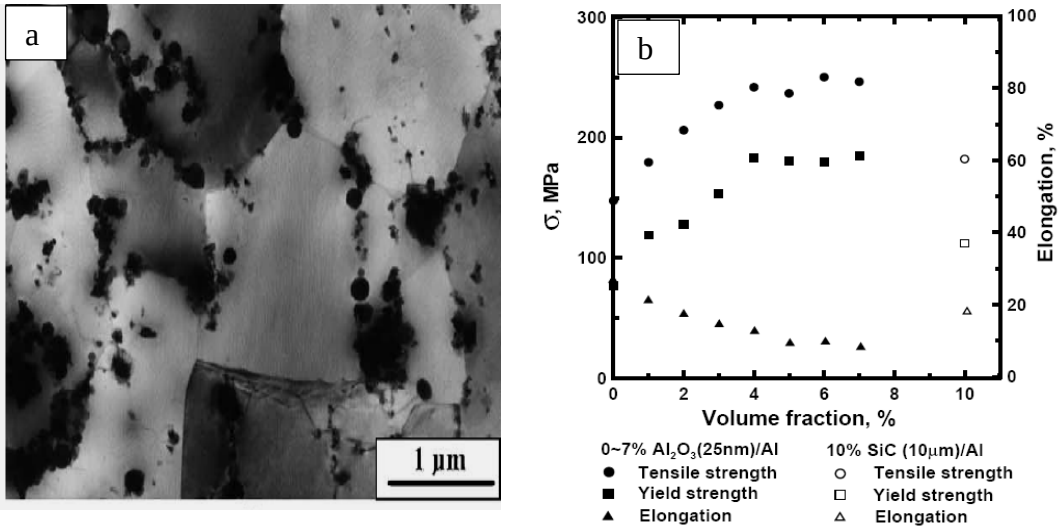

Fig. 2-5 (a) TEM image of the aluminium based composite reinforced with 4 vol. % Al_2O_3 nanoparticles, and (b) mechanical properties of the produced composites based on the different SiC loading contents [36].

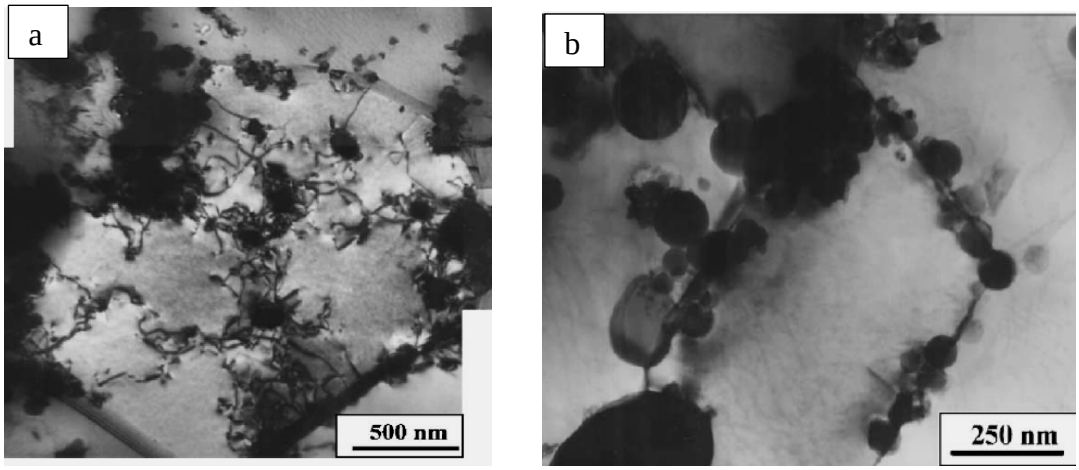

Fig. 2-6: (a) TEM images representing the distribution of the Al_2O_3 nanoparticles and dislocation structure for the loading content of around 2% after tensile test, and (b) TEM picture of aluminium based composites reinforced with 5% vol. Al_2O_3 nanoparticles representing the agglomeration of particulates on the grain boundary [36].

This is of interest due to some beneficial effects including perfect bonding between the matrix and particle, simple controlling the matrix structure, simplicity, low processing cost for production of different materials at various processing conditions compared to other processing routes [9].

It has been shown that the liquid based fabrication methods can be used for production of the aluminium matrix composites reinforced with SiC particles. However, the large discrepancy between the thermal expansion coefficients of SiC particles and the aluminium matrix associated with poor wettability between liquid aluminium, and these particles are key challenges in production of these composites [101].

These problems can be escalated due to the formation of detrimental products as a result of undesirable reaction between SiC particles and liquid aluminium in the form of brittle aluminium carbide phases (Al_4C_3) [25]. Schultz et al. [103] has demonstrated the implementation of reactive wetting associated with stir mixing to distribute the nanoparticles within liquid metal for Al–Cu–Mg composites reinforced with nanoalumina particles and were produced using gravity and squeeze casting. Achieved results have shown that the utilization of reactive wetting for Al_2O_3 nanoparticles as reinforcement for Al–Cu–Mg alloys accompanied by stir mixing can significantly enhance the hardness of gravity cast specimens. This is happening if the reaction between the reinforcement and the matrix can be in the on-going or completed status at the time of solidification. It has been suggested that a small amount of clustering can bring about particle engulfment and Orowan strengthening, but enhancing the formation of clusters can result in particle pushing and grain refinement strengthening that can be explained based on the Hall–Petch relation.

It has been demonstrated by TEM analysis (Fig. 2-7) that squeeze cast sample represents the formation of isolated particles within the grains rather than at grain boundaries. This represents that the higher solidification rate of squeeze casting can result in particle pushing, thereby stimulating engulfment of larger particles compared to the gravity cast samples [103]. As shown in Fig. 2-7(b), the segregated intermetallic phase, which is rich in copper with small amounts of Ni, Fe and Al, is more susceptible to be segregated at grain boundaries rather than grain interiors. This study has approved that the squeeze casting process can be considered as a reliable process to stimulate the engulfment of nanoparticles within solidifying matrix, but this study has not reported any fundamental relationship

between the effects of squeeze casting process and the nanoparticles engulfment during solidification.

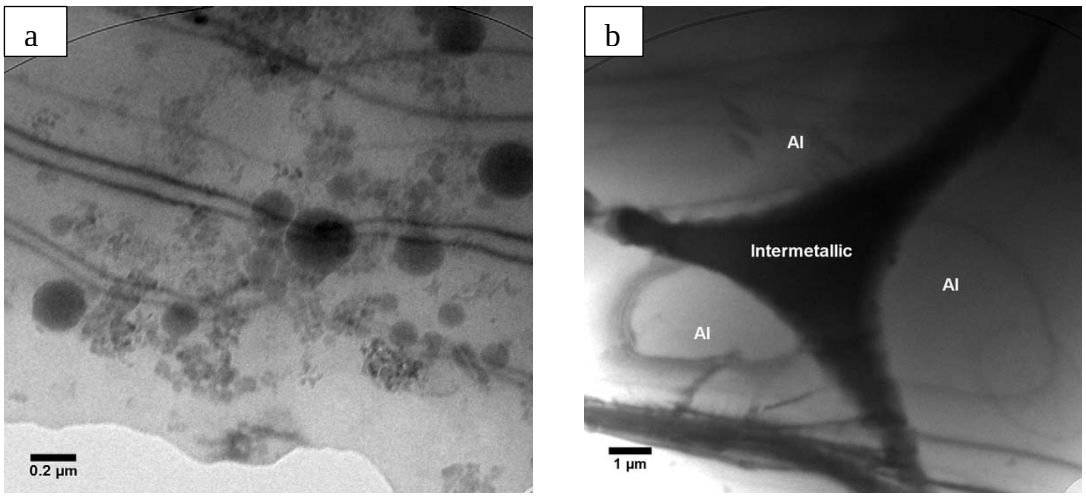

Fig. 2-7: TEM pictures representing (a) the squeeze cast Al–Mg composites reinforced with 5 wt. %Mg–2.5 wt%Al_2O_{3np} after 5 min stirring, and (b) intermetallic phase solidified at triple juncture point of (a) [103].

AMCs reinforced with nanoparticles also suffer from the agglomeration of nanoparticles which is the common problem associated with manufacturing process especially liquid based methods such as stir casting [74]. Hashmi et al. [74] have shown that this is related to the large surface-to-volume ratio and low wettability of nanoparticles in most liquid metals, preventing these nanoparticles to be dispersed uniformly during most liquid state process such as stir casting [20, 104].

Different approaches have been utilized to disperse nanoparticles into aluminium matrix using liquid based methods. For instance, ultrasonic technique was implemented for dispersion of nanoparticles such as Al_2O_3 nanoparticulates [105], hybrid SiC and B_4C [106]. It has been reported [93] that casting process using ultrasonic waves has this ability to produce some cavitation in the liquid metals, thereby effectively dispersing SiC nanoparticles into magnesium and A356 aluminium alloy to produce high performance metal matrix composites.

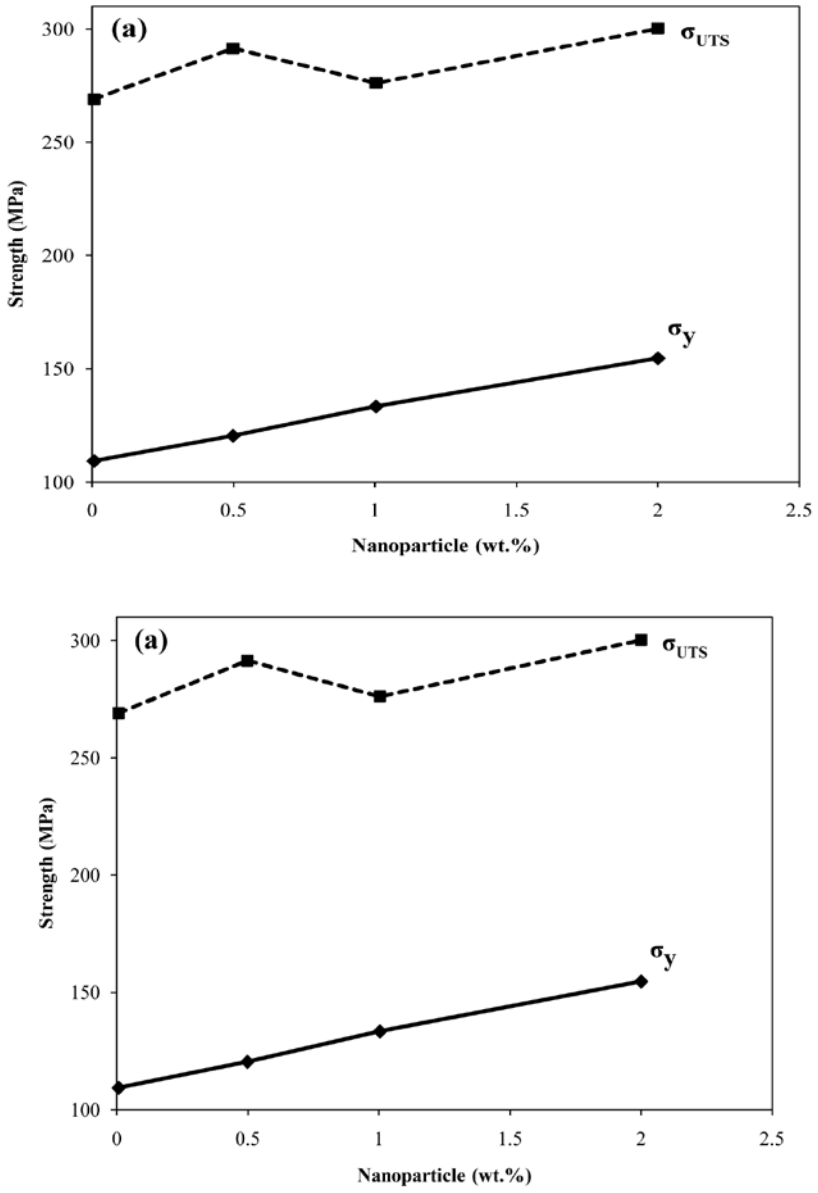

Fig. 2-8: Tensile properties of A356 aluminium alloy reinforced with SiC nanoparticles [93].

As shown in Fig. 2-8, Yang et al. [93] have shown that the low volume fraction of SiC nanoparticles (2%) can be dispersed uniformly within aluminium matrix, resulting in improving the tensile yield strength of the produced composite by about 50%. The achieved mechanical properties outperform those obtained from those composites produced using the same fraction of micron-sized SiC particles. The ultrasonic fabrication method, however, is not applicable when large-volume

AMCs, fortified with nanoparticles, are needed due to high possibility of particle clustering.

Semi-solid processes (SSP) has been demonstrated as an effective manufacturing route in manufacturing AMCs reinforced with micron-sized ceramic particles [107, 108], and can also be considered as a promising manufacturing route to distribute nanoparticles within solidified aluminium matrix. This is attributed to the supporting role of matrix solid particles in confinement of nanoparticles during semi-solid processes [109, 110].

Most researches have focused on investigating the mechanical properties of the AMCs produced using semi-solid processing reinforced mainly with micro-sized particles [111, 112]. The AMCs fortified with nanoparticles, however, are receiving more attention as alternative composites used in different industries such as automobile, aerospace and electronics, attributed to the enhanced mechanical properties of these composites.

Jiang et al. [113] have demonstrated the effectiveness of the rheocasting process on enhancing the mechanical properties of the 7075 aluminium alloy reinforced with SiC nanoparticles (0.5-1%) composites. It has been shown that the tensile yield strength and ultimate strength of composite produced by rheoforming process were enhanced compared with those produced using extrusion and the rheoforming process. It has been demonstrated that by increasing the stirring time from 5 min to 20 min, the tensile properties of the produced composites were enhanced attributed to the reduced grain size generated after this, as shown in Fig. 2-9.

It was also reported by Jiang et al. [113] that the pressure applied during rheocasting process can significantly enhance the mechanical properties of the produced composites, attributed to the diminished porosity due to the application of the pressure and also strengthening stemmed from dislocations. Additionally, mechanical properties have been enhanced due to the increase of the SiC nanoparticles loading content from 0.5% to 1%, but it has been reported that further enhancement of the loading content of SiC nanoparticles diminishes the tensile properties.

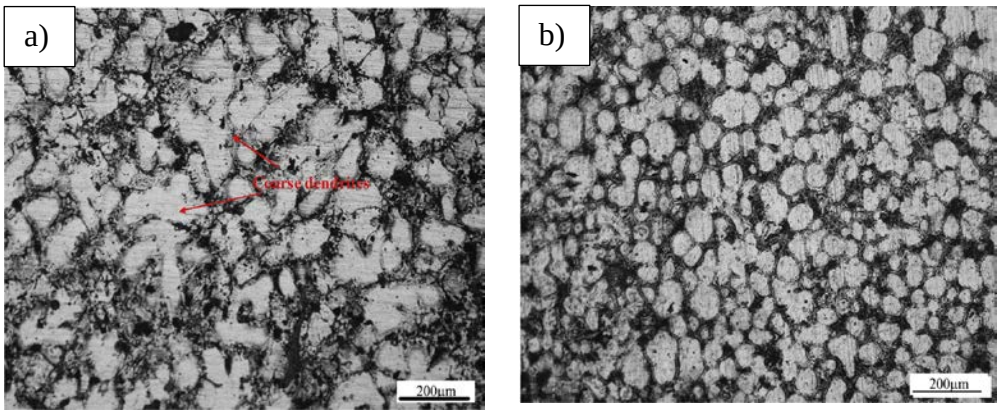

Fig. 2-9: Micrograph of the rheoformed 7075 AMCs reinforced with SiC nanoparticles after stirring times of (a) 5 min and (b) 10 min [113].

Despite the growing demand for AMCs, there are few studies on manufacturing AMCs reinforced with nanoparticles using semi-solid processing in the literatures. This is, therefore, essential to implement more studies to develop the existing manufacturing routes to produce less expensive but high performance AMCs reinforced with nanoparticles for different applications.

2.9 Strengthening mechanisms of MMCs reinforced with nanoparticles

The high mechanical properties of MMCs reinforced with nanoparticles are attributed to the several strengthening mechanisms contributing in enhancing the tensile strength. These mechanisms include load transfer effect, Hall-Petch strengthening, Orowan strengthening, thermally activated dislocation generated due to the considerable difference between coefficient of thermal expansion (CTE) and elastic modulus (EM) mismatch between the particles and the matrix leading to generating the geometrically necessary dislocations (GNDs) [36, 114].

2.9.1.1 Load Transfer Effect

It has been approved that the loads transfer from the matrix material, i.e. ductile component, to the reinforcements, i.e. hard and rigid component, can contribute in strengthening of the based material. A modified Shear Lag model proposed by Nardone and Prewo [115] is usually utilized to anticipate the effect of load bearing in strengthening ascribed to the load transfer from particulate to the matrix phase [116]:

$$\Delta\sigma_l = \vartheta_p \sigma_m \left[\frac{(l+t)A}{4l}\right] \quad (2\text{-}1)$$

where ϑ_p is the volume fraction of the particles, σ_m is the yield strength of the unreinforced matrix, l and t are the size of the particulate parallel and perpendicular to the loading direction, respectively. Eq. (2-1) can be replaced with the following equation for particulate reinforcements.

$$\Delta\sigma_l = \frac{1}{2}\vartheta_p \sigma_m \quad (2\text{-}2)$$

2.9.1.2 Hall-Petch Strengthening

It was reported that the grain size can exert a strong influence on the tensile strength of the materials, attributed to the effect of grain boundaries on blocking the movement of dislocation trough the materials. This is ascribed to existence of the grains with the different orientation and considerable disorder aspect of these regions compared to other sections of the material, inhibiting the movement of dislocations in determined slip planes [117]. It has been shown that incorporation of nanoparticles within the metal matrices can significantly stimulate drop in the grain size of the matrix during milling process [53]. It has also demonstrated that the change of the reinforcement content in the Al–SiC nanocomposite powders is found to have significant influence on the crystallite size of the matrix after planetary milling [118].

The strength can be related to the average grain size using Eq. (2-3).

$$\Delta\sigma_{H-P} = \frac{K_y}{\sqrt{d}} \quad (2\text{-}2)$$

where K_y stands for the strengthening coefficient attributed to the characteristic constant of each material. It has been asserted that the nanoparticles have a strong efficacy in controlling the grain growth of the AMMCs during fabrication process due to significant interplay of them with grain boundaries as pinning points, thereby harnessing the grain growth effectively.

It has been clarified that the enhancing the ϑ_p (volume fraction) and the diminishing the d_p (particle diameter) can result in manifestation of the finer structure, as theoretically modeled by the Zener equation [119]:

$$d_m = \frac{4\alpha d_p}{3\vartheta_p} \quad (2\text{-}3)$$

where α is a proportional constant.

2.9.1.3 Orowan Strengthening

The main concept of the Orowan strengthening is defined as a stress that must be imposed to force a dislocation to by-pass an obstacle, i.e. particulate, which can also be considered as the resistance of distributed particles in the matrix to the passing of dislocations. When there are micron-sized particulates and therefore the inter-particle spacing is large, the Orowan effect does not have a strong contribution in strengthening [120]. In contrast, the Orowan strengthening plays an important role when there are significant amount of the well-dispersed nanoparticles within the matrix of composite [121, 122]. This, in turn, enhances the resistance to the creep and thermal stability even when the loading content of nanoparticles are small (vol.<1%), attributed to the bowing needed for dislocations to bypass the nanoparticles that can be asserted by the TEM observation, disclosing the strong dislocation bowing and tangling around the distributed particles [116, 123]. Chen at al. [116] have shown profound effect of nanoparticles in strengthening the metal matrices based on difference in the coefficients of thermal expansion between the matrix and reinforcing particles and more importantly the Orowan strengthening mechanism. They have demonstrated that the relative contribution of Orowan strengthening effect increases with decreasing size of nanoparticles.

The Orowan effect can be defined by the following expression [117]:

$$\Delta\sigma_{\mathrm{Orowan}} = \frac{0.13bG}{d_p\left(\sqrt[3]{\frac{1}{2}\vartheta_p}-1\right)}\ln\left(\frac{d_p}{2b}\right) \qquad (2\text{-}4)$$

where b is the Burger's vector, and G is the matrix shear modulus, ϑ_p is the volume fraction percentage of the particulate and d_P is the particulate diameter.

2.9.1.4 Thermally-activated Dislocation Strengthening

The mismatch in coefficient of thermal expansion (CTE) between the particles and the metal matrix surrounding the particles can result in generation of thermally-activated dislocation during cooling of the composites to accommodate the stresses produced due to this mismatch in CTE. The density of thermally-

activated dislocation produced due to CTE mismatch can be calculated using the following expression [119]:

$$\rho^{CTE} = \frac{A\Delta\alpha\Delta T\vartheta_p}{bd_p(1-\vartheta_p)} \quad (2\text{-}5)$$

where A is a geometric constant, $\Delta\alpha$ is the difference in CTE, and ΔT is the difference between test and processing or heat treatment temperatures, b is the burger vector of the matrix and ϑ_p is the volume fraction percentage of the particulate. The Taylor equation [124] can be used to calculate the strengthening brought about due to thermally-activated dislocation as follows:

$$\Delta\sigma^{CTE} = \sqrt{3}\beta Gb\sqrt{\rho^{CTE}} \quad (2\text{-}6)$$

where β is a constant, G is the shear modulus of the matrix, b is the value of burger vector of the matrix.

2.9.1.5 Geometrically Necessary Dislocations Strengthening

The mismatch between the elastic modulus (EM) of the particles and the surrounding matrix can generate the geometrically necessary dislocations during deformation process to accommodate the mismatch stresses. The density of GNDs can be calculated using Eq. (2-7), where ε is the strain generated during deformation [124].

$$\rho^{EM} = \frac{6\vartheta_p}{\pi {d_p}^3}\varepsilon \quad (2\text{-}7)$$

The strengthening generated due to the formation of GNDs can be calculated using Eq. (2-8).

$$\Delta\sigma^{GNDs} = \sqrt{3}\beta Gb\sqrt{\rho^{GNDs}} \quad (2\text{-}8)$$

The final strength of the produced composite (σ_c) as a result of aforementioned strengthening mechanisms can be calculated by summing the noted strengthening values to the single strengthening effects, $\Delta\sigma_i$, added to the principal yield strength of the unreinforced matrix (σ_m), as follows:

$$\sigma_c = \sigma_m + \sum_i \Delta\sigma_i \quad (2\text{-}9)$$

There are different approaches to estimate the resulted strength from above mentioned strengthening contributors considering the superposition of the noted strengthening [116, 125]. A simple method (Eq. (2-10)) [125] represents

estimation of the final tensile properties of the composite by summing the root of the squares related to the each strengthening contributors, as:

$$\sigma_c = \sigma_m + \sqrt{\sum_i \Delta\sigma_i{}^2} \quad (2\text{-}10)$$

Zhang and Chen [116, 126] have proposed another common approach considering the Orowan strengthening mechanism, thermally-activated dislocation strengthening, and load-bearing effect:

$$\sigma_c = \left(1 + 0.5\vartheta_p\right)\left(\sigma_m + A + B + \frac{AB}{\sigma_m}\right) \quad (2\text{-}11)$$

where A represents the CTE mismatch, and B is the coefficient demonstrates the Orowan effect:

$$A = 1.25Gb\sqrt{\frac{12\vartheta_p \Delta\alpha \Delta T}{b d_p (1-\vartheta_p)}} \quad (2\text{-}12)$$

$$B = \frac{0.13Gb}{d_p\left(\left(\frac{1}{2\vartheta_p}\right)^{1/3}-1\right)} \ln\frac{d_P}{2b} \quad (2\text{-}13)$$

Few studies can be found in the literature that principally investigated the strengthening mechanisms of metal matrix composites reinforced with graphene sheets to generate the general strengthening model. This shortage does not provide a comprehensive assessment and comparison of the suggested models, resulted in simple presentation of the results without any in-depth investigation of the results. It has been reported by Gupta et al. [127] that the limited formation of aluminium carbide (Al_4C_3) at the interface of reinforcement and matrix can play an important role in strengthening the matrix. Ci et al. [128] have also shown that the presence of small amount of carbide at the interface of the CNT and matrix can improve the interfacial bonding. Accordingly, due to the high possibility for formation of Al_4C_3 at the interface of graphene sheets and aluminium matrix, the effect of formation of Al_4C_3 in strengthening the aluminium matrix in this PhD thesis needs also to be considered carefully.

Fig. 2-10 [129] represents the efficacy of all strengthening contributors and the produced strengthening calculated based on Eq. (2-11) related to adding a 2 wt.% Al_2O_3 into the aluminium matrix manufactured at 400 °C, indicating the proposed strengthening model is consistent with experimental data. As shown in Fig. 2-10, thermally-activated dislocation and Orowan strengthening mechanisms are prevalent compared to other strengthening mechanisms, especially for

nanoparticles with size lower than 50 nm. As the loading content of nanoparticles reinforcing the MMCs is limited to the small percentage to diminish the determinate effect of these reinforcements on the electrical and thermal conductivity, very small contribution from load transfer is expected.

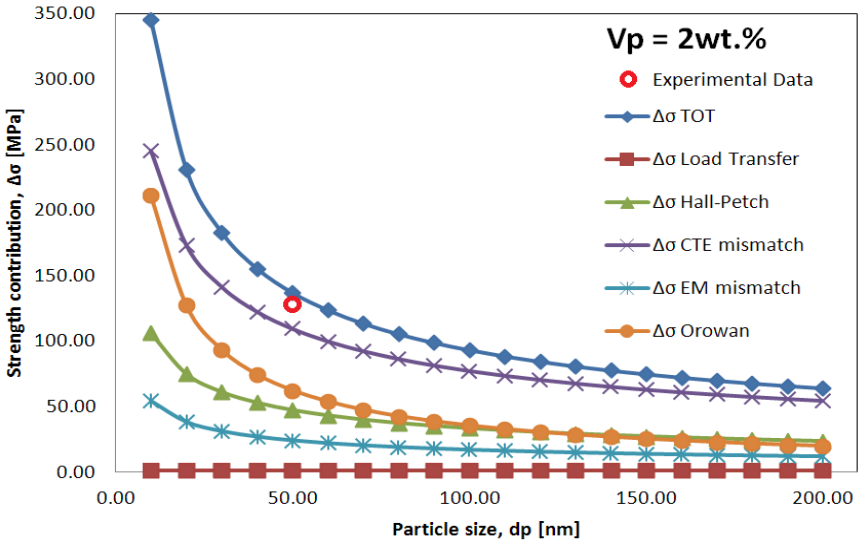

Fig. 2-10: Effect of different strengthening mechanisms and final strengthening enhancement produced by adding 2 wt.% Al_2O_3 into the aluminium matrix [129].

2.10 Conclusions

The attainment of superior enhancement in strength and ductility for aluminium matrix alloys reinforced with nanoparticles is very crucial in most industrial applications. According to the literature studies conducted in this chapter, manufacturing aluminium matrix composites with solid or liquid states processing methods usually results in agglomeration of nanoparticles due to their higher surface-to-volume ratio and the lower wettability in most metallic melt. This, in turn, deteriorates the mechanical properties of these composites, attributed to providing easy path for rapid movement of cracks trough the grain boundaries occupied with agglomerated nanoparticles, pushed away from solidification front. Studies have shown the profound potential of graphene sheets in manipulating the physical properties and most specifically agglomeration of oxide metals to enhance the ability of these composites for storing the electrochemical energy. This has opened a new window in implementation of graphene sheets on ceramic

nanoparticles to diminish their propensity for agglomeration, thereby prompting uniform distribution of them within metal matrix of the produced composites. This idea was also supported by reviewing the research implemented on solidification behaviour of nanoparticles, demonstrating the higher propensity of the particles with high thermal conductivity to be engulfed within solidifying matrix. Based on the aforementioned results achieved from reviewing the different studies, this study aims at exploiting the exception properties of graphene sheets to manipulate the physical and chemical properties of nanoparticles. It is expected that this manipulation can enhance the tendency of these particles for engulfment within aluminium matrix, thereby augmenting the uniform distribution of these nanoparticles in the matrix. The successful implementation of this manufacturing strategy can solve an open issue in fabrication of the metal matrix composites by simultaneous enhancement of the tensile ductility and strength, which is believed that they are mutually exclusive due to severe agglomeration of nanoparticles in the most suggested manufacturing routes.

Chapter 3 Enhanced tensile properties of aluminium matrix composites reinforced with graphene encapsulated SiC nanoparticles

3.1 Statement

Due to a high propensity of nano-particles to agglomerate, making aluminium matrix composites with a uniform dispersion of the nano-particles using liquid routes is an exceptionally difficult task. This chapter represents results of the initial investigation implemented at the beginning of this PhD study to analyse the feasibility of incorporating of graphene sheets within aluminium matrix to diminish the agglomeration of nanoparticles by encapsulating SiC nanoparticles using graphene sheets during ball milling. The main facilities used to produce the composites are Fritsch Pulverisette P5 planetary ball milling machine for manufacturing composite powder and stir casting machine to fabricate the casting samples. The microstructural investigation was implemented making use of a Philips CM200 TEM at an accelerating voltage of 200 kV and Field Emission Scanning Electron Microscopy (FE-SEM) performed in a HITACHI S4160 and JEOL JSM-7500FA.

Regarding experimental procedure used in this chapter to fabricate the final composites, the milled mixture was incorporated into A356 molten alloy using non-contact ultrasonic vibration method. Two different shapes for graphene sheets were characterised usinghigh resolution TEM, including onion-like shells encapsulating SiC particles and disk-shaped graphene nanosheets. Tensile tests showed 45% and 84% improvement in yield strength and tensile ductility, respectively. The former was ascribed to the Orowan strengthening mechanism, while the latter is due primarily to the fiber pull-out mechanism, brought about by the alteration of the solidification mechanism from particle pushing to particle engulfment during solidification as a consequence of high thermal conductive graphene sheets encapsulating SiC particles. The next chapters are going to elaborate the results provided in this chapter by revealing the main mechanisms involved in solidification, strengthening and incorporation of SiC nanoparticles encapsulated by graphene sheets.

Composites: Part A 68 (2015) 155–163

Contents lists available at ScienceDirect

Composites: Part A

journal homepage: www.elsevier.com/locate/compositesa

Enhanced tensile properties of aluminium matrix composites reinforced with graphene encapsulated SiC nanoparticles

A. Fadavi Boostani [a], S. Tahamtan [b], Z.Y. Jiang [a,*], D. Wei [c], S. Yazdani [d], R. Azari Khosroshahi [d], R. Taherzadeh Mousavian [e], J. Xu [b], X. Zhang [b], D. Gong [b]

[a] School of Mechanical, Materials and Mechatronic Engineering, University of Wollongong, NSW 2522, Australia
[b] State Key Laboratory of Rolling and Automation, Northeastern University, Shenyang, Liaoning 110004, China
[c] School of Electrical, Mechanical and Mechatronic Systems, University of Technology, Sydney, NSW 2007, Australia
[d] Faculty of Materials Engineering, Sahand University of Technology, Tabriz, Iran
[e] Department of Metallurgy, Zanjan Branch, Islamic Azad University, Zanjan 45156-58145, Iran

ARTICLE INFO

Article history:
Received 19 May 2014
Received in revised form 3 September 2014
Accepted 1 October 2014
Available online 14 October 2014

Keywords:
A. Metal-matrix composites (MMCs)
A. Graphene sheets
B. Mechanical properties
E. Casting

ABSTRACT

Due to a high propensity of nano-particles to agglomerate, making aluminium matrix composites with a uniform dispersion of the nano-particles using liquid routes is an exceptionally difficult task. In this study, an innovative approach was utilised to prevent agglomeration of nano-particle by encapsulating SiC nano-particles using graphene sheets during ball milling. Subsequently, the milled mixture was incorporated into A356 molten alloy using non-contact ultrasonic vibration method. Two different shapes for graphene sheets were characterised using HRTEM, including onion-like shells encapsulating SiC particles and disk-shaped graphene nanosheets. This resulted in 45% and 84% improvement in yield strength and tensile ductility, respectively. The former was ascribed to the Orowan strengthening mechanism, while the latter is due primarily to the fiber pull-out mechanism, brought about by the alteration of the solidification mechanism from particle pushing to particle engulfment during solidification as a consequence of high thermal conductive graphene sheets encapsulating SiC particles.

1. Introduction

The achievement of both strength and ductility for aluminium alloys reinforced with ceramic particulates is very useful for a wide range of safety applications. However, although aluminium alloys reinforced with ceramic particulates enhance the tensile strength, they suffer from inadequate ductility [1,2]. This is, in fact, a well-known bottleneck that limits the widespread engineering application of micro-composites especially when there is high ceramic particle content [3,4].

To attain a higher strength and retain ductility of the composite, nano-sized ceramic particles are often used [5,6]. The result is a metal matrix nano-composite (MMNC) [7,8]. In such cases, it is extremely challenging to distribute and disperse the nano-particles uniformly in the metal matrix. This is especially true for using liquid based processing routes such as casting, because of the large surface to volume ratio and the poor wettability of nano-particles in most metallic melts [9,10]. It was found that composites manufactured specifically by liquid methods such as stir casting suffer from particle pushing [11], resulting in rejection and agglomeration of particles from the growing solid/liquid interface during solidification. These problems easily induce the agglomeration and clustering of the nano-particles in the matrix, prompting low tensile properties, especially ductility, associated with intergranular fracture mode in the final solidified material [12–14].

The key to prolonged ductility is, therefore, to disperse these nano-particles into the grain interior, rather than having them agglomerated and concentrated at the grain boundaries, which can endanger elongation by causing cracks in nano-particles settled at the grain boundaries [13]. The former is accomplished by manipulating the shape of the interface and its curvature, controlling the interaction between the particle and the interface. It has also been suggested that the shape of the interface behind the particle is also dependent on the thermal conductivity of the particle and the melt [15,16]. Khan and Rohatgi [16] showed that when the thermal conductivity of the particle is greater than that of the melt, the shape of the interface behind the particle changes from convex to concave. This difference in interface curvature brings about engulfment of particles in the matrix instead of segregation and pushing into the interdendritic regions, conferring improved tensile properties on the produced composites [17].

* Corresponding author. Tel.: +61 02 42214545.
E-mail address: jiang@uow.edu.au (Z.Y. Jiang).

http://dx.doi.org/10.1016/j.compositesa.2014.10.010
1359-835X/

Many researchers have focused on using innovative methods to incorporate nano-particles into the molten aluminium, making an MMNC with a suitable dispersion and avoiding nano-particle agglomeration [10]. The milling of nano-particles with metallic powders such as aluminium and ultrasonic assisted casting methods, especially in the semi-solid state, are the most important methods which have been proposed in this regard. However, these methods are still in development, especially where a high reinforcement loading is sought [3,14,18] in the implementation of thermal models to predict the interaction at the solid/liquid interface during solidification.

In addition to the unprecedented characteristic of graphene, i.e. a single-atom-thick sheet of sp^2 hybridised carbon atoms, as a strengthening nanofiller in the world of polymer matrix composites [19,20], recent studies have shown that graphene can also be considered as an effective reinforcement for metal matrices [21]. However, to the best of our knowledge, most of these studies [21,22] have only considered the mechanical property changes after the implantation of graphene nanosheets (GNSs) as a new nano filler for metal matrix composites, but exploiting the promising characteristics of GNSs, such as the high thermal conductivity and anchoring nano particles, to harness the structural uniqueness and full potential of utilising nano-particles during the fabrication process remains largely unexplored. For instance, it has been reported that graphene sheets possess the unique feature of having a two-dimensional shell(s) which can nucleate and anchor nano-particles on the edges and surface [23,24], however, the ability of graphene sheets to alleviate the agglomeration of nano-particles during solid and liquid processing for the production of meal matrix composites has hitherto not been reported.

In this study, an innovative nanocapsulating route is implemented to exploit the high thermal conductivity and flexibility of graphene sheets as wrapping shells to diminish the pushing and agglomeration of SiC nano-particles during milling and the subsequent semi-solid casting process. The effect of using 1 vol.% GNSs to alleviate the agglomeration of nano SiC particles and subsequent enhancement in tensile properties of the composite, produced using a process encompassing milling and semi-solid stir casting, was investigated using high resolution transmission electron microscopy (HRTEM) and tensile tests, respectively. In order to gain insight into the relationship between the microstructure of the fabricated composite and its tensile properties, two mathematical models were developed, making use of the Orowan strengthening mechanism, and the models were further validated with tensile test results.

2. Experimental procedures

In order to prepare a mixture containing nano SiC and GNSs reinforcements, high purity aluminium powder (45 μm, supplied from Alpha Aesar Company with 99.5% purity), a sufficient amount of nano-β-SiC particles (45 nm, supplied from Nanostructured & Amorphous Materials, Inc.) and pure pristine monolayer graphene with the average lateral size of 550 nm (supplied from Graphene Supermarket) were used.

The ball milling process was performed in a Fritsch Pulverisette P5 planetary ball mill without interruption under high purity (99.999%) argon gas in a liquid nitrogen environment (cryomilling). During cryomilling, liquid nitrogen was constantly added to compensate for evaporation. The stainless steel vial was sealed with an elastomeric O ring. The stainless steel balls to powder weight ratio is 15:1, and the rotation rate of the vial is 250 rpm under a total milling time of 2 h. The amount of GNSs and SiC nano-particles was adjusted to 83 wt.% SiC and 17 wt.% graphene. These components were milled for 0.5 h without aluminium powder. Subsequently, the milling was continued for 1.5 h by adding aluminium powder to the mixture, containing graphene and SiC, by setting the aluminium weight equal to 45 wt.% of the total SiC and graphene powders, to enhance the incorporation of the nano SiC particles into the molten aluminium.

Powder injection into molten A356 aluminium alloy was conducted with high purity (99.999%) argon atmosphere (6 l/min) in the semi-solid state. Table 1 demonstrates the chemical composition of the A356 alloy used in this study. Two distinct methods including (a) as received SiC particles and (b) composite powder containing aluminium powder and SiC particles encapsulated by graphene sheets (prepared, as noted above, by the milling process) were utilised. After the entire alloy in the crucible was melted, it was cooled to 605 °C and held at this temperature. This temperature lies in the solid–liquid range and corresponds to a solid fraction of about 0.30 [25].

Then, stirring of the semi-solid alloy (using a graphite impeller) at 400 rpm was initiated, while prepared powders were added to the uniformly formed vortex over a time period of approximately 5 min associated with adding 1 wt.% Mg as a wetting agent. Simultaneously, non-contact ultrasonic casting was utilised to apply vibration to the prepared melt. This was done using an ultrasonic chamber (Bandelin-Germany Make – Model: RK – 100H), which can vibrate at a frequency of 35 kHz. After the completion of particle feeding, mixing was continued for an extra 1 min. Finally, the composite slurry was poured into a pre-heated cast iron mould using a bottom-pouring system. The composites fabricated using as-received SiC particles and composite powder are denoted herein as AR-SiC and preform samples, respectively.

The density of the samples was measured by the Archimedes method in order to calculate the porosity of the samples. In addition, in order to investigate the formation of GNSs in the matrix and around the SiC particles in the composite, HRTEM was employed using a Philips CM200 at an accelerating voltage of 200 kV. The morphology evolution of the powders during milling and the fracture behaviour of the fabricated composites were characterised using Field Emission Scanning Electron Microscopy (FE-SEM) performed in HITACHI S4160, JEOL JEM-2011 and JEOL JSM-7500FA.Tensile testing was carried out using a Hounsfield universal test machine at a cross-head speed of 0.5 mm s^{-1}. The dog-bone shaped tensile specimens had a gauge size of 6 mm in diameter and 30 mm in length, according to ASTM: B557M-10.

3. Results and discussion

3.1. Morphological characterization of powders

Fig. 1(a) shows the morphology of Al–55 wt.% SiC–12 wt.% graphene powder (preform), set to reach the final composition after casting (A357–3 vol.% SiC-1 vol.% graphene). As shown in Fig. 1(a), the size of the agglomerated particles after milling is smaller than 1 μm, which can accommodate better dissolution and lower agglomeration during subsequent semi-solid stir casting. Basically, the dissolution of finer milled powders in the melt is easier than that of larger agglomerated ones. Three important phenomena are responsible for formation of nanodispersions before solidification. First, the dissolution of aluminium powders during injection of powders into the melt. In fact, aluminium powders act as a carrier for ceramic particles to the melt and protect them from any contact

Table 1
Chemical composition of A356 alloy used in this study (wt.%).

Al	Si	Fe	Cu	Mn	Mg	Zn	Ti
Bal.	7.0	<0.2	<0.2	<0.1	<0.1	<0.1	<0.2

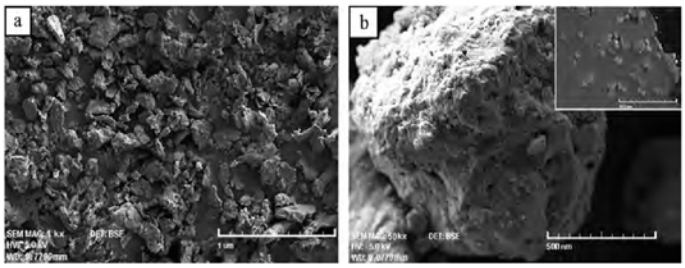

Fig. 1. (a) Morphology of Al–55 wt.% SiC–12 wt.% graphene powder and (b) high magnification image of (a).

with the surface of the melt and alumina layer, and after their dissolution, the nanoparticles will be released in the matrix. Second, the power of ultrasonic vibration causes the agglomerated particles not being sintered. In fact, it is envisaged that aluminium powders which are in the inner part of an agglomerated nanoparticles act as a binder at 605 °C to avoid particles separation and release, which only ultrasonic vibration could separate these nanoparticles during stirring. Finally, the importance of using semi-solid stirring must be considered. Indeed, a high amount of shear stress during mechanical blending in the semi-solid stirring causes the agglomerated particles to easily separate from each other.

Fig. 1(b) demonstrates the high magnification image of the agglomerated particles in Fig. 1(a). As can be seen in Fig. 1(b) and corresponding cross section as a right corner image, a uniform distribution of SiC particles inside the aluminium matrix was achieved after the milling process, due to the formation of graphene sheets around SiC particles in the first step of milling. In fact, it is believed that the formation of graphene sheets can be a good strategy to diminish the high propensity of nano-particles for agglomeration during the milling process.

HRTEM experiments have been utilised to reveal the formation and dispersion of graphene sheets around SiC particles and inside the preform sample. Fig. 2(a) demonstrates the representative HRTEM image of graphene sheets encapsulating SiC particles during the milling process, appearing in the form of onion-like shells around the SiC particles. It can be seen that this innovative process has a unique capability to encapsulate SiC particles with bilayer or trilayer graphene sheets bent around the SiC particles.

As shown in Fig. 2(a), the outer graphene shells (white arrow) tightly surrounded SiC particles without any gap, following the surface curvature of the ceramic particles in order to minimise surface energy of system including particles and graphene shells. Basically, the impact forces produced during the initial step of milling is what bends the sp^2 around the SiC particles, thus forming these onion-like shells.

Fig. 2(b) demonstrates the TEM image of SiC particle distribution in the composite powder. As can be seen, a uniform distribution of SiC particles is achieved. In fact, besides the unique characteristic of this process for producing a bilayer or trilayer graphene shell encapsulating the SiC particles (Fig. 2(a)), this process is also able to prevent the agglomeration of nano SiC particles in the milled powder, as shown in Fig. 2(b), substantiating the results shown in Fig. 1(b). As shown in Fig. 2(c), the TEM elemental X-ray map also authenticates the formation of well-dispersed SiC particles throughout the composite powder.

3.2. Composite structure

3.2.1. FE-SEM investigations

Fig. 3 represents FE-SEM microstructure of AR-SiC (Fig. 3(a)) and preform (Fig. 3(b)) samples, respectively. There are four important points that can be deduced from Fig. 3. First, the formation of agglomerated SiC nanoparticles is observed in AR-SiC sample (Fig. 3(a)) compared with a uniform distribution of these particles in the preform sample (Fig. 3(b)), despite the fact that some clusters remain in the matrix (black arrows in Fig. 3(b)). As shown in Fig. 3(a) by black arrows, SiC nanoparticles in AR-SiC sample have this propensity to be agglomerated within aluminium matrix associated with formation of microvoids at the interface of these particles and surrounding matrix, resulting in lower tensile properties.

Second, the remain of nano-gaseous pores after stirring seems to be inevitable during the semi-solid state process for both samples due to a high viscosity of the melt, even when ultrasonic waves were used. Third, the amount of nanoparticles is considerably higher for preform sample containing graphene nanosheets and aluminium powders. Forth, the presence of air gap in the agglomerated ceramic particles and formation of solidification shrinkages around these agglomerated particles could be seen in Fig. 3(a). There is also some evidence of formation of nanopores within the matrix.

3.2.2. TEM investigations

In Section 3.2.2, nanostructures of the produced composites were characterized using TEM, associated with schematic illustrations to give a better insight into the effect of graphene sheets on the nanostructures of the samples. Additionally, the effect of graphene sheets on manipulation of solidification behaviour of the samples, playing an important role in manifestation of the aforementioned nanostructures, is investigated in Section 3.2.3.

Fig. 4 represents TEM nanostructure images of AR-SiC (Fig. 4(a) and (b)) and preform samples (Fig. 4(c–f)) after semi-solid stir casting. Fig. 4(b), (d) and (f) are schematic illustrations corresponding to the nanostructures seen in Fig. 4(a), (c) and (e), respectively. As shown in Fig. 4(a), nano SiC particles in the AR-SiC sample have a high tendency to agglomerate during stir casting in order to reduce their free surface energy. As can be seen in Fig. 4(a), the vast majority of SiC particles in the AR-SiC sample have a high propensity to agglomerate at grain boundaries instead of within the grain interior, and this is attributed to the effect of the particle pushing mechanism during solidification, as shown by arrows in Fig. 4(b). However, as can be seen in Fig. 4(c), in the case of preform samples, the majority of well-dispersed SiC particles reside in the grain interior rather than at the grain boundaries, and this is ascribed to the effect of the particle engulfment mechanism during solidification, as demonstrated by arrows in Fig. 4(d).

In fact, the better distribution of SiC particles especially in the grain interior of the preform sample compared to the formation of agglomerated SiC particles at the grain boundaries of the AR-SiC sample can be related to various parameters involving manufacturing processes (e.g. ball milling and semi-solid routes) and other mechanisms controlling the solidification process after semi-solid casting.

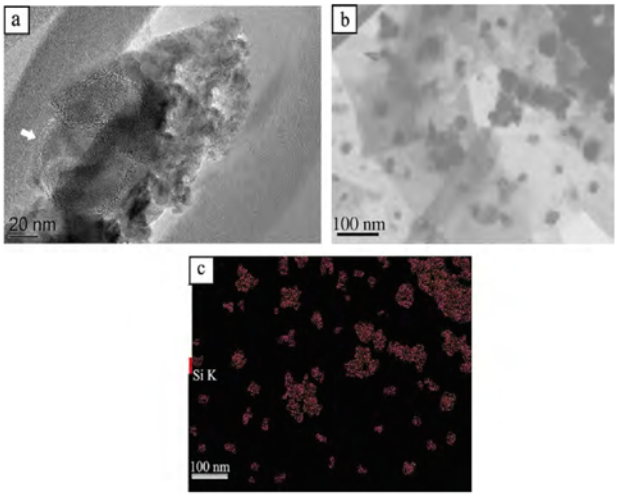

Fig. 2. (a) HRTEM images of SiC particle encapsulated by trilayer GNSs, (b) TEM image of SiC particles in composite powder and (c) elemental TEM X-ray map of (b). (For interpretation of the references to colour in this figure legend, the reader is referred to the web version of this article.)

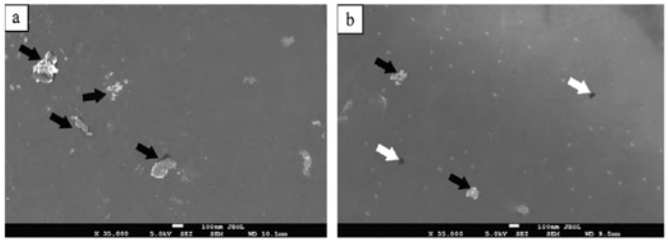

Fig. 3. FE-SEM micrograph of (a) AR-SiC and (b) preform samples.

First, regarding the role of milling, it is believed that graphene shells wrapping nano SiC particles can be in charge of the uniform dispersion of these particles in the milled composite powder, as shown in Fig. 2(c). From an energetic standpoint, the quasi-spherical carbon and onions are the most stable form of carbon particles [26]. When the highly curved graphene sheets are obtained as a result of high flexibility of graphene sheets and impact forces applied during ball milling, they are in a metastable state in the light of the theory of minimization of surface area, so the need to minimize the energy drives this curling up to spherical forms like onions. Under this circumstance, nano SiC particles can be a favourable substrate to be wrapped by highly curved graphene sheets which in turn diminishes the total energy of system by alleviating the agglomeration of nano SiC particles.

Second, semi-solid processing also plays an important role in the uniform distribution of the SiC particles in the preform sample. In fact, it is believed that creation of a vortex in the semi-solid stirring process breaks solid dendrites at 605 °C because of higher friction between the SiC particles and the aluminium alloy matrix. This further induces a homogeneous distribution of the SiC particles in the matrix of the solidified A356 composite. In addition, the sedimentation of the SiC particles decreases at the semi-solid state stirring temperature [27], which can also result in a homogeneous distribution of the SiC particles because of the presence of a solid phase [28].

During the solidification process, instead, it is believed that the particle engulfment mechanism governs the solidification process of the preform sample, rather than the particle pushing mechanism, which is activated in the AR-SiC sample. Generally, it has been proven that the particle engulfment mechanism results in the formation of isolated particles inside the grains of metal matrix during solidification, and the particle pushing mechanism leads to the formation of agglomerated particles at grain boundaries and in the last freezing zones of the solidified material [29].

3.2.3. Solidification mechanisms

The current models addressing the incorporation of particles into a solidifying matrix can be categorised into three classes: (i) the kinetic models that predict the velocity of the solid/liquid interface which is critical for the transition from particle pushing to engulfment [30], (ii) the thermodynamic models [31] which are closely related to classical heterogeneous nucleation theory and (iii) the models based on the ratio of the thermophysical properties of the particles and the melt [32]. The latter model predicts

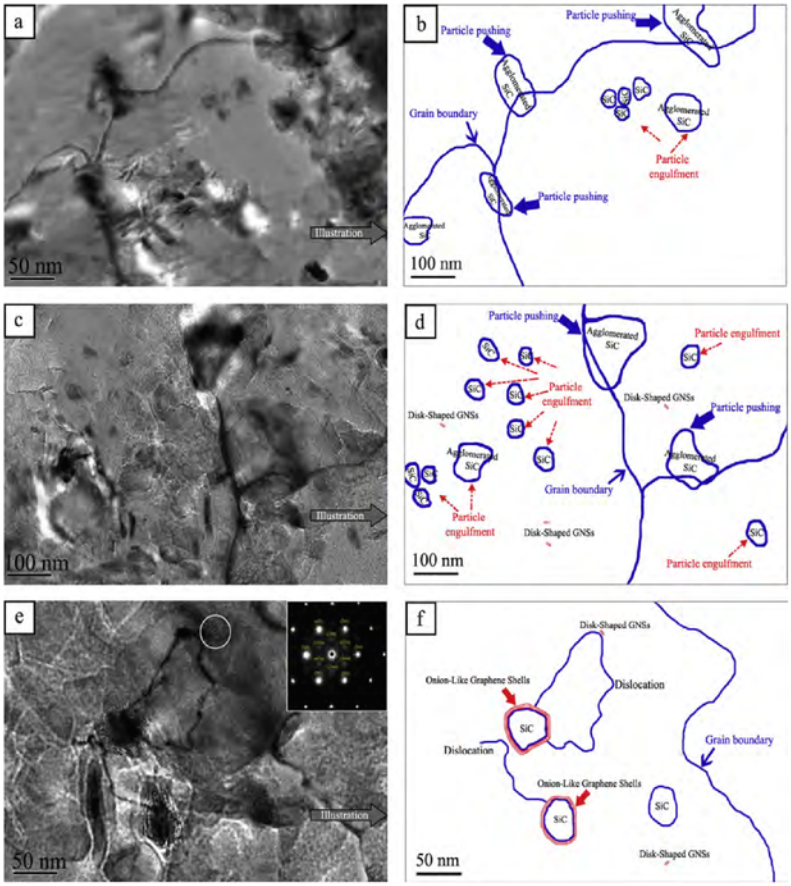

Fig. 4. TEM micrograph of (a) AR-SiC sample, (b) schematic representation of (a), (c) preform sample, (d) schematic representation of (c), (e) high magnification image of preform sample associated with selected area diffraction (SAD) pattern of specified region, and (f) schematic representation of (e). (For interpretation of the references to colour in this figure legend, the reader is referred to the web version of this article.)

the incorporation ability in general, that is, a dependence of the incorporation behaviour on the processing conditions. Any dependence on the morphology of the interface is not included.

The models based on the thermophysical characteristics rely on the thermal conductivity of particles and liquid using Eq. (1) [33]. The subscripts P and l refer to properties of the particles and the liquid, respectively.

$$K_P > K_l \quad \text{for engulfment} \tag{1}$$

The models based on heat diffusivity [34] characteristics are based on Eq. (2) using the thermal conductivity (k), the specific heat (c_P) and the density (ρ):

$$\sqrt{\frac{K_P \cdot \rho_P \cdot C_P^P}{K_l \cdot \rho_l \cdot C_P^l}} > 1 \quad \text{for engulfment} \tag{2}$$

These two models show that by enhancing the thermal conductivity of particles incorporated into the liquid matrix, the possibility of particle engulfment through the grains of the solidifying matrix increases owing to change of the interface shape from convex to concave [15,16,32,33], facilitating the engulfment of particle through the matrix during solidification [15]. In essence, the lower thermal conductivity of the particles affects the temperature gradient ahead of solidification front and therefore acts as a barrier to the removal of the heat necessary for further solidification and consequently inhibits particle engulfment.

In this study, it is expected that the thermal conductivity of SiC particles encapsulated by graphene shells is much larger than those which are not encapsulated, as a result of high thermal conductivity of graphene shell covered SiC particles [35,36]. This is because the thermal conductivity of graphene shells on SiC particles is better conserved in bilayer and trilayer GNSs than in single layer GNSs [37]. According to Eqs. (1) and (2), this high thermal conductivity of the SiC particles in the preform samples results in the incorporation of most SiC particles in grain interiors rather than at grain boundaries, as shown in Fig. 4(c) and corresponding schematic illustration (Fig. 4(d)).

Fig. 4(e) represents a high magnification TEM image of the preform sample containing engulfed SiC particles. The inset in Fig. 4(e) demonstrates the selected area diffraction (SAD) pattern

obtained from the selected disk-shaped region of Fig. 4(e), demonstrating that this region contains GNSs with a preferred crystallographic relationship of $\langle 111\rangle_{Al}//\langle 0001\rangle_{GNSs}$ to the matrix. Fig. 4(f) shows the schematic demonstration of Fig. 4(e), representing the presence of SiC particles encapsulated by graphene shells and some disk-shaped GNSs dispersed in the matrix.

3.3. Tensile properties

Fig. 5 represents tensile properties of the preform and AR-SiC samples. Insets are sketches illustrating the microstructure corresponding to different samples. As shown in Fig. 5, the tensile strength and ductility of preform samples are improved by about 45% and 84% compared to AR-SiC samples, respectively. These superior tensile properties are ascribed to the effect of three possible important strengthening mechanisms: (i) the Orowan strengthening mechanism related to uniform distribution of SiC particles not only at the grain boundaries but most importantly in the grain interiors as well, (ii) enhanced dislocation density as a result of the large mismatch between the thermal expansion coefficient of GNSs and the aluminium matrix, and finally (iii) the fiber pull-out toughening mechanism.

As illustrated in the schematic image of Fig. 4, the microstructure of the preform sample contains SiC nano-particles encapsulated by graphene shells and some dispersed disk-shaped GNSs inside the grains of the aluminium matrix. In fact, graphene sheets play two important roles in enhancing the tensile properties of the preform sample. First, they reduce the susceptibility of SiC particles to cracking as a result of the onion-like shells around these particles, as shown in Fig. 4(e) and (f). This, in turn, enhances the threshold stress limit of the SiC particles cracking during tensile stress, resulting in higher tensile properties especially tensile elongation of the preform sample (Fig. 5). Second, these onion-like graphene shells around the SiC particles can block the movement of dislocation passing through the matrix, and make it difficult to reach the grain boundaries at the low stress levels associated with the higher yield stress of the preform sample (225 MPa) compared to the AR-SiC sample (155 MPa). Along with this unique role of the onion-like graphene shells in hampering the dislocation crossing the SiC particles through the matrix, disk-shaped GNSs dispersed within the matrix can also take a same synergic role in hampering dislocation movement within the matrix.

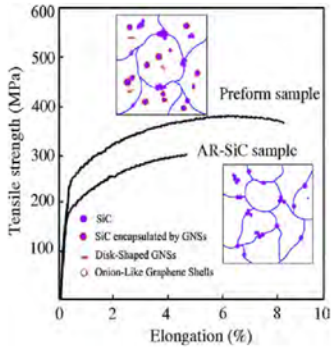

Fig. 5. Stress–strain curve of AR-SiC and preform samples accompanied with schematic illustration of their nanostructures. (For interpretation of the references to colour in this figure legend, the reader is referred to the web version of this article.)

3.3.1. Strengthening models

Eq. (3) can be employed to measure the increment in yield strength ($\Delta\sigma_y$) of the processed composite as a result of the interfering effect of disk-shaped GNSs with dislocations sliding on (111) the slip plane of the aluminium matrix, provided that the particles cannot be sheared by dislocations and are well-dispersed in the slip plane of the matrix phase [38]. In this equation, M (3) is the Taylor factor for polycrystalline FCC alloys, G (25 GPa) is the shear modulus of the aluminium matrix, b (0.25 nm) is the magnitude of the Burgers vector of dislocation, ϑ (0.35) is Poisson's ratio, f (0.01) is the volume fraction of the GNSs, d (10 nm) and t (3 nm) are the average diameter and thickness of at least 100 disk-shaped GNSs measured using HRTEM analysis, respectively.

$$\sigma_y^{\text{Disk}} = \frac{MGb}{2\pi\sqrt{1-\vartheta}}\left(\frac{1}{0.931\sqrt{\frac{0.306\pi d_t t_t}{f}} - \frac{\pi d}{8} - 1.061 t_t}\right)\ln\frac{1.225 t_t}{b} \quad (3)$$

Calculated results from Eq. (3), using the above-noted values, demonstrate that enhancement in the yield strength $\left(\Delta\sigma_y^{\text{Disk}} = 229\ \text{MPa}\right)$ of the preform sample as a result of disk-shaped GNSs is significantly larger than the experimental values $\left(\Delta\sigma_y = \sigma_y^{\text{preform}} - \sigma_y^{\text{AR-SiC}} = 70\ \text{MPa}\right)$ obtained from tensile tests (Fig. 5). This difference between predicted and experimental values for $\Delta\sigma_y$ as a result of the Orowan strengthening mechanism can be attributed to the formation of graphene with two different shapes including disk-shaped and onion-like morphologies. Indeed, the total volume fraction (f) of disk-shaped GNSs was set to 0.01 during the above-mentioned calculation; however, as shown in Fig. 4(e) and (f), graphene can also be found in the form of onion-like shells encapsulating SiC particles. So, in order to clarify the weight of onion-like graphene shells encapsulating SiC particles in yield strength increment compared to disk-shaped GNSs dispersed in the matrix of the preform sample, a modified version of the Orowan strengthening mechanism applicable for round-shaped particles is used in Eq. (4) [38]:

$$\Delta\sigma_y^{\text{Onion}} = \frac{MGb}{2\pi\sqrt{1-\vartheta}\left(\frac{0.779}{\sqrt{f}} - 0.785\right)d}\ln\frac{0.785 d}{b} \quad (4)$$

In this equation, all parameters have the same values as Eq. (3) unless the d parameter, related to the size of the onion-like graphene shells encapsulating the SiC particles through the matrix, is set to 46 nm, under this assumption that at least two graphene layers have covered the SiC particles. This was calculated by investigating more than 100 nano SiC particles, with a diameter of 45 nm and provided there is no agglomeration of the SiC particles, and all pure GNSs have been converted into onion-like shells. The results show that by considering these primary conditions, the maximum enhancement in yield strength of the preform sample, as a result of onion-like graphene shells around SiC particles, is limited to 58 MPa. This value is in good agreement with results of tensile tests with a better approximation, making Eq. (4) the main governing model for predicting tensile properties of the preform sample. Indeed, these calculations demonstrate that the maximum increment is induced due to the fact that the formation of disk-shaped GNSs particles through the matrix can be about 4 times $\left(\frac{\Delta\sigma_y^{\text{Disk-shaped GNSs}}}{\Delta\sigma_y^{\text{Onion-liked GNSs}}} = 3.95\right)$ bigger than the one endued by onion-like graphene shells, evincing the major role of disk-shaped GNSs in enhancing the yield strength of the preform sample. Therefore, it can be seen that the achievement of a 45% improvement in the yield strength of the preform sample, over that of the AR-SiC sample is attributed primarily to the higher contribution of onion-like

graphene shells encapsulating SiC particles. There are a number of reasons for the lower yield strength of the preform sample compared to the values predicted by Eq. (3) ($\Delta\sigma_y^{Disk} = 229$ MPa):

First, disk-shaped GNSs are assumed to have a habit plane perpendicular to the slip plane of aluminium (1 1 1) in the model presented. However, in fact, GNSs lie on the slip plane of the aluminium matrix. Hence, it is predicted that the amount of interaction between GNSs and dislocation gliding on the matrix slip plane is lower than in the suggested model. Nevertheless, SiC particles coated by onion-like graphene shells interact with slip planes more easily as a result of their three dimensional circular shape, which means that they have at least some sections which interact with most active slip planes during the deformation process. Second, it is also anticipated that the number of GNSs which are able to survive agglomeration, to form the undesirable graphite structure during the manufacturing process through Van der Waals interactions, is not as high as to have the strong effect suggested by the model presented (Eq. (3)). Finally, as shown in Fig. 4(e and f), disk-shaped GNSs have not been dispersed uniformly throughout the entire matrix, making it hard for them to interact with dislocation effectively.

On the other hand, it should be noted that in addition to the Orowan strengthening mechanism which confers higher yield strength on the preform sample, there are other strengthening mechanisms which play an important role in boosting the tensile properties of the composite produced. One of these is the thermally induced dislocation generated via a considerable difference between the thermal expansion coefficient of the aluminium and the graphene ($\alpha_{Al} = 21.4 \times 10^{-6}$/k, $\alpha_{graphene} = -6 \times 10^{-6}$/k at 300 k [39], $\alpha_{graphene} = 0.9 \times 10^{-6}$/k at 873–1073 K [40]) during solidification. As shown in Fig. 4(e), there is a high possibility in the formation of thermally induced dislocation through the matrix during solidification.

In addition to the above-mentioned strengthening mechanism, the other reason for the higher tensile properties of the preform sample compared with the AR-SiC sample is related to the lower porosity content (1.6% ± 0.3) introduced in the sample compared to the AR-SiC sample (4% ± 0.6). This lower porosity content of the preform sample can be attributed to the milling of SiC particles with aluminium powder that causes close contact between these powders and removes the air gap between them.

3.3.2. Fracture behaviour

Fig. 6(a) and (b) show the fractographic image of the AR-SiC and preform samples after tensile tests, respectively. As can be seen in Fig. 6(a), the fracture surface of the AR-SiC sample contains cleavage surfaces (white arrow) and some big dimples (white circle), responsible for the lower tensile ductility of the AR-SiC sample, as compared to the preform sample. In fact, the agglomeration of particles in the AR-SiC sample (Fig. 6(a) and (b)), especially at the grain boundaries, as a result of particle pushing, can facilitate the cracking of these agglomerated particles under lower stresses, and accommodate a low energy path along the grain boundaries (intergranular fracture) for crack propagation resulting in the lower tensile properties of the AR-SiC sample. In fact, externally applied load is generally transferred from particle-lacking zones to particle-rich zones in a composite, with the damage being generated in particle-rich zones because of the higher stress concentration at small strains [28]. Furthermore, agglomerated particles are suitable sites for damage accumulation and local particle-rich zones are the most appropriate nucleation sites of cracks [1,41,42].

However, in the case of the preform sample, as shown in Fig. 6(b), no evidence of cleavage surfaces or big dimples was observed on the fracture surfaces, demonstrating the ductile failure of the transgranular mode. More importantly, as demonstrated by black arrows in Fig. 6(b), in addition to the unique characteristic of GNSs in blockading dislocation within the grains, they also have another interesting macroscopic feature for preventing crack propagation during the fracture process under the fiber pull-out toughening mechanism. Under such circumstances, growing cracks encounter pull-out fibers, increasing the energy needed for propagation by diminishing the load transferred from the matrix to the dispersed reinforcements resulting in more ductility [43].

3.3.3. Characterization of the SiC/matrix interface

The properties of MMCs are affected significantly by the characteristics of the interface between the matrix and reinforcement [44,45]. Reinforcing particles are thermodynamically unstable and endure reaction at the SiC/matrix interface, depending on processing temperature and time. Interfacial reactions often cause the removal of desirable elements from molten alloy, increasing melt viscosity and reducing castability [46]. SiC reinforcement is not stable thermodynamically in contact with molten aluminium alloys and therefore, Al_4C_3 formation is expected depending on the temperature, environment and other parameters [1].

Fig. 7(a) and (b) show HRTEM images of the SiC/matrix interface in the case of AR-SiC and preform samples, respectively. Formation of Al_4C_3 at 605 °C and in the presence of about 7 wt.% Si is difficult [43,47], and consequently the detection of Al_4C_3 is not an easy task. However, the results obtained, as shown in Fig. 7(a), indicate its formation at nanoscale (2–5 nm) with a rod-like structure, as shown in right corner inset of Fig. 7(a). As seen in Fig. 7(a), in the case of the AR-SiC samples, the Al_4C_3 layer is formed around the SiC particle while in the case of the preform sample (Fig. 7(b)), Al_4C_3 is formed only in some damaged areas of GNSs (white arrows). As demonstrated by inset of Fig. 7(b), the formation of Al_4C_3 has also been approved by SAD pattern taken from the damaged area of graphene sheets encapsulating SiC particles. Therefore, in the former, the ability for load transfer from the matrix to the SiC particles is reduced, while in the latter, it

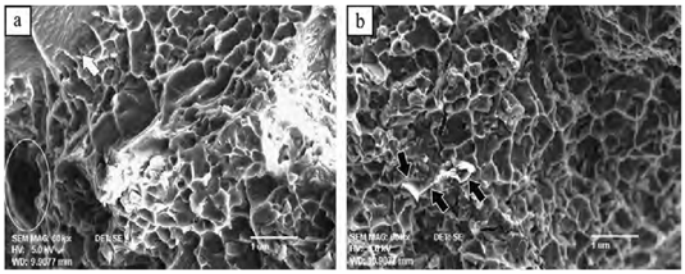

Fig. 6. Fracture surfaces of (a) AR-SiC and (b) preform samples.

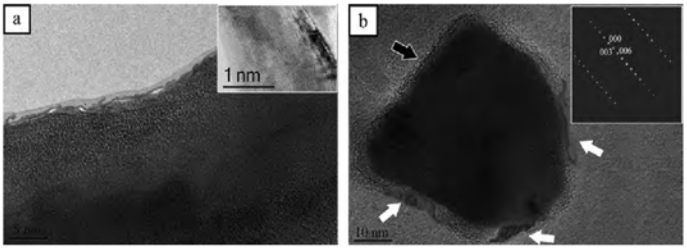

Fig. 7. TEM microstructures of a SiC particle showing SiC/matrix interface in the case of (a) AR-SiC and (b) preform samples. The rod-like structure and SAD pattern of Al_4C_3 are representing in the insets of (a) and (b), respectively.

increases. Additionally, particle-rich zones produced as a result of severe agglomeration in the AR-SiC sample, limit the flow of liquid before complete solidification of the composite and therefore, the interfaces in particle-rich zones are defective. Since these zones rapidly lose their load-bearing capability, the strength of the composite containing agglomerated particles is lower than those without particle agglomeration [48]. In fact, agglomerated particles contain many inner smaller particles without any contact with the matrix. These inner fine particles are easily displaced on each other during loading due to a weak mechanical bonding, leading them to being conjoined. There is an air gap between these fine particles in which a defect-free interface could not be formed between agglomerated particles and matrix (Fig. 3(a)).

More importantly, it is anticipated that the interface between SiC particles and the surrounding matrix is stronger in the preform sample than in the AR-SiC sample as a result of the rough and wavy surface of the graphene shells encapsulating the SiC particles. Indeed, it should be noted that graphene will be wrinkled during heating, as shown by the black arrow in Fig. 7(b), due to its different behaviour and it will expand during cooling and solidification [49]. This rough topography of the interface augments interfacial friction in the interfacial zone of the SiC particles and the adjacent matrix during sliding of debonded particles in the fracture which, in turn, permits realisation of more toughness in the preform sample.

Moreover, the wrinkling phenomenon during solidification of the composite can lead to the formation of a low-defect interface between the aluminium matrix and the nano-particles, leading to an increment in the tensile strength of the composite. Additionally, the Al_4C_3 layer around the SiC particles in the AR-SiC sample cracks easily because it has a greater likelihood of containing a flaw(s) which can initiate cracks and lead to a weaker interface.

4. Conclusions

This study proposes an innovative fabrication method, making use of encapsulating and high thermal conductivity promising features of graphene, for manufacturing aluminium-based composite reinforced with nano SiC particles. The former enables the agglomeration of nano SiC particles during powder milling and subsequent liquid processing to be diminished, and the latter made a useful change in the solidification mechanism from pushing to the engulfment of particles.

The augmented tensile properties of this composite can be ascribed mainly to the strengthening effect of the graphene sheets manifested in the form of onion-like encapsulating shells for the nano SiC particles dispersed throughout the aluminium matrix. Having considered the Orowan strengthening mechanism, two different models were investigated, emphasizing the major role of nano SiC particles encapsulated by onion-like graphene shells in attaining greater tensile properties. This improvement is also attributed to thermally induced dislocation brought about by considerable difference in thermal coefficient expansion of the graphene and aluminium matrix.

The fractographic investigations have also demonstrated that higher tensile ductility of composites containing graphene can be ascribed to lower agglomeration of SiC particulates as well as fiber pile-up mechanism. The former reduces the dimple size and the latter augments the energy needed for crack propagation through the matrix.

Acknowledgments

The authors would like to acknowledge the use of facilities (ARC-LE0237478) within the University of Wollongong (UOW) Electron Microscopy Centre and especially the great assistance of Dr. Gilberto Casillas. Authors also thank Dr. David Mitchel and Mr. Mitchel Nancarrow for their valuable support.

References

[1] Hong S-J, Kim H-M, Huh D, Suryanarayana C, Chun BS. Effect of clustering on the mechanical properties of SiC particulate-reinforced aluminum alloy 2024 metal matrix composites. Mater Sci Eng A 2003;347(1–2):198–204.
[2] Llorca J, Martínez JL, Elices M. Reinforcement fracture and tensile ductility in sphere-reinforced metal-matrix composites. Fatigue Fract Eng Mater Struct 1997;20(5):689–702.
[3] Kai XZ, Li ZQ, Fan GL, Guo Q, Xiong DB, Zhang WL, et al. Enhanced strength and ductility in particulate-reinforced aluminum matrix composites fabricated by flake powder metallurgy. Mater Sci Eng A 2013;587:46–53.
[4] Lewandowski JJ, Junt WH. Intrinsic and extrinsic fracture mechanisms in inorganic composite systems. Warrendale, Pennsylvania: TMS; 1995.
[5] El-Mahallawi I, Abdelkader H, Yousef L, Amer A, Mayer J, Schwedt A. Influence of Al_2O_3 nano-dispersions on microstructure features and mechanical properties of cast and T6 heat-treated Al Si hypoeutectic alloys. Mater Sci Eng A 2012;556:76–87.
[6] El-Mahallawi IS, Shash Y, Eigenfeld K, Mahmoud TS, Ragaie RM, Shash AY, et al. Influence of nanodispersions on strength–ductility properties of semisolid cast A356 Al alloy. Mater Sci Technol 2010;26(10):1226–31.
[7] Rajmohan T, Palanikumar K, Arumugam S. Synthesis and characterization of sintered hybrid aluminium matrix composites reinforced with nanocopper oxide particles and microsilicon carbide particles. Compos B Eng 2014;59:43–9.
[8] Ahamed H, Senthilkumar V. Role of nano-size reinforcement and milling on the synthesis of nano-crystalline aluminium alloy composites by mechanical alloying. J Alloy Compd 2010;505(2):772–82.
[9] León CA, Mendoza-Suarez G, Drew RL. Wettability and spreading kinetics of molten aluminum on copper-coated ceramics. J Mater Sci 2006;41(16):5081–7.
[10] Su H, Gao W, Feng Z, Lu Z. Processing, microstructure and tensile properties of nano-sized Al_2O_3 particle reinforced aluminum matrix composites. Mater Des 2012;36:590–6.
[11] Hashim J, Looney L, Hashmi MSJ. Metal matrix composites: production by the stir casting method. J Mater Process Technol 1999;92–93:1–7.
[12] Kok M. Production and mechanical properties of Al_2O_3 particle-reinforced 2024 aluminium alloy composites. J Mater Process Technol 2005;161(3):381–7.

[13] Murphy AM, Howard SJ, Clyne TW. Characterisation of severity of particle clustering and its effect on fracture of particulate MMCs. Mater Sci Technol 1998;14(9–10):959–68.
[14] Yang Y, Lan J, Li X. Study on bulk aluminum matrix nano-composite fabricated by ultrasonic dispersion of nano-sized SiC particles in molten aluminum alloy. Mater Sci Eng A 2004;380(1–2):378–83.
[15] Agaliotis EM, Rosenberger MR, Ares AE, Schvezov CE. Influence of the shape of the particles in the solidification of composite materials. Proc Mater Sci 2012;1:58–63.
[16] Khan MA, Rohatgi PK. A numerical study of thermal interaction of solidification fronts with spherical particles during solidification of metal-matrix composite materials. Compos Eng 1993;3(10):995–1006.
[17] Hashim J, Looney L, Hashmi MSJ. Particle distribution in cast metal matrix composites—Part I. J Mater Process Technol 2002;123(2):251–7.
[18] Hemanth J. Development and property evaluation of aluminum alloy reinforced with nano-ZrO_2 metal matrix composites (NMMCs). Mater Sci Eng A 2009;507(1–2):110–3.
[19] Singh V, Joung D, Zhai L, Das S, Khondaker SI, Seal S. Graphene based materials: past, present and future. Prog Mater Sci 2011;56(8):1178–271.
[20] Potts JR, Dreyer DR, Bielawski CW, Ruoff RS. Graphene-based polymer nanocomposites. Polymer 2011;52(1):5–25.
[21] Chen L-Y, Konishi H, Fehrenbacher A, Ma C, Xu J-Q, Choi H, et al. Novel nanoprocessing route for bulk graphene nanoplatelets reinforced metal matrix nanocomposites. Scr Mater 2012;67(1):29–32.
[22] Bartolucci SF, Paras J, Rafiee MA, Rafiee J, Lee S, Kapoor D, et al. Graphene–aluminum nanocomposites. Mater Sci Eng A 2011;528(27):7933–7.
[23] Lightcap IV, Kosel TH, Kamat PV. Anchoring semiconductor and metal nanoparticles on a two-dimensional catalyst mat. Storing and shuttling electrons with reduced graphene oxide. Nano Lett 2010;10(2):577–83.
[24] Pham VH, Dang TT, Hur SH, Kim EJ, Chung JS. Highly conductive poly(methyl methacrylate) (PMMA)-reduced graphene oxide composite prepared by self-assembly of PMMA latex and graphene oxide through electrostatic interaction. ACS Appl Mater Interfaces 2012;4(5):2630–6.
[25] Naher S, Brabazon D, Looney L. Development and assessment of a new quick quench stir caster design for the production of metal matrix composites. J Mater Process Technol 2005;166(3):430–9.
[26] Ugarte D. Curling and closure of graphitic networks under electron-beam irradiation. Nature 1992;359(6397):707–9.
[27] Zhang H, Geng L, Guan L, Huang L. Effects of SiC particle pretreatment and stirring parameters on the microstructure and mechanical properties of SiCp/Al–6.8Mg composites fabricated by semi-solid stirring technique. Mater Sci Eng A 2010;528(1):513–8.
[28] Xu Z, Yan J, Chen W, Yang S. Effect of ultrasonic vibration on the grain refinement and SiC particle distribution in Zn-based composite filler metal. Mater Lett 2008;62(17–18):2615–8.
[29] Juretzko F, Stefanescu D, Dhindaw B, Sen S, Curreri P. Particle engulfment and pushing by solidifying interfaces: Part 1 ground experiments. Metall Mater Trans A 1998;29(6):1691–6.
[30] Pötschke J, Rogge V. On the behaviour of foreign particles at an advancing solid–liquid interface. J Cryst Growth 1989;94(3):726–38.
[31] Omenyi SN, Neumann AW. Thermodynamic aspects of particle engulfment by solidifying melts. J Appl Phys 1976;47(9):3956–62.
[32] Surappa MK, Rohatgi PK. Heat diffusivity criterion for the entrapment of particles by a moving solid–liquid interface. J Mater Sci 1981;16(2):562–4.
[33] Bolling GF, Cissé J. A theory for the interaction of particles with a solidifying front. J Cryst Growth 1971;10(1):56–66.
[34] Surappa MK, Rohatgi PK. Preparation and properties of cast aluminium–ceramic particle composites. J Mater Sci 1981;16(4):983–93.
[35] Faugeras C, Faugeras B, Orlita M, Potemski M, Nair RR, Geim AK. Thermal conductivity of graphene in Corbino membrane geometry. ACS Nano 2010;4(4):1889–92.
[36] Joshi RP, Neudeck PG, Fazi C. Analysis of the temperature dependent thermal conductivity of silicon carbide for high temperature applications. J Appl Phys 2000;88(1):265–9.
[37] Muñoz E, Lu J, Yakobson BI. Ballistic thermal conductance of graphene ribbons. Nano Lett 2010;10(5):1652–6.
[38] Nie JF. Effects of precipitate shape and orientation on dispersion strengthening in magnesium alloys. Scr Mater 2003;48(8):1009–15.
[39] Bao W, Miao F, Chen Z, Zhang H, Jang W, Dames C, et al. Controlled ripple texturing of suspended graphene and ultrathin graphite membranes. Nat Nano 2009;4(9):562–6.
[40] Nelson JB, Riley DP. The thermal expansion of graphite from 15 °C to 800 °C: Part I. Experimental. Proc Phys Soc 1945;57(6):477.
[41] Wu Y, Lavernia EJ. Strengthening behavior of particulate reinforced MMCs. Scr Metall Mater 1992;27(2):173–8.
[42] Conlon KT, Wilkinson DS. Effect of particle distribution on deformation and damage of two-phase alloys. Mater Sci Eng A 2001;317(1–2):108–14.
[43] Deng CF, Wang DZ, Zhang XX, Li AB. Processing and properties of carbon nanotubes reinforced aluminum composites. Mater Sci Eng A 2007;444(1–2):138–45.
[44] Chu K, Jia C-C, Jiang L-K, Li W-S. Improvement of interface and mechanical properties in carbon nanotube reinforced Cu–Cr matrix composites. Mater Des 2013;45:407–11.
[45] Zhang QQ, Wu GQ, Huang Z, Tao Y. Effects of particle/matrix interfaces on the mechanical properties for SiCp or YAl2p reinforced Mg–Li composites. J Alloy Compd 2014;588:1–6.
[46] Asthana R. Reinforced cast metals: Part II evolution of the interface. J Mater Sci 1998;33(8):1959–80.
[47] Lee J-C, Byun J-Y, Park S-B, Lee H-I. Prediction of Si contents to suppress the formation of Al_4C_3 in the SiCp/Al composite. Acta Mater 1998;46(5):1771–80.
[48] Ma P-C, Mo S-Y, Tang B-Z, Kim J-K. Dispersion, interfacial interaction and re-agglomeration of functionalized carbon nanotubes in epoxy composites. Carbon 2010;48(6):1824–34.
[49] Yoon D, Son Y-W, Cheong H. Negative thermal expansion coefficient of graphene measured by raman spectroscopy. Nano Lett 2011;11(8):3227–31.

Chapter 4 Graphene sheets encapsulating SiC nanoparticles: A roadmap towards enhancing tensile ductility of metal matrix composites

4.1 Statement

This chapter aims to investigate the solidification mechanism coming into practice during incorporation of SiC nanoparticles encapsulated by graphene sheets within advancing solid/liquid interface. To this end, a new solidification model taking into account the alteration of the solidification mechanism from particle pushing to particle engulfment, making use of at least 40% enhancement in higher thermal conductivity and diminished repelling forces of SiC nanoparticles tuned by encapsulating graphene sheets was suggested.

Regarding experimental procedure implemented in this chapter, β-SiC nanoparticles were well dispersed in a matrix of aluminium making use of encapsulation capacity of graphene sheets during ball milling process, semi-solid stirring of the aluminium melt, ultrasonic treatment, and pressure application during solidification. Tensile tests have shown that this nanostructure manipulation can make about 350% and 258% enhancement in yield strength and tensile ductility, respectively, compared to that of unreinforced aluminum alloy. Fractographic experiments also disclosed a dimple fracture surface for the semi-solid-processed aluminium matrix composite reinforced by the nanoparticles that were encapsulated by graphene sheets using ball-milling process compared with the cleavage fracture surface of those fortified without the application of graphene.

To achieve a more intuitive understanding of strengthening mechanisms of graphene sheets within aluminium matrix, which is not covered by Chapter 3, this chapter will present a novel analytical model demonstrating the significant effect of thermal activated dislocation in strengthening due to considerable mismatch between thermal expansion coefficient of graphene sheets and aluminium matrix.

Materials Science & Engineering A 648 (2015) 92–103

Contents lists available at ScienceDirect

Materials Science & Engineering A

journal homepage: www.elsevier.com/locate/msea

Graphene sheets encapsulating SiC nanoparticles: A roadmap towards enhancing tensile ductility of metal matrix composites

A. Fadavi Boostani [a], R. Taherzadeh Mousavian [b], S. Tahamtan [c], S. Yazdani [b], R. Azari Khosroshahi [b], D. Wei [d], J.Z. Xu [c], D. Gong [c], X.M. Zhang [c], Z.Y. Jiang [a,e,*]

[a] School of Mechanical, Materials and Mechatronic Engineering, University of Wollongong, NSW 2522, Australia
[b] Faculty of Materials Engineering, Sahand University of Technology, Tabriz, Iran
[c] State Key Laboratory of Rolling and Automation, Northeastern University, Shenyang, Liaoning 110004, China
[d] School of Electrical, Mechanical and Mechatronic Systems, University of Technology, Sydney, NSW 2007, Australia
[e] School of Materials and Metallurgy, University of Science and Technology Liaoning, Anshan 114051, China

ARTICLE INFO

Article history:
Received 28 March 2015
Received in revised form
7 September 2015
Accepted 11 September 2015
Available online 15 September 2015

Keywords:
Composites
Semisolid processing
Powder metallurgy
Electron microscopy
Fracture

ABSTRACT

In this study, β-SiC nanoparticles were well dispersed in a matrix of aluminium making use of encapsulation capacity of graphene sheets, semi-solid stirring of the aluminium melt, ultrasonic treatment, and pressure application during solidification. A new solidification model taking into account the alteration of the solidification mechanism from particle pushing to particle engulfment, making use of at least 40% enhancement in higher thermal conductivity and diminished repelling forces of SiC nanoparticles tuned by encapsulating graphene sheets was suggested. This nanostructure manipulation can make about 350% and 258% enhancement in yield strength and tensile ductility, respectively, compared to that of unreinforced aluminum alloy. The results achieved based on the devised analytical model have shown the significant effect of thermal activated dislocation in strengthening due to considerable mismatch between thermal expansion coefficient of graphene sheets and aluminium matrix. Fractographic observations disclosed a dimple fracture surface for the semi-solid-processed aluminium matrix composite reinforced by the nanoparticles that were encapsulated by graphene sheets using ball-milling process compared with the cleavage fracture surface of those fortified without the application of graphene.

1. Introduction

Composites produced by mixing nanoparticles with molten metal are particularly susceptible to particle clustering due to the large surface-to-volume ratio and the poor wettability of nanoparticles in most metallic melt [1,2]. Different methods have been utilised to overcome this problem not only in liquid but also in solid routes including semi-solid stirring [3], ultrasonic treatment [2,4] and ball milling [5–11]. However, nanoparticles used in these methods still suffer from poor wetting behaviour or weak interfacial bonding to matrix, agglomeration among themselves with Van-der-Waals force, inhomogeneous distribution in the matrices and degraded thermal stability at high temperature processing. The question, which arises here, is whether graphene, i.e. a single-atom-thick sheet of sp^2 hybridised carbon atoms, has the ability to manipulate the interaction between the nanoparticles and the interface to achieve better incorporation of these particles within the solidifying matrix.

Recent studies have shown that in addition to graphene's ability as a strengthening nanofiller in polymer matrix composites [12,13], it can also be considered as an effective reinforcement for metal matrices [14,15]. However, nonuniform dispersion of graphene sheets within the composite matrix can diminish the tensile properties in that they are increasing crack initiation sites, thereby diminishing the composite performance [16]. Wang et al. [17] has also proposed powder metallurgy route, established based on the flake metallurgy, which showed the effect of implementation graphene nanosheets in enhancing the tensile properties of aluminium based composites. The suggested method, however, was not highly successful in conferring superior tensile properties to the produced composites due to the nonuniform distribution of the graphene sheets within the matrix. Bastwros et al. [18] has also attributed augmentation in the tensile properties to the formation of graphene sheets or aluminium carbide within the

* Corresponding author.
E-mail addresses: afb496@uowmail.edu.au (A. Fadavi Boostani), jiang@uow.edu.au (Z.Y. Jiang).

http://dx.doi.org/10.1016/j.msea.2015.09.050
0921-5093/

matrix of Al6061 aluminium alloy.

It has been demonstrated that graphene sheets have the exceptional characteristic of being a unique conducive substrate for the nucleation and anchoring of nanoparticles on the edges and surface [19], however, the unique ability of graphene sheets to alleviate the agglomeration of nanoparticles for the production of meal matrix composites has hitherto not been explored.

One of the criteria, which causes the particles to be enshrouded by the solidification front (particle engulfment) is the ratio between the thermal conductivity of the particle and the melt, which influences the topography of the interface and, thereby, the nature of the interaction, (pushing or engulfment) between particle and the interface. It has also been suggested that the shape of the interface behind the particle also depends on the thermal conductivity of the particle and the melt [20,21]. Khan et al. [21] showed that when the thermal conductivity of the particle is greater than that of the melt, the shape of the interface behind the particle changes from convex to concave. This difference in interfacial curvature brings about engulfment of particles in the matrix instead of their being segregated and pushed in the interdendritic regions, giving the composite improved tensile properties [22].

In this study, nano-fabrication method is employed making use of the encapsulation capacity of graphene sheets to diminish the agglomeration of SiC nanoparticles in the milling process, and enabling these particles not to be repelled during subsequent liquid processing routes, as a result of higher thermal conductivity of SiC nanoparticles wrapped by graphene sheets. The fabrication process includes adding 1 Vol% graphene sheets to alleviate the agglomeration of SiC nanoparticles during milling and subsequent pressure assisted (PA) semi-solid process to produce A357-3 Vol% SiC-1 Vol% graphene aluminium alloy. The nanostructure of the samples produced was investigated using high resolution transmission electron microscopy (HRTEM), and was correlated to the tensile test results.

2. Experimental procedure

2.1. Preparation of reinforcing phase

A High purity aluminium powder with a mean particle size of 45 μm (supplied by Alpha Aesar company with 99.5% purity), a sufficient amount of β-SiC nanoparticles with A mean particle size of 45 nm (supplied by Nanostructured & amorphous Materials, Inc.) and a pristine monolayer graphene with an average lateral size of 550 nm (supplied by Graphene Supermarket) were used as starting raw materials. Fig. 1 shows the morphology of β-SiC nanoparticles. their considerable agglomeration could be observed from this figure, indicating that the first problem of aluminium matrix nanocomposite fabrication Is the severe agglomeration of ceramic nanoparticles before their incorporation into the melt.

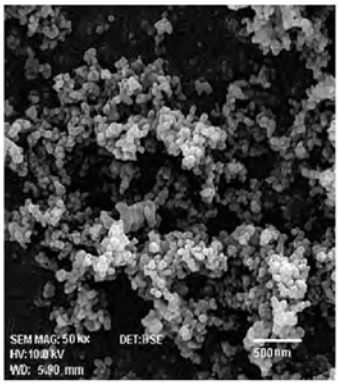

Fig. 1. Morphology of β-SiC nanoparticles.

In order to separate the agglomerated nanoparticles as well as encapsulating them by graphene sheets, a Fritsch Pulverisette P5 planetary ball mill was used without interruption under high purity (99.99%) argon gas. The stainless steel vial was sealed with an elastomeric O ring. The stainless steel balls-to-powder weight ratio was 15:1, and the rotation rate of the vial was 250 rpm under a total milling time of 2 h. The amount of graphene nano sheets (GNSs) and SiC nanoparticles was set to 83 Wt% SiC and 17 Wt% graphene. These components were ball-milled for 0.5 h without aluminium powder. Subsequently, the milling was continued for another 1.5 h by adding aluminium powder to the mixture, which contained graphene and SiC, by setting the aluminium weight equal to 45 Wt% of the total SiC and graphene powders, to make a preform for better incorporation of the SiC nanoparticles into the molten aluminium.

2.2. Preparation of the balk composite

The balk composites were manufactured using injection of the prepared powder into molten A357 aluminium alloy under an atmosphere controlled by high purity (99.999%) argon gas (6 l/min) in a semi-solid state. Table 1 shows chemical composition of matrix alloy used in this study.

After the entire alloy in the crucible was melted, it was cooled down slowly to 605 °C and held at this temperature. This temperature lies in the solid-liquid range and corresponds to a solid fraction of about 0.30. Then, 1 Wt% Mg as a wetting agent was added and stirring of the semi-solid alloy (using a ceramic coated stainless steel impeller) at 400 rpm was initiated, while prepared powders along with 1 Wt% Mg (as a wetting agent) were added to the uniformly formed vortex over a time period of approximately 5 min to increase the incorporation rate of SiC nanoparticles within the liquid aluminium [23]. Simultaneously, non-contact ultrasonic casting using an ultrasonic chamber (Bandelin-Germany Make-Model: RK-100H) was utilised to apply vibration to the prepared melt at a frequency of 35 kHz. Pressure was applied to the slurry immediately after filling the die cavity using a 250 t vertical hydraulic press held for 15 s until solidification was completed. The die was preheated at 300 °C before semi-solid stirring. Mechanical and microstructural properties of three different samples including NT, PT and PGT were investigated in this study. Table 2 represents a nomination system used to identify different specimens in the rest of this paper.

2.3. Material characterisation

The density of the samples was measured by the Archimedes method in order to calculate the porosity of the samples. In order to investigate the formation of graphene nanosheets (GNSs) in the matrix and around the SiC nanoparticles in the composite, HRTEM analysis was employed using a Philips CM200 at an accelerating voltage of 200 kV. Additionally, GNSs were characterised by Raman spectroscopy, measured at 514.5 nm excitation, using a JY HR800 (JobinYvon, Horiba) Raman spectrometer. The

Table 1
Chemical composition of the A357alloy used in this study (Wt%).

Al	Si	Fe	Cu	Mn	Mg	Zn	Ti
Bal.	7.0	< 0.2	< 0.2	< 0.1	< 0.3	< 0.1	< 0.2

Table 2
Nomination system of the specimens.

Name used in the paper	Different treatment applied on samples		
	Ball milling	Pressure	Graphene
NT	-	-	-
PT	*	*	-
PGT	*	*	*

microstructure of the powders and bulk samples along with the fracture behaviour of the fabricated composites were characterised using Field Emission Scanning Electron Microscopy (FE-SEM) performed in HITACHI S4160 and JEOL JSM-7500FA. Tensile test was carried out using a Hounsfield universal test machine at a cross-head speed of 0.5 mm s^{-1}. The dog-bone shaped tensile specimens had a gauge size of 6 mm in diameter and 30 mm in length, according to ASTM: B557M-10.

In order to investigate the homogeneity of distribution of SiC nanoparticles in different samples, the quadrat method [24] was performed on 30 FE-SEM images of different areas of each sample at 60 K magnification. A grid encompassing 36 quadrats was placed on the captured images spanning an area of 924 × 924 pixels in size. To diminish the bias introduced by edge effects, the total number of particles was counted for those located completely inside each quadrat and the ones in contact with the left and bottom quadrat sides. It should be noted that the size of cells was adjusted about twice the size of the mean area per particle since it is the most appropriate cell size as determined by Karnezis et al. [25].

3. Results and discussion

3.1. Powder samples

Fig. 2(a) represents the microstructure of reinforcing powders used for the production of PGT sample. The chemical composition of this powder was set to Al-55 Wt% SiC-12 Wt% graphene, resulting in adjustment of the final composition of PGT sample (A357-3 Vol% SiC-1 Vol% graphene). The purpose for the milling of nanoparticles with aluminium powders is to make a condition for the nanoparticles for separation from the agglomerated form due to the ball to powder and powder to vial collisions. In fact, aluminium powders act as glue for the nanoparticles not to be reattached after separation. The aluminium powders then slowly release the separated nanoparticles into the melt. However, our previous examinations indicated that the milling of aluminium with nanoparticles would not lead to an ideal separation of nanoparticles. It was obtained in our previous investigations that graphene sheets are capable to avoid reattachment of the separated nanoparticles by wrapping them, making them restricted from each other [15]. The average particle size of the composite powders after ball-milling is a key parameter to facilitate their dissolution in the melt.

In fact, Ostwald process makes it easier for small powders to be dissolved into the aluminium melt due to higher specific surface area than larger particles [26].

It was found that aluminium powders easily release the nanoparticles if the composite powders have a lower average particle size. Otherwise, due to possible fast sintering of the aluminium powders just by incorporation, the release of nanoparticles might be difficult, leading to possible remain of large sized composite powders even after semi-solid stirring and ultrasonic treatment. Fig. 2(a) shows that the size of the composite powders after ball-milling is smaller than 5 μm, which facilitates better release of nanoparticles and lower agglomeration during subsequent semi-solid stirring. As can be seen in the inset of Fig. 2(b), which is a high magnification micrograph of Fig. 1(a), SiC nanoparticles have been distributed uniformly within the aluminium matrix.

The composite powder produced can also play a significant role as a protective carrier of SiC nanoparticles to the melt by diminishing their contact with the alumina layer which covers on surface of the molten aluminium. It is envisaged that vibration induced by semi-solid stirring along with subsequent ultrasonic vibration can facilitate separation of micro-sized composite powders, as shown in Fig. 2(a), within the melt. The separated nanoparticles can then be released into the melt and remained apart during stirring even as solidification proceeds, resulting in a uniform distribution of them within the solidified matrix. In fact, the second problem of nanocomposite fabrication is the pushing of separated nanoparticles ahead of the solidification front, which leads to their clustering along the grain boundaries.

The results of HRTEM experiments proved the unique ability of graphene sheets to encapsulate the SiC nanoparticles within the powder mixture. As shown in Fig. 3(a), these sheets have encapsulated SiC nanoparticles and formed bilayer or trilayer onion-like shells. As demonstrated in Fig. 3(a), the outer graphene shells tightly surround SiC nanoparticles without any gap, following the surface curvature of the ceramic particle in order to minimise their surface energy. The impact forces produced during the initial step of ball-milling is what bends the sp^2 around the SiC nanoparticles, thus forming these onion-like shells and their formation is attributed to the fact that the quasi-spherical and onions shapes carbon are the most stable form of carbon particles [27].

As predicted by the theory of minimisation of surface area, the impact forces applied during ball milling together with the high flexibility of the graphene sheets cause the formation of these spherical onion-like shapes. Under these circumstances, highly curved graphene sheets tend to wrap the SiC nanoparticles and to diminish the total energy of the system by alleviating the agglomeration of SiC nanoparticles. Fig. 3(b) illustrates the TEM

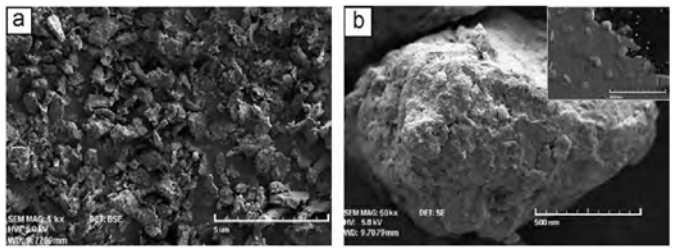

Fig. 2. (a) Morphology of Al-55 Wt% SiC-12 Wt% graphene composite powder and (b) high magnification image of (a).

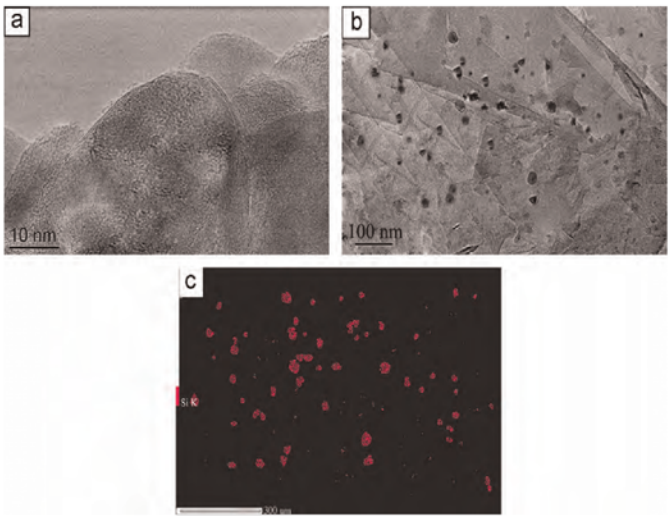

Fig. 3. (a) HRTEM images of SiC nanoparticles encapsulated by bilayer GNSs, (b) TEM image of SiC nanoparticles in composite powder and (c) elemental TEM x-ray map of (b).

image of SiC nanoparticle distribution in the composite powder.

As can be seen in Fig. 3(b), a uniform distribution of SiC nanoparticles is achieved, authenticating the results shown in Fig. 2 (b). The TEM elemental x-ray map (Fig. 3(c)) also confirms the formation of well-dispersed SiC nanoparticles throughout the composite powder.

As shown in Fig. 4, the Raman spectrum also confirms the presence of GNSs by demonstration a symmetric low frequency 2D peak at 2700 cm^{-1} in accordance with previously reported data for graphene [28,29]. The sharp and intense 2D band was observed at 2700 cm^{-1}, suggesting few layers of pristine graphene with an I_D/I_G ratio value of 1.33 higher than 0.84 for the pure one, evincing the existence of some defects in the graphene structure during the ball milling process due to the rupturing of the symmetric hexagonal network of graphene layers. The absence of multiplicity in the D peak suggests the presence of less than ten layers of graphene as it is noted that more than ten layers will lead to a 3D graphite structure [30] which further leads to splitting of the D peak into D_1 and D_2 [31]. As can be seen in Fig. 3, the D band was observed in the vicinity of 1320 cm^{-1} whereas G-band was observed at 1580 cm^{-1}.

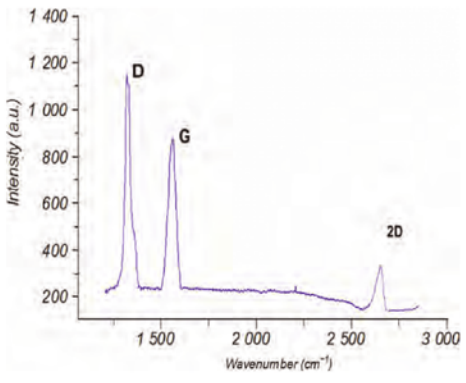

Fig. 4. Raman spectra of produced composite powder.

3.2. Bulk samples

3.2.1. Solidification mechanism

It is believed that for particles with a thermal conductivity lower than the melt, the interface accelerates as it approaches and encapsulates the front half of the particle, and then decelerates as it encapsulates the remaining half of the particle. In fact, the interface appears with a convex shape facing the particle for low thermal conductivity ratios ($K_P/K_l < 1$), resulting in the pushing of the particle ahead of the solidification front [28]. For high thermal conductivity ratios ($K_P/K_l > 1$), instead, the phenomenon is the opposite and the interface becomes concave facing the particle and tending to entrap it.

Although, as noted above, the thermal conductivity ratio criteria can give a good approximation of the possibility of particle engulfment or pushing, it is still immature to take into account all reported effective parameters, such as drag force [29], molecular surface forces [30], solid/liquid interfaces [31] and particle velocity. This study suggests a new solidification model which considers all of these parameters in order to predict the pushing and engulfment of SiC nanoparticles within the aluminium matrix during the process. Fig. 5 illustrates the schematic of this model. Fig. 5 (a) shows the microstructure of a sample subjected to deformation using PA semi-solid process associated with a higher magnification picture (Fig. 5(b)) of the selected region in Fig. 5(a).

As shown in Fig. 5(a), globular α-aluminium particles, which are the predominant structure in most sections of the sample, have the propensity to be rearranged in the form of clustered particles as a consequence of temperature and applied deformation changes during the process. As illustrated in Fig. 5(c), the temperature field is locally distorted in the vicinity of the particle because the thermal conductivity of the particle is different from that of the melt. It has been proven that for particles with high thermal conductivity ratios ($K_P/K_l > 1$), the temperature field diverges near the particle, resulting in the particle having a lower temperature than the surrounding liquid. It is expected that the thermal conductivity of SiC nanoparticles encapsulated by

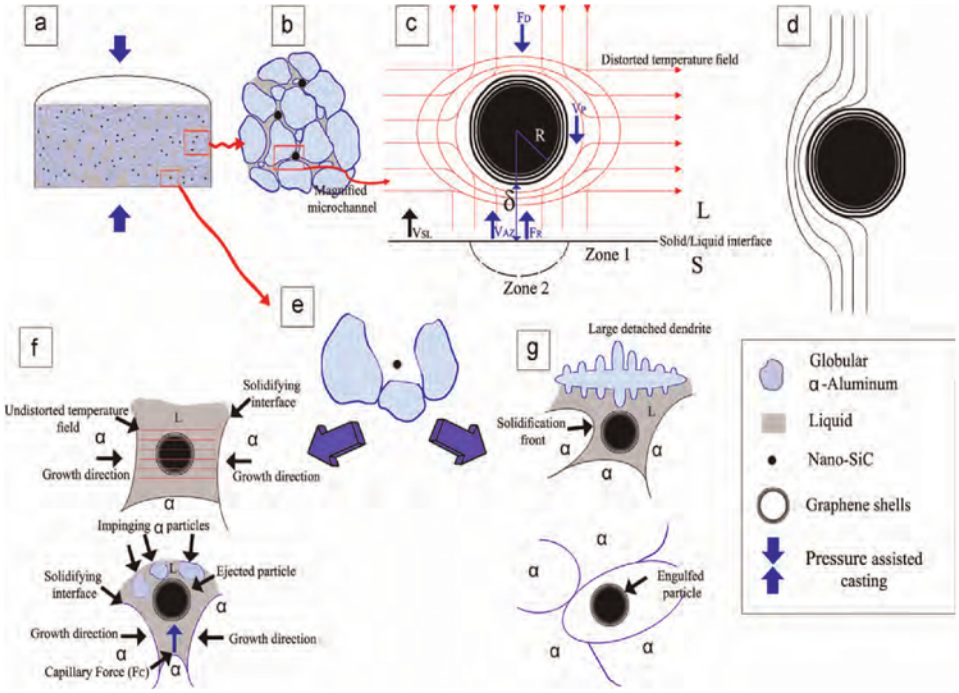

Fig. 5. Schematic illustration of the microstructural evolution during the semi-solid forming process.

graphene shells is much larger than those which are not encapsulated, as a result of the high thermal conductivity of graphene shell covered SiC nanoparticles [32,33].

Thus, it can be seen that a SiC nanoparticle encapsulated with graphene shells demonstrates higher thermal conductivity ratios, resulting in the kind of distortion shown schematically in Fig. 5(c).

Fig. 5(c), represents the magnified illustration of the microchannel located in the specified region of Fig. 5(b), and shows most of the forces as well as the temperature field exerted on the SiC nanoparticle during the process.

In order to elucidate the actual weight of graphene sheets on tunning the thermal conductivity of SiC nanoparticles encapsulated by them, the thermal conductivity of different composites reinforced with various contents of SiC nanoparticles was investigated. The final result of PGT sample is presented here, showing that thermal conductivity of this sample is 160 W/mK slightly lower than 175 W/mK reported [34] for A356 aluminium alloy. Then having considered the effective field approach suggested by Kanaun–Levin [35], the following model was suggested to correlate the thermal conductivity of PGT sample to the composite constituents.

$$K_C = K_m\left(1 + \frac{3V_P(K_{eff} - K_m)}{3K_m + (1 - V_P)(K_{eff} - K_m)}\right) \quad (1)$$

where K_C, K_m, and V_P are representing the thermal conductivity of composite, matrix, and volume fraction percentage of SiC nanoparticles, respectively. K_{eff} stands for the effective thermal conductivity of SiC nanoparticles encapsulated by graphene sheets. The main purpose of above-mentioned calculations is to determine this value. Substitution of K_C=160 W/Km, K_m=175 W/Km [34] and V_P=0.03 into Eq. (1) yields an effective thermal conductivity (K_{eff}) value of 421 W/Km for SiC nanoparticles. This value is 40% larger than even the reported value for pure SiC particle (300 W/Km [36]), substantiating the major role of graphene sheets on enhancing the thermal conductivity of SiC nanoparticles. In fact, for nanoparticles encapsulated by two-dimensional materials such as graphene sheets in this case, the effect of encapsulating sheets can be substantial. This is attributed to this fact that, albeit the total thickness of the sheets may be very small (of the order of 0.35–2 nm for monolayer to multi-layer graphene sheets, respectively), its relative thickness (standardized to the "core" nano particle size) may be substantial, if the "core" nano particles have nanoscale sizes.

As shown in Fig. 5(c), SiC nanoparticles are subjected to the repulsive forces (F_R) exerted by the solidification front calculated by Eq. (2) [37], where δ is defined as the gap distance between the SiC nanoparticle and the advancing solidification interface:

$$F_R = 2\pi B \int_0^{\infty} \frac{rdr}{\delta^3(r)} \quad (2)$$

The movement of the particle as a result of this repulsive force, generates a flow of liquid metal underneath the particles exerting a drag force (F_D) given by Eq. (3) [38]:

$$F_D = 12\pi^2\eta V_P \int_0^{R_P} rdr \int_0^{r} \frac{\rho d\rho}{\delta^3(\rho)} = V_P\psi \quad (3)$$

In Eq. (3), V_p and η are the velocity of the particle and the viscosity of the liquid metal, respectively. ψ is defined using Eq. (4)

$$\psi = 12\pi^2\eta \int_0^{R_P} rdr \int_0^{r} \frac{\rho d\rho}{\delta^3(\rho)} \quad (4)$$

During the pressure assisted casting process, the particles are subjected to liquid flow forces generated by pressure applied during casting, so that the SiC nanoparticles are accelerated towards the solidification front according to Eq. (5)

$$m\frac{dV_P}{dt} = F_R + F_D \tag{5}$$

In Eq. (5), m is defined as the mass of the particle. As shown in Fig. 5(c), it is assumed that the solidification front moves towards the particle with an imposed velocity of V_{SL}. According to the model shown in Fig. 5, zone 1 of the advancing solid/liquid interface, unaffected by the particle, tends to keep moving during solidification with a velocity of V_{SL} even after interaction with the particle. Therefore, the variation of δ versus the time of solidification can be defined according to Eq. (6)

$$\frac{d\delta}{dt} = V_P - V \tag{6}$$

Eq. (6) can also be rewritten as

$$m\frac{dV_P}{d\delta}(V_P - V_{SL}) = F_R + F_D \tag{7}$$

Eq. (7) makes it possible to ascertain the boundary conditions above which the type of particle solidification changes from particle pushing to particle engulfment. In fact, when V_P is equal to V_{SL}, $\frac{d\delta}{dt} = 0$, making $F_R = -F_D$ and resulting in particle pushing.

Since the value of m in Eq. (7) in most cases is small, $F_R \cong F_D$, and Eq. (3) can be written in the following form

$$V_P(\delta) = -\frac{F_R(\delta)}{\varphi(\delta)} \tag{8}$$

By advancing zone 1, i.e. the unaffected plane region of the solid/liquid interface as shown in Fig. 5(d), during solidification, the amount of δ diminishes. This, in turn, enhances both F_R and ψ. However, δ cannot decrease indefinitely as a result of the high under-cooling which produces due repulsive force (F_R). This consequently slows down the affected zone (V_{AZ}), but the unaffected zone (zone 1 in Fig. 5(c)) still advances at velocity V_{SL}, resulting in the engulfment of the particle by the solidifying matrix, as shown in Fig. 5(d). It has been shown recently that graphene sheets are opaque and this diminishes the van der Waals forces (vdW) of the substrate, and the amount of this opacity can be increased by increasing the number of graphene sheets covering the substrate [39]. So, graphene shells encapsulating SiC nanoparticles could be expected to have this exceptional effect on diminishing the repulsive vdW force (F_R) generated normally between particles and the advancing solidification front, and preventing the particles from being repelled as δ reduces during the advancement of the solid/liquid interface. Investigation of the nanostructure of balk samples presented in Section 3.2.2.1 has proved the significant effect of numbers of graphene shells encapsulating SiC nanoparticles on repelling them from the advancing solidification front.

From a thermo-mechanical standpoint as well, the mechanical force produced by the friction and the impact of the globular α-aluminium particles bring about turbulent melt convection during the PA semi-solid process [40]. This turbulent melt flow eliminates the local distortion temperature fields near the particles and makes them uniform, as illustrated in Fig. 5(f). The generated turbulent flow can simultaneously break some dendrite arms, which remain from previous semi-solid stirring and disintegrate them into smaller particles [41]. These detached particles can result in the formation of an equiaxed grain structure due to the grain multiplication mechanism resulting in the confinement of SiC nanoparticles impinged upon by α particles blocking the ejection of the SiC nanoparticle capacitated by the capillary forces (F_c) generated between advancing solidification fronts. It is postulated that this phenomenon, in turn, can facilitate the accommodation of SiC nanoparticles encapsulated by graphene shells within the grain interior, i.e. particle engulfment, as depicted in Fig. 5(f). The principle behind this type of particle engulfment is the mechanism of mechanical entrapment. Having considered the incorporation of a particle into the solid using mechanical entrapment, it has been suggested that this mechanism can occur on multiple solidification fronts as they advance to engulf a particle [31,42]. In addition to the impinging effect initiated by small particles, there is also the possibility of the small particles being captured between the advancing globular α-aluminium phases accomplished using large droplets or dendrite fragments produced during semi-solid forming, as illustrated in Fig. 5(g).

Simultaneously, the pressure applied during the casting process increases the liquidus temperature of the alloy, according to Clausius–Clapeyron (Eq. (9))

$$\frac{\Delta T_S}{\Delta P} = \frac{T_S(V_l - V_S)}{\Delta H_S} \tag{9}$$

In Eq. (9), T_S, ΔH, ΔP, V_l and V_S correspond to the equilibrium solidification temperature, the changes of applied pressure, the specific volumes of the liquid and solid, respectively. It has been shown that the expected enhancement in the solidification temperature is about 6 K per 100 MPa of pressure [43]. Having considered this enhancement in the liquidus temperature and high thermal conductivity ratios ($K_P/K_l > 1$), the total undercooling near the SiC nanoparticle encapsulated by the graphene shells is increased. It is postulated that this, in turn, can stimulate the preferential nucleation of α-aluminium on the surfaces of the reinforcements as postulated by the Classical Spherical Cap (CSCM) model of heterogeneous nucleation [44].

Therefore, it was concluded that graphene sheets have two important roles; first, they avoid the reattachment of separated nanoparticles during ball-milling process. Second, they remain on the nanoparticles during stirring and solidification resulted in the engulfment of the nanoparticles, leading to the semi-ideal distribution of nanoparticles in a matrix of aluminum.

3.2.2. Microstructural characterization

3.2.2.1. Optical characterization. Fig. 6 demonstrates the optical images of PT and PGT samples. As shown by arrows in Fig. 6(a), SiC nanoparticles have a higher tendency to be agglomerated in PT sample. In fact, the only effect of pressure application is fragmentation of eutectic silicon particles without any considerable change in alleviating the agglomeration of SiC nanoparticles. SiC nanoparticles in PGT sample, however, shows no tendency for agglomeration (Fig. 6(b)) associated with a uniform distribution of these particles within aluminium matrix (Fig. 6(c)).

3.2.2.2. FE-SEM characterisation. Fig. 7 represents the semi-solid structure of PGT samples rapidly quenched from 580 °C to room temperate in order to trace the solidification phenomena taking place during semi-solid deformation. This temperature was selected lower than working temperature (605 °C) for better monitoring all solidification mechanisms. Fig. 7(a) shows the nucleation of α-aluminium phase around SiC nanoparticle (black circle), which follows the CSCM model [45]. The white circle in Fig. 7 (b) illustrates the preceding mechanism for the engulfment of one SiC nanoparticle between the advancing globular α-aluminium phases as shown in Fig. 5(f). Fig. 7(b) also shows how a SiC nanoparticle was captured by the detached dendrite (black arrow) between the solidifying α-aluminium phases, demonstrating the mechanism presented in Fig. 5(g). In addition to the above-mentioned effect, the PA semi-solid process can augment the heat

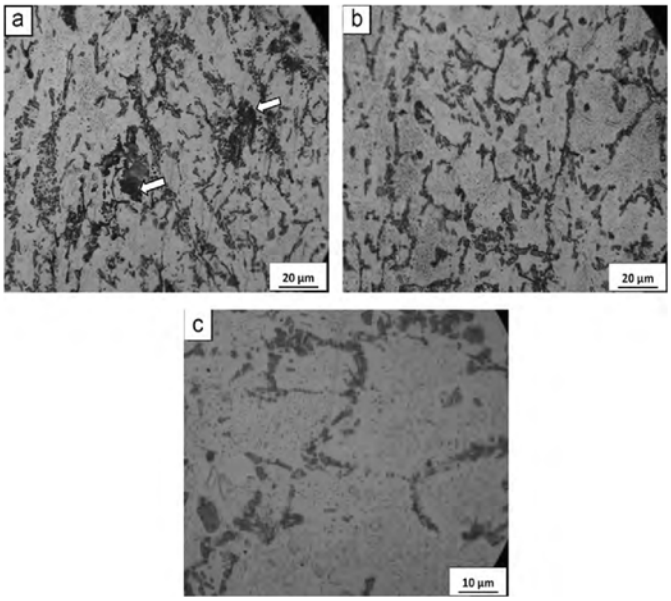

Fig. 6. Optical images of (a) PT, (b) PGT and (c) high magnification picture of (b).

transfer and consequently the cooling rate and, as a result, the primary α-aluminium particles become smaller and closer to spherical. This, as a result, can facilitate entrapment of SiC nanoparticles between the primary α-aluminium particles.

Fig. 8 demonstrates the FE-SEM microstructure of the NT (Fig. 8(a)), PT (Fig. 8(b)) and the PGT samples (Fig. 8(c)).

There are four major discrepancies making the microstructure of the PGT sample distinct from the ones observed for the NT and PT samples.

First, the SiC nanoparticles have been dispersed uniformly within the aluminium matrix in the PGT sample, but they tend to be agglomerated in the NT and PT samples (black arrows). Second, microvoids are predominant in the matrix (white arrow) and in the vicinity of agglomerated particles (black arrow) in NT sample, but microvoids in PT sample preferentially formed within agglomerated particles (black arrow) as a result of applied solidification pressure diminishing the voids formed within matrix.

PGT sample, however, has a minimum porosity content (0.7 ± 0.1) compared to NT (4 ± 0.3) and PT samples ($1.3\% \pm 0.10$) attributed to the effect of pressure and uniform distribution of SiC nanoparticles in lessoning the microvoids formed within matrix and between agglomerated SiC particles [11,46,47], respectively. Additionally, there is a lower tendency for formation of microvoids at the interface of SiC nanoparticles and matrix due to the high negative thermal coefficient expansion of graphene sheets ($\alpha_{graphene} = -6 \times 10^{-6}$/k at 300 K [48], $\alpha_{graphene} = 0.9 \times 10^{-6}$/k at 873–1073 K [49]) compared with surrounding aluminium matrix ($\alpha_{Al} = 21.4 \times 10^{-6}$/k), making it expanded interestingly during solidification resulted in defectless interface between the SiC nanoparticles and aluminium matrix.

To achieve a better insight about the effect of graphene sheets on the uniform distribution of SiC nanoparticles, the quadrat method [24] was implemented on the FE-SEM pictures as explained in the experimental section. Results, as shown in Fig. 9, have substantiated the effectiveness of the graphene encapsulation process in conferring uniform distribution on the SiC nanoparticles in PGT sample. As shown in Fig. 9 and substantiated mathematically, clustered arrangement of SiC nanoparticles within NT sample follows the negative binomial model, whereas the distribution of SiC nanoparticles in PT sample is demonstrating a moderate divergence from the negative binomial model, representing the better distribution for SiC nanoparticles with a

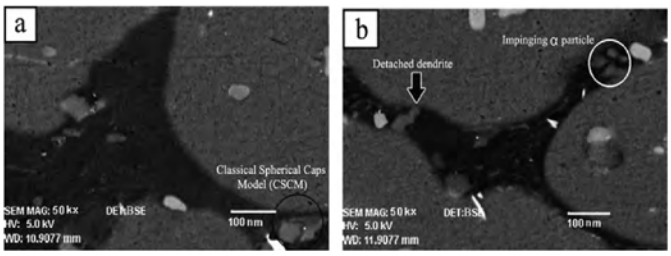

Fig. 7. Microstructure of PGT quenched samples (a) CSM model, (b) mechanical capturing.

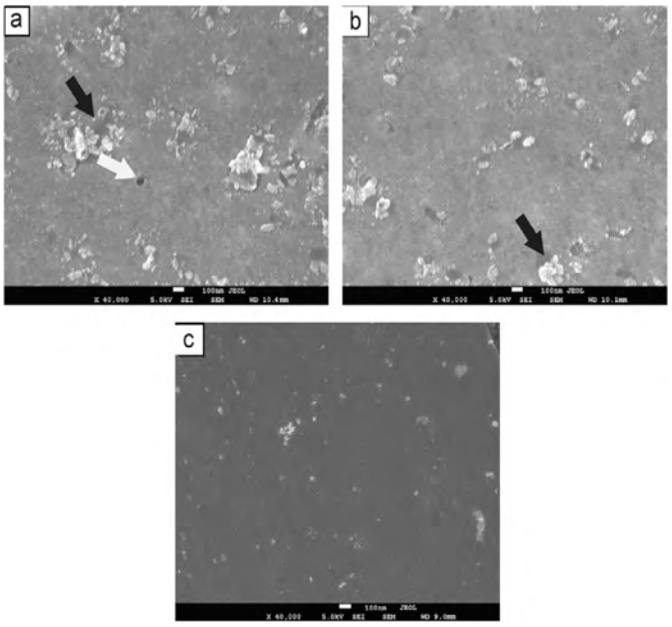

Fig.8. FE-SEM micrograph of (a) NT, (b) PT and (C) PGT samples.

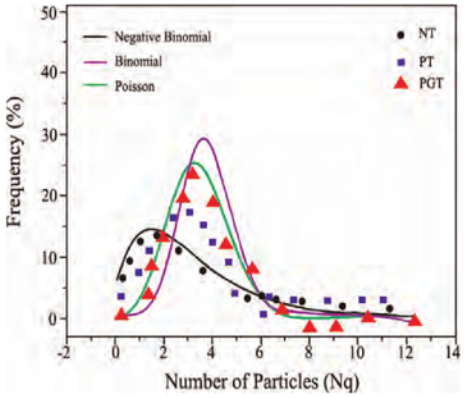

Fig. 9. Results of quadrat analysis based on the theoretical distribution curves associated with experimental results for different samples.

moderate degree of agglomeration, as shown in Fig. 8(b). However, as shown in Fig. 9, the corresponding distribution for PGT sample is representing a trend similar to the Poisson and binomial model, authenticating the uniform distribution of SiC nanoparticles, as shown in Fig. 8(c).

3.2.2.3. TEM investigation

3.2.2.3.1. Characterisation of the SiC/Matrix Interface. The effect of graphene sheets on the interface of SiC nanoparticles and aluminium matrix was investigated using TEM study (Fig. 10). As the stirring temperature was 605 °C and about 7 %wt Si was present in the matrix, therefore, no intensive reaction might be occurred between the molten aluminium and SiC nanoparticles. However, it should be studied that how the graphene layer could affect the

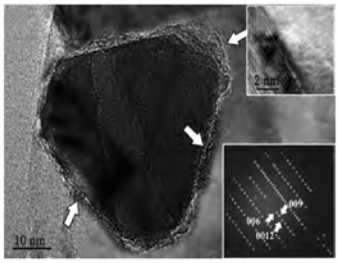

Fig. 10. The interface between SiC nanoparticle and matrix associated with selected area diffraction pattern of Al_4C_3 in the inset.

interface between aluminium matrix and SiC nanoparticles. Fig. 10 shows the occurrence of a reaction between aluminium matrix and graphene layer around the nanoparticles. In fact, it seems that the presence of graphene could avoid the possible reaction between aluminium matrix and SiC nanoparticles, while this layer itself seems to be involved a relatively intensive reaction with the aluminium matrix. As shown in Fig. 10, there is evidence of Al_4C_3 formation between the graphene layers with aluminium matrix. The inset of Fig. 10 shows the formation of Al_4C_3, as can be seen by the selected area diffraction pattern (SAD) taken from the damaged area of the graphene sheets (white arrows) encapsulating SiC nanoparticles. It has also been approved that formation of Al_4C_3 can facilitated bonding between aluminium matrix and reinforcement resulted in improved load transfer and consequently higher tensile properties [50]. The upper inset of Fig. 10 shows the HRTEM picture related to the formation of nano-sized rod-shaped aluminium carbide (NRAC) at the interface of graphene sheets encapsulating SiC nanoparticles and aluminium matrix. This shows that in spite of the results reported by Bartolucci et al. [16] about detrimental effect of Al_4C_3 formation on the mechanical

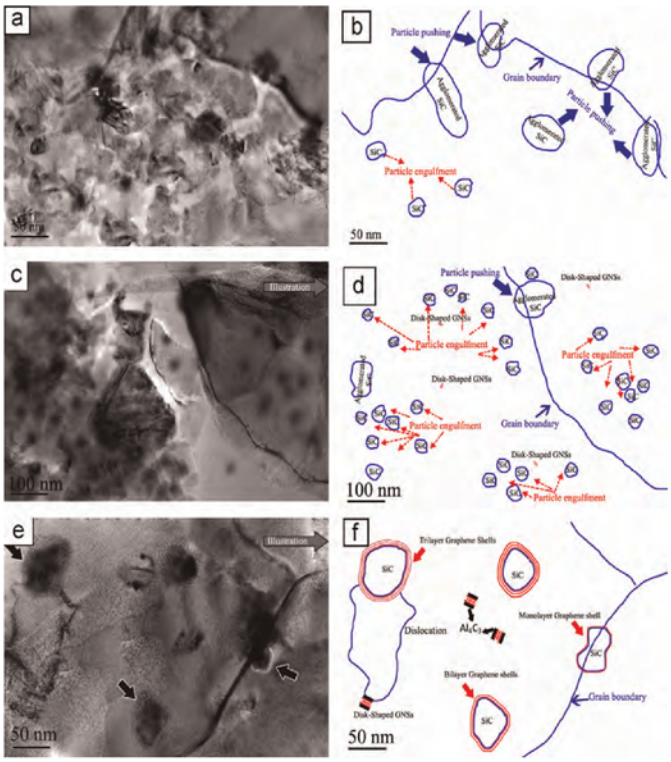

Fig. 11. TEM micrograph of (a) NT sample, (b) schematic representation of (a), (c) PGT sample, (d) schematic representation of (c), (e) high magnification image of PGT sample associated, and (f) a schematic representation of (e).

properties of aluminium based composites, formation of NRAC results in prompting the pining and therefore better mechanical bonding of SiC nanoparticle into the aluminium matrix due to formation of the void free interface in the region not affected by the NRAC, as shown in Fig. 10. This is consistent with the results achieved by the Ci et al. [51] that the presence of small amount of carbide at the interface of the CNT and matrix can improve the interfacial bonding. The HRTEM characterization of NRAC in this study also shed light the ambiguity raised by Bastwros et al. [18] about the possibility of Al_4C_3 formation in the aluminium based composite reinforced with graphene.

3.2.2.3.2. Characterisation of the nanostructure. Fig. 11 represents TEM nanostructure images of NT (Fig. 11(a)) and PGT samples (Fig. 11(c, e)).

Fig. 11(b), (d) and (f) are schematic illustrations corresponding to Fig. 11(a), (c) and (e), respectively. As demonstrated in Fig. 11(a), there is a high tendency for the agglomeration of SiC nanoparticles in the NT sample because their free surface energy diminishes. More importantly, the higher propensity of SiC nanoparticles in the NT sample for agglomeration at the grain boundaries rather than that at the grain interior, as shown in Fig. 11 (a), is ascribed to the effect of particle pushing mechanism during solidification, as demonstrated by arrows in Fig. 11(b).

As shown in Fig. 11(c), SiC nanoparticles in the PGT sample exhibit a higher tendency to reside in the grain interior rather than at the grain boundaries, substantiating the fact that particle engulfment mechanism predominates during solidification rather than particle pushing mechanism, as can be seen in Fig. 11(d). By analysing the embedded nanoparticles in the matrix, it was found that aluminum powders successfully released the graphene encapsulating nanoparticles into the melt and due to the aforementioned thermal mechanisms, they were not pushed by the solidification ahead, and graphene layer did not leave the nanoparticles during stirring and solidification. It could be seen that graphene layer(s) was remained on the nanoparticles. In fact, this uniform dispersion of SiC nanoparticles in the PGT sample, unlike those agglomerated at the grain boundaries of the NT sample can be ascribed to various parameters involved in the manufacturing processes (e.g. ball milling and PA semi-solid stirring). It is believed that the creation of a vortex in the semi-solid stirring process breaks solid dendrites at 605 °C because of the higher friction between the SiC nanoparticles and the aluminium matrix. This further induces a homogeneous distribution of the SiC nanoparticles in the matrix of the solidified composite. The sedimentation of the SiC nanoparticles also decreases at the semi-solid stirring temperatures [3], which can also result in a homogeneous distribution of the SiC nanoparticles because of the presence of a solid phase [45]. More importantly, application of pressure during solidification can augment the mechanical confinement of SiC nanoparticles (Fig. 5(f) and (g)) within the aluminium matrix and thereby ascertaining their better distribution.

Fig. 11(e) represents the settlement of the SiC nanoparticle encapsulated by monolayer graphene at the grain boundaries compared with those covered by bilayer and trilayer resided

Table 3
The average values of yield stress (YS), ultimate tensile strength (UTS) and total elongation (%) of samples.

Samples	Yield strength (YS)	Ultimate tensile strength (UTS)	Elongation (E)	Porosity (%)
A357	75 ± 2	125 ± 3	2 ± 0.3	3 ± 0.1
NT	95 ± 6	149 ± 7	3 ± 0.5	4 ± 0.3
PT	186 ± 8	245 ± 11	8 ± 1	1.3 ± 0.1
PGT	337 ± 9	448 ± 13	12 ± 1	0.7 ± 0.1

within the grain boundaries. As shown in Fig. 11(e), SiC nanoparticles encapsulated by a monolayer graphene sheet are settled at the grain boundaries, but those encapsulated by bilayer or trilayer graphene sheets have the propensity to be engulfed within the grain boundaries, illustrating the lower repelling vdW force of the advancing solidification front for these particles. SiC nanoparticles in the NT sample, however, are preferentially agglomerated at grain boundaries due to the strong repelling vdW force between these particles and the approaching solid/liquid interface which pushes them away to the last solidification region located normally between grains [52].

3.3. Tensile properties

Table 3 represents the average values of yield stress (YS), tensile strength (UTS), and total elongation (%) of samples studied. It should be noted that irrespective of a higher porosity amount of NT sample in respect to A357, however, a higher amount of ductility was obtained for NT sample, showing the effect of semi-solid stirring, which causes the fragmentation of the corresponding dendrites and formation of coaxial grains [53].

Also, it could be observed that ultrasonic treatment aided to exit of gases during stirring, leading to the formation of a lower amount of porosities irrespective of nanoparticles incorporation that increases the porosity amount in the final composite. This, in turn, is resulted in diminishing the YS and UTS values of NT sample. A higher amounts of YS and UTS were obtained for PT sample due to the considerable elimination of porosities and fragmentation of 3D silicon platelets as a result of pressure application during solidification [54]. According to Table 3, the YS and UTS of PGT sample are considerably higher than PT sample by 81% and 82% ascribed to the lower agglomeration of SiC nanoparticles and consequently lower porosities of this sample. This enhancement in tensile properties because of incorporation of graphene sheets within aluminium matrix is also consistent with the one reported by Bae et al. [55], attributed mainly to the better load transfer from the matrix to the graphene sheets. Additionally, uniform dispersion of SiC nanoparticles encapsulated with graphene sheets and disk-shaped GNSs (DSGS) within matrix grains can facilitates strain hardening of PGT sample, as shown in Fig. 11 (e). The engulfed SiC nanoparticles also can block the dislocation movement within the aluminium grains, as shown in Fig. 11(e), thereby diminishing the dislocation density at grain boundaries resulted in higher ductility.

To demonstrate the actual effect of graphene sheets on enhancing the tensile properties of produced composites, a new analytical model (Eq. (10)) was introduced by incorporating a modified shear-lag model (continuum mechanics approach) and an enhanced dislocation density model (micromechanics strengthening approach) into the model proposed by Ramakrishnan [56], as the latter generally is used for micron-sized particles.

$$\sigma_y^{PGT} = \sigma_y^{NT}(1+\omega_L^{DSGS})(1+\omega_T)(1+\omega_{Orowan}^{DSGS}+\omega_{Orowan}^{OLGS}) \quad (10)$$

To devise the aforementioned equation, the strengthening mechanisms such as load bearing (ω_l), thermal enhanced dislocation density (ω_T), and Orowan (ω_{Orowan}) for DSGS and onion-liked graphene sheets (OLGS) encapsulating SiC nanoparticles are considered as major improvement factors, enhancing the yield strength of NT sample (σ_y^{NT}) to the anticipated yield strength of the PGT sample (σ_y^{PGT}).

Wang et al. [17] has demonstrated that the main strengthening mechanism of the aluminium based composite reinforced with graphene is stress transfer from aluminium matrix to the graphene sheets. The modified shear lag model proposed by Nardone and Prewo [57] stated that the transformation of load from the ductile matrix to the hard reinforcements (i.e. ceramic and graphene) can fortify the matrix subjected to the external load. The classical shear lag model [58] was used to clarify the mechanism of load transfer from the composite matrix to the embedded DSGS. To this end, the two-dimensional elastic configuration was considered for a platelet of length L, thickness t and elastic modulus E, which is bonded to a matrix material of thickness λ.

Having considered the aspect ratio of the graphene plate (let $s=L/t$) and the matrix strain (e_m), normal and shear stress along the graphene flake can be calculated, respectively, as follows [59]:

$$\sigma_f = E_f e_m\left[1-\frac{\cosh(ns\frac{x}{L})}{\cosh(\frac{ns}{2})}\right] \quad (11)$$

$$\tau_P = nE_f e_m\left[\frac{\sinh(s\frac{x}{L})}{\cosh(\frac{ns}{2})}\right] \quad (12)$$

In these equations, n can be defined as $n=\sqrt{\frac{2G_m}{E_f}(\frac{t}{\lambda})}$ in which G_m represents the shear modulus of the matrix. Therefore, the maximum load transfer from the matrix to the graphene platelet is attainable for the composite with the higher value of ns. To reach this, it is necessary to reduce the distance between the graphene platelets (λ) and simultaneously diminish their thickness, as thickness (t) affects the n with square root but it has an inverse relationship with S ($S=L/t$). At this stage, it is also necessary to introduce a new parameter to correlate the ns value of the graphene platelet with the load-bearing improvement factor (ω_l) affected mainly by the volume fraction of the reinforcements [56]. To find the ω_l value, it is imperative to ascertain the inter-particle spacing, as a function of the total graphene volume fraction (V_{Gr}). Hence, the ω_l parameter is defined as

$$\omega_l = \sqrt{\frac{2G_m L^2}{E_f \lambda_{eff} t}} \quad (13)$$

where λ_{eff} is an effective inter-particle spacing between the graphene sheets within the matrix, and can be calculated using Eq. (14) [60]:

$$\lambda_{eff}^{DSGS} = 0.931\sqrt{\frac{0.306\pi dt}{V_{Gr}^{DSGS}}}-\frac{\pi d}{8}-1.061t \quad (14)$$

Putting the values of G_m=25 GPa, d=40 nm, t=15 nm, E_f=1000 GPa and λ_{eff}=495 nm into Eq. (13) results in a ω_l value of 0.10 for the DSGS. It should be noted that the V_{Gr}^{DSGS} has been set to 0.18% of the total volume of the graphene (V_{Gr}=0.01) added as a raw material, and is measured along with other microstructural features such as L and t using image analysis of at least 30 HRTEM micrographs.

The enhancement in yield strength of PGT sample due to the considerable mismatch between thermal expansion coefficient of graphene sheets (-6×10^{-6}/k at 300 k [48]), encapsulating SiC nanoparticles, and aluminium matrix ($0.9\times10^{-6}\,k^{-1}$ at 873–

1073 K [49]) can be devised using Eq. (15) based on the Taylor dislocation strengthening equation [61].

$$\omega_T = \frac{\sqrt{3}\beta G_m b}{\sigma_y^{NT}}\sqrt{\frac{12V_p\Delta\alpha\Delta T}{bd_p}} \tag{15}$$

where G_m (25 GPa) is the shear modulus of the aluminium matrix, b (0.25 nm) is the magnitude of the Burgers vector of dislocation, ΔT is the difference between fabrication temperature (605 °C) and temperature at which the tensile properties were measured (25 °C), $\Delta\alpha$ is the difference between the thermal expansion coefficient of the aluminium and the graphene ($\Delta\alpha = 27.4\times10^{-6}/k$), V_p is the total volume fraction of SiC nanoparticles encapsulated by graphene shells (0.03), d_{Gr} is related to the average diameter of the graphene sheets and shells within the aluminium matrix (45 nm), and σ_y^{NT} is the yield strength of the NT sample (95 MPa). Thus, the calculated value for ω_T is 3.211 is much larger than other strengthening contributors and therefore plays a major role in the strengthening the matrix.

To determine the strengthening contribution of DSGS and the OLGS under the Orowan strengthening mechanism, two different models can be utilised [60].

$$\omega_{Orowan}^{DSGS} = \frac{MGb}{2\pi\sqrt{1-\vartheta}\,\sigma_y^{NT}}\left(\frac{1}{0.931\sqrt{\frac{0.306\pi dt}{V_{Gr}^{Disc}}-\frac{\pi d}{8}}-1.061t}\right)\ln\frac{1.225t}{b} \tag{16}$$

$$\omega_{Orowan}^{OLGS} = \frac{MGb}{2\pi\sqrt{1-\vartheta}\,\sigma_y^{NT}\left(\frac{0.779}{\sqrt{V_{Gr}^{Onion}}}-0.785\right)d}\ln\frac{0.785\,d}{b} \tag{17}$$

In these equations, M (3) is the Taylor factor for polycrystalline FCC alloys, G (25 GPa) is the shear modulus of the aluminium matrix, b (0.25 nm) is the magnitude of the Burgers vector of dislocation, ϑ (0.35) is the Poisson's ratio, σ_y^{NT} is the yield strength of the NT sample, V_{Gr}^{DSGS} (0.0018) and V_{Gr}^{OLGS} (0.0082) are the effective volume fractions of the DSGS and the OLGS calculated based on image analysis of 30 HRTEM micrographs, respectively. Parameters of L (40 nm), d (45 nm) and t (10 nm) are the average length, diameter and thickness of at least 40 DSGS and OLGS measured using HRTEM analysis, respectively.

The investigation of Eqs. (16) and (17), using the noted values, giving the values of 0.33 and 0.24 for ω_{Orowan}^{DSGS} and ω_{Orowan}^{OLGS}, respectively. This is demonstrating the greater role of the DSGS in strengthening as compared to the DSGS ones. Having considered the ω_L^{DSGS} = 0.1, ω_T=3.211, ω_{Orowan}^{DSGS} = 0.33 and ω_{Orowan}^{OLGS} = 0.24, σ_y^{PGT} is predicted to be around 690 MPa, which is larger than the value obtained experimentally (337 MPa).

The lower yield strength of the PGT sample compared to the one predicted by presented model is attributed to some reasons: (i) the total volume fraction of the DSGS is assumed to have a habit plane perpendicular to the slip plane of the aluminium (111) in the model presented, however, some of them could settle on the slip plane of the aluminium matrix resulting in lower interaction between them and the gliding dislocations; (ii) graphitization through Van der Waals interactions between some graphene sheets during the manufacturing process, resulted in the formation of unwrapped-graphene and hence agglomerated SiC nanoparticles, thereby levelling off the strengthening generated by thermal activated dislocations.

3.3.1. *Fracture behaviour*

Fig. 12 shows an FE-SEM micrograph of the fracture surfaces of the NT and PGT samples. The fracture surface of the PGT sample contains many small dimples accompanied by ductile fracture, as shown in Fig. 12(a). In contrast, as shown in Fig. 12(b), the fracture surface of the NT sample contains cleavage surfaces (black arrow) and some large dimples (black circle), deteriorating the tensile ductility of the NT sample, as compared to the PGT sample.

In fact, having agglomerated particles at the grain boundaries, the NT sample is more prone to crack initiation, facilitating and accommodating, in turn, a low energy path for crack propagation even after initiation resulted in intergranular fracture [62]. In fact, externally applied load is generally transferred from particle-lacking zones to particle-rich zones in a composite, with the damage being generated in particle-rich zones because of the higher stress concentration at small strains [4,63]. Agglomerated particles are suitable sites for damage accumulation and local particle-rich zones are the most appropriate nucleation sites of cracks [64–67].

Regarding the PGT sample, the fracture surface, as shown in Fig. 12(a), does not provide any evidence of cleavage surfaces or large dimples, showing ductile failure under the transgranular mode. More importantly, as demonstrated by the black arrow in Fig. 12(a), in addition to the unique characteristic of disk-shaped graphene sheets in hampering dislocation movement trough the grains, they also have another interesting macroscopic feature for preventing crack propagation during the fracture process under the fiber pull-out toughening mechanism. Under such circumstances, growing cracks encounter pull-out fibers, increasing the energy needed for propagation by diminishing the load transfer from the matrix to the dispersed reinforcements and resulting in more ductility [68].

4. Conclusions

This study demonstrates important implications for the implementation of graphene sheets to alleviate the agglomeration of nanoparticles in solid and consequent liquid processing routes. This is achieved using promising feature of graphene sheets to wrap the nanoparticles resulting in higher thermal conductivity

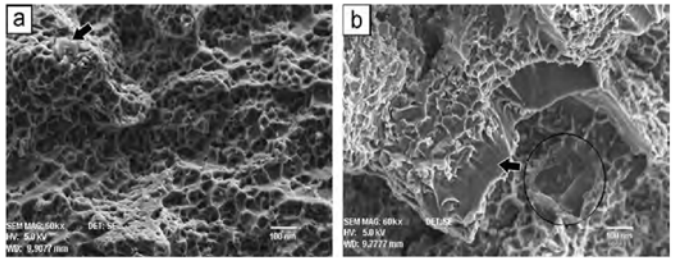

Fig. 12. Fracture surfaces of (a) PGT and (b) NT samples.

and tuning the repelling forces of the SiC nanoparticles, stimulating the engulfment of these particles within the matrix rather allowing them to be agglomerated at the grain boundaries. This confers superior enhancement on the yield strength and tensile elongation of composites by 350% and 258%, respectively, compared to the ones of A357 aluminium alloy. The suggested analytical model has shown the profound effect of thermal activated dislocations in strengthening compared to the other strengthening mechanisms. The fractographic results also demonstrate the effective role of graphene sheets in manifestation of dimple and pull-out fracture surfaces. The former was attributed to the role of graphene sheets in diminishing the agglomeration of SiC nanoparticles, and the latter ascribed to the blocking capacity of graphene sheets in crack movement.

Acknowledgments

The authors would like to acknowledge the use of facilities (ARC-LE0237478) within the University of Wollongong (UOW) Electron Microscopy Centre and especially the great assistance of Dr. Gilberto Casillas. Authors also thank Dr. David Mitchel and Mr. Mitchel Nancarrow for their valuable support.

References

[1] C.A. León, G. Mendoza-Suarez, R.L. Drew, J. Mater. Sci. 41 (2006) 5081–5087.
[2] H. Su, W. Gao, Z. Feng, Z. Lu, Mater. Des. 36 (2012) 590–596.
[3] H. Zhang, L. Geng, L. Guan, L. Huang, Mater. Sci. Eng.: A 528 (2010) 513–518.
[4] Z. Xu, J. Yan, W. Chen, S. Yang, Mater. Lett. 62 (2008) 2615–2618.
[5] A.M.K. Esawi, K. Morsi, A. Sayed, A.A. Gawad, P. Borah, Mater. Sci. Eng.: A 508 (2009) 167–173.
[6] K. Morsi, A.M.K. Esawi, P. Borah, S. Lanka, A. Sayed, M. Taher, Mater. Sci. Eng.: A 527 (2010) 5686–5690.
[7] S. Mula, K. Mondal, S. Ghosh, S.K. Pabi, Mater. Sci. Eng.: A 527 (2010) 3757–3763.
[8] S. Tahamtan, A. Halvaee, M. Emamy, Z.Y. Jiang, A. Fadavi Boostani, Mater. Sci. Eng.: A 619 (2014) 190–198.
[9] N. Valibeygloo, R.A. Khosroshahi, R.T. Mousavian, Int. J. Mine. Metall. Mater. 20 (2013) 978–985.
[10] M. Roshan, T.R. Mousavian, H. Ebrahimkhani, A. Mosleh, J. Min. Metall. Sect. B: Metall. 49 (2013) 299–305.
[11] N. Beigi Khosroshahi, R. Azari Khosroshahi, R. Taherzadeh Mousavian, D. Brabazon, Ceram. Int. 40 (2014) 12149–12159.
[12] V. Singh, D. Joung, L. Zhai, S. Das, S.I. Khondaker, S. Seal, Prog. Mater. Sci. 56 (2011) 1178–1271.
[13] J.R. Potts, D.R. Dreyer, C.W. Bielawski, R.S. Ruoff, Polymer 52 (2011) 5–25.
[14] L.-Y. Chen, H. Konishi, A. Fehrenbacher, C. Ma, J.-Q. Xu, H. Choi, H.-F. Xu, F. E. Pfefferkorn, X.-C. Li, Scr. Mater. 67 (2012) 29–32.
[15] A. Fadavi Boostani, S. Tahamtan, Z.Y. Jiang, D. Wei, S. Yazdani, R. Azari Khosroshahi, R. Taherzadeh Mousavian, J. Xu, X. Zhang, D. Gong, Compos. A: Appl. Sci. Manuf. 68 (2015) 155–163.
[16] S.F. Bartolucci, J. Paras, M.A. Rafiee, J. Rafiee, S. Lee, D. Kapoor, N. Koratkar, Mater. Sci. Eng.: A 528 (2011) 7933–7937.
[17] J. Wang, Z. Li, G. Fan, H. Pan, Z. Chen, D. Zhang, Scr. Mater. 66 (2012) 594–597.
[18] M. Bastwros, G.-Y. Kim, C. Zhu, K. Zhang, S. Wang, X. Tang, X. Wang, Compos. B: Eng. 60 (2014) 111–118.
[19] I.V. Lightcap, T.H. Kosel, P.V. Kamat, Nano Lett. 10 (2010) 577–583.
[20] E.M. Agaliotis, M.R. Rosenberger, A.E. Ares, C.E. Schvezov, Proc. Mater. Sci. 1 (2012) 58–63.
[21] M.A. Khan, P.K. Rohatgi, Compos. Eng. 3 (1993) 995–1006.
[22] J. Hashim, L. Looney, M.S.J. Hashmi, J. Mater. Process. Technol. 123 (2002) 251–257.
[23] N. Beigi Khosroshahi, R. Taherzadeh Mousavian, R. Azari Khosroshahi, D. Brabazon, Mater. Des. 83 (2015) 678–688.
[24] I. Sabirov, O. Kolednik, R.Z. Valiev, R. Pippan, Acta Mater. 53 (2005) 4919–4930.
[25] P.A. Karnezis, G. Durrant, B. Cantor, Mater. Charact. 40 (1998) 97–109.
[26] G. Gao, London: Imperial College Press, 2004.
[27] D. Ugarte, Nature 359 (1992) 707–709.
[28] M.K. Surappa, P.K. Rohatgi, J. Mater. Sci. 16 (1981) 562–564.
[29] S.C. Tjong, Mater. Sci. Eng.: R: Rep. 74 (2013) 281–350.
[30] L. Hadji, Math. Comput. Model. 36 (2002) 147–156.
[31] E. Lavernia, T.S. Srivatsan, J. Mater. Sci. 45 (2010) 287–325.
[32] C. Faugeras, B. Faugeras, M. Orlita, M. Potemski, R.R. Nair, A.K. Geim, ACS Nano 4 (2010) 1889–1892.
[33] R.P. Joshi, P.G. Neudeck, C. Fazi, J. Appl. Phys. 88 (2000) 265–269.
[34] S.I. Bakhtiyarov, R.A. Overfelt, S.G. Teodorescu, J. Mater. Sci. 36 (2001) 4643–4648.
[35] S. Kanaun, V. Levin, Recent advances in mathematical modelling of composite materials, 1994, pp. 1–58.
[36] G.A. Slack, J. Appl. Phys. 35 (1964) 3460–3466.
[37] G.F. Bolling, J. Cissé, J. Cryst. Growth 10 (1971) 56–66.
[38] A.A. Chernov, D.E. Temkin, A.M. Mel'nikova, Sov. Phys. Crystallogr. 21 (1976) 726–736.
[39] F. Mugele, Nat. Mater. 11 (2012) 182–183.
[40] A. Fadavi Boostani, S. Tahamtan, Trans. Nonferr. Met. Soc. China 20 (2010) 1608–1614.
[41] A. Fadavi Boostani, S. Tahamtan, Mater. Des. 31 (2010) 3769–3776.
[42] T.S. Srivatsan, E.J. Lavernia, J. Mater. Sci. 27 (1992) 5965–5981.
[43] T.M. Yue, G.A. Chadwick, J. Mater. Process. Technol. 58 (1996) 302–307.
[44] L. Gránásy, T. Pusztai, D. Saylor, J.A. Warren, Phys. Rev. Lett. 98 (2007) 035703.
[45] A.L. Greer, A.M. Bunn, A. Tronche, P.V. Evans, D.J. Bristow, Acta Mater. 48 (2000) 2823–2835.
[46] M. Mohammadpour, R.A. Khosroshahi, R.T. Mousavian, D. Brabazon, Metall. Mater. Trans. B 46 (2015) 12–19.
[47] S. Soltani, R. Azari Khosroshahi, R. Taherzadeh Mousavian, Z.-Y. Jiang, A. Fadavi Boostani, D. Brabazon, Rare Met. 34 (2015) 1–10.
[48] W. Bao, F. Miao, Z. Chen, H. Zhang, W. Jang, C. Dames, C.N. Lau, Nat Nano, 4 (2009) 562–566.
[49] J.B. Nelson, D.P. Riley, Proc. Phys. Soc. 57 (1945) 477.
[50] L.M. Tham, M. Gupta, L. Cheng, Acta Mater. 49 (2001) 3243–3253.
[51] L. Ci, Z. Ryu, N.Y. Jin-Phillipp, M. Rühle, Acta Mater. 54 (2006) 5367–5375.
[52] F. Juretzko, D. Stefanescu, B. Dhindaw, S. Sen, P. Curreri, Metall. Mater. Trans. A 29 (1998) 1691–1696.
[53] Y. Yang, J. Lan, X. Li, Mater. Sci. Eng.: A 380 (2004) 378–383.
[54] V. Dao, S. Zhao, W. Lin, C. Zhang, Mater. Sci. Eng.: A 558 (2012) 95–102.
[55] S.E. Shin, H.J. Choi, J.H. Shin, D.H. Bae, Carbon.
[56] N. Ramakrishnan, Acta Mater. 44 (1996) 69–77.
[57] V.C. Nardone, K.M. Prewo, Scr. Metall. 20 (1986) 43–48.
[58] T. Jiang, R. Huang, Y. Zhu, Adv. Funct. Mater. 24 (2014) 396–402.
[59] A.S. Carrara, F.J. Mcgarry, J. Compos. Mater. 2 (1968) 222–243.
[60] J.F. Nie, Scr. Mater. 48 (2003) 1009–1015.
[61] C.S. Goh, J. Wei, L.C. Lee, M. Gupta, Acta Mater. 55 (2007) 5115–5121.
[62] A. Fadavi Boostani, S. Tahamtan, J. Alloy. Compd. 481 (2009) 220–227.
[63] S. Tahamtan, A. Fadavi Boostani, Trans. Nonferr. Met. Soc. China 20 (3) (2010) s781–s787.
[64] S.-J. Hong, H.-M. Kim, D. Huh, C. Suryanarayana, B.S. Chun, Mater. Sci. Eng.: A 347 (2003) 198–204.
[65] Y. Wu, E.J. Lavernia, Scr. Metall. Mater. 27 (1992) 173–178.
[66] K.T. Conlon, D.S. Wilkinson, Mater. Sci. Eng.: A 317 (2001) 108–114.
[67] S. Tahamtan, A. Fadavi Boostani, H. Nazemi, J. Alloy. Compd. 468 (2009) 107–114.
[68] C.F. Deng, D.Z. Wang, X.X. Zhang, A.B. Li, Mater. Sci. Eng.: A 444 (2007) 138–145.

Chapter 5 Solvothermal-assisted graphene encapsulation of SiC nanoparticles: A new horizon toward toughening aluminium matrix nanocomposites

5.1 Statement

Due to the uncontrolled nature of ball milling process on number of graphene sheets encapsulating SiC nanoparticles and some evidence of having SiC nanoparticles without any graphene sheets wrapping around them in the produced composites, discussed in Chapters 3 and 4, this chapter presents an innovative fabrication route to diminish the agglomeration of SiC nanoparticles using graphene encapsulating method stimulated by a solvothermal process. This study has showed that the solvothermal process is a process that can be controlled by adjusting the process parameters such as temperature and gas flow, but controlling the phenomena happening in the milling process is difficult, resulting in nonuniform formation of graphene sheets wrapping SiC nanoparticles.

In the case of the experimental procedure utilized in this chapter, the SiC nanoparticles, wrapped by graphene sheets using the solvothermal process, were incorporated into A357 molten alloy using a liquid processing route. To have a better insight about the effect of graphene sheets on the distribution of SiC nanoparticles in the produced composites, high resolution transmission electron microscopy (HRTEM) was implemented, showing uniform distribution of SiC nanoparticles wrapped by onion-liked graphene shells within the matrix of composite. Tensile tests have demonstrated that tweaking the nanostructure of the aluminium metal matrix composites can bring about 273% and 400% augmentation in yield strength and tensile ductility, respectively, compared to the unreinforced one. This is attributed to the manipulation of solidification mechanism of SiC nanoparticles from pushing to engulfment, ensued from imparting higher thermal conductivity to these particles by onion-liked graphene sheets. Fractographic observations have revealed the transgranular facture mode activated due to nano-void coalescence fracture mechanism in composites reinforced with graphene sheets associated with prolonged ductility.

Materials Science & Engineering A 653 (2016) 99–107

Contents lists available at ScienceDirect

Materials Science & Engineering A

journal homepage: www.elsevier.com/locate/msea

Solvothermal-assisted graphene encapsulation of SiC nanoparticles: A new horizon toward toughening aluminium matrix nanocomposites

A. Fadavi Boostani [a], R. Taherzadeh Mousavian [b], S. Tahamtan [c], S. Yazdani [b], R. Azari Khosroshahi [b], D. Wei [d], J. Xu [c], X. Zhang [c], Z.Y. Jiang [a,*]

[a] School of Mechanical, Materials and Mechatronic Engineering, University of Wollongong, NSW 2522, Australia
[b] Faculty of Materials Engineering, Sahand University of Technology, Tabriz, Iran
[c] State Key Laboratory of Rolling and Automation, Northeastern University, Shenyang, Liaoning 110004, China
[d] School of Electrical, Mechanical and Mechatronic Systems, University of Technology, Sydney, NSW 2007, Australia

ARTICLE INFO

Article history:
Received 10 November 2015
Received in revised form
2 December 2015
Accepted 7 December 2015
Available online 9 December 2015

Keywords:
Composites
Semi-solid processing
Mechanical characterisation
Electron microscopy
Fracture

ABSTRACT

Agglomeration of ceramic nanoparticles is a key challenge during manufacturing aluminium matrix composites in both solid and liquid methods. This study presents an innovative fabrication route to diminish the agglomeration of SiC nanoparticles using graphene encapsulating method stimulated by a solvothermal process. The produced SiC nanoparticles were then incorporated into A357 molten alloy using a liquid processing route. HRTEM investigations have shown the uniform distribution of SiC nanoparticles wrapped by onion-liked graphene shells within the matrix of composite, conferring 273% and 400% enhancement in yield strength and tensile ductility, respectively, compared to the unreinforced one. This is attributed to the manipulation of solidification mechanism of SiC nanoparticles from pushing to engulfment, ensued from imparting higher thermal conductivity to these particles by onion-liked graphene sheets. Fractographic observations have revealed the transgranular facture mode activated due to nano-void coalescence fracture mechanism in composites reinforced with graphene sheets associated with prolonged ductility. A devised analytical strengthening model has also demonstrated the profound efficacy of thermal activated dislocation mechanism in fortifying the matrix, brought about by the exceptional negative thermal expansion coefficient of graphene sheets.

1. Introduction

Enhancing the tensile properties of aluminium matrix composites (AMCs) is of interest for different industrial applications especially in automobile industries, necessitating a uniform dispersion of ceramic particles within the matrix [1,2]. This, however, is more challenging task for nanoparticles due to higher propensity of them to be agglomerated during fabrication process, especially liquid routes, ascribed to the large surface to volume ratio and the poor wettability of nanoparticles in most metallic melts [3,4]. The agglomeration of nanoparticles is attributed to their pushing from advancing solid/liquid interface during solidification [5,6], resulting in settlement of them at grain boundaries. This, in turn, deteriorates the tensile elongation of produced composites due to facilitating low energy path for crack propagation trough the agglomerated regions located at grain boundaries [7]. To be harnessed, it is crucial to manipulate the solidification behaviour of nanoparticles from being pushed to be engulfed within solidified matrix, accomplished by alternating the shape of the advancing solid/liquid interface from convex to concave. This is, in turn, administered by augmenting the thermal conductivity of the reinforcing particles compared to the melt [8,9]. To date, apart previous studies conducted on improving the incorporation rate and uniform distribution of nanoparticles within liquid matrix [10,11], the invented methods are not highly successful in alteration the topology of advancing solid/liquid interface by manipulating the thermal conductivity of composite constituents due to their so-called fixed intrinsic nature.

However, it has been shown that graphene, i.e. a single-atom-thick sheet of sp^2 hybridised carbon atoms, has this unique functionality to be utilised as two-dimensional shell(s) that can nucleate and anchor nanoparticles on the edges and surface [12,13], and more interestingly as a functionally graded coating to manipulate some intrinsic properties of particles such as wetting [14]. To this end, authors have recently demonstrated the higher propensity of SiC nanoparticles encapsulated by graphene sheets to be

* Corresponding author.
E-mail addresses: afb496@uowmail.edu.au (A. Fadavi Boostani), jiang@uow.edu.au (Z.Y. Jiang).

http://dx.doi.org/10.1016/j.msea.2015.12.008
0921-5093/

uniformly dispersed and engulfed within solidifying aluminium matrix [15], attributed to the higher thermal conductivity of graphene sheets compared to the SiC particles at higher processing temperatures [16,17]. This can open a new window in revolutionizing the implementation of graphene sheets in metal matrix composites (MMCs) more behind the reported ordinary role as a nanofiller in enhancing the mechanical properties of MMCs [18,19]. The invented graphene encapsulating process [15], however, has some drawbacks pertinent to the uncontrolled nature of milling process, bringing about an inhomogeneity in number of onion-liked graphene shells (OLGS) wrapping SiC nanoparticles [20]. This, in turn, can deteriorate the propensity of SiC nanoparticles for engulfment within solidifying aluminium matrix [20], attributed to diminution in the opacity of graphene sheets due to change in the number of layers [14], thereby manipulating the van der Waals forces (vdW) of the substrate [20]. Following the attention has been given to invent a controllable graphene encapsulation process, this study aims at introducing an innovative solvothermal approach, leading to self-assembly of SiC nanoparticles into OLGS.

Production of crumpled or folded graphene sheets using solvothermal process is of interest theoretically and experimentally [21,22]. Produced graphene sheets demonstrate high flexibility, endowing high capability of encapsulation for different applications such as drug delivery, photocatalysis, solar cells, and electrical energy storage systems [23–25].

This promising encapsulating feature of graphene sheets, however, has not been reported before that can effectively manipulate the solidification and agglomeration behaviour of nanoparticles to render superior tensile ductility to MMCs.

This study, therefore, aims at exploiting this promising feature of graphene sheets to diminish the agglomeration of SiC nanoparticles in the A357 aluminium based composites to enhance the tensile properties especially tensile elongation. The nanostructure and mechanical properties of the produced composites were studied by high resolution transmission electron microscopy (HRTEM) and tensile tests, respectively. A mathematical model was devised based on the Orowan, geometrically necessary dislocations, shear lag and thermal activated dislocation strengthening mechanisms, and the model was further authenticated by tensile test results.

2. Experimental procedures

In order to produce a well-dispersed suspension of SiC nanoparticles, SiC nanoparticles (45 nm, supplied from Nanostructured & Amorphous Materials, Inc.) were subjected to oxidation using a mixture of sulphuric acid and hydrogen peroxide (30% H_2O_2: 97% H_2SO_4= 1:4 in volume). Accordingly, a horn sonicator was utilised to disperse oxidised SiC nanoparticles into distilled water for 10 min, accompanied by another 1 h sonication in a water bath sonicator. To functionalize surface of SiC nanoparticles, 10 wt% aminopropyltriethoxysilane (APS) (97%, Sigma Aldrich) was added to the prepared suspension.

To reach a well dispersed suspension of APS–SiC–graphene oxide (GO), the aqueous APS–SiC suspension was added slowly to the GO suspension (0.3 mg/mL, Research Grade Single Layer Graphene Oxide Water Dispersion supplied from US Research Nanomaterials, Inc.) while stirring at room temperature, resulting in generation of an amide bond between the Terminal NH_2 groups on APS–SiC nanoparticles with COOH groups on GO.

To prepare SiC nanoparticles encapsulated by graphene, the prepared suspension (APS–SiC–GO) was nebulised by an ultrasonic atomizer (97 kPa, UN-511, Alfesa Pharm Co., Japan). This resulted in production of solvothermal droplets carried by N_2 gas at a flow rate of 1 L/min to flow through a preheated horizontal tube at 700 °C for 3 s. The force generated as a result of generation the bonds between SiC nanoparticles and GO and the rapid solvent evaporation at 700 °C, resulted in encapsulation of SiC nanoparticles by graphene sheets.

Table 1
Chemical composition of A357 alloy used in this study (wt%).

Ti	Zn	Mg	Mn	Cu	Fe	Si	Al
< 0.2	< 0.1	< 0.3	< 0.1	< 0.2	< 0.2	7.0	Bal.

Injection of powder into the molten A357 aluminium alloy was carried out using high purity (99.999%) argon atmosphere (6 L/min) in the semi-solid state. Chemical composition of the A357 alloy used in this study has been demonstrated in Table 1.

The alloy was cooled down to 605 °C after melting and held at this temperature corresponding to a solid fraction of about 0.30 [26], followed by stirring the melt, using a graphite impeller at 400 rpm, associated with continuous feeding of SiC nanoparticles (3 vol%) to the uniformly formed vortex over a time period of approximately 5 min associated with adding 1 wt% Mg as a wetting agent.

SiC nanoparticles were resourced using two different methods including (a) non-treated as-received SiC nanoparticles, and (b) SiC nanoparticles encapsulated by onion-liked graphene shells (OLGS), prepared using a solvothermal process. Composite samples manufactured using the former and the latter are called in this study as NT-SiC and AR-SiC samples, respectively. SiC nanoparticles, prepared using the solvothermal process, for AR-SiC samples were ball milled with aluminium powder and then injected into the liquid aluminium. The ball milling was done using a Fritsch Pulverisette P5 planetary ball mill under high purity (99.99%) argon gas in a liquid nitrogen environment (cryomilling) for 1 h to make a preform for better incorporation of the SiC nanoparticles into the molten aluminium. During cryomilling, liquid nitrogen was constantly added to compensate for evaporation. The stainless steel vial was sealed with an elastomeric O ring. The stainless steel balls to powder weight ratio is 15:1, and the rotation rate of the vial is 250 rpm. Regarding NT-SiC sample, a mixture of as-received SiC nanoparticles and aluminium powder were ball milled using the same procedure used for AR-SiC sample.

After the completion of particle feeding, mixing was continued for an extra 1 min. Finally, prepared composite slurry was poured at 600 °C into a pre-heated cast iron mould with 100 mm in diameter and 50 mm in depth using a bottom-pouring system.

The Archimedes method was utilised to measure the density of the samples. High resolution transmition electron microscopy was used using a Philips CM200 and JEOL JEM-2010 at an accelerating voltage of 200 kV. Microstructure of samples was investigated using a Field Emission Scanning Electron Microscopy (FE-SEM), performed in a HITACHI S4160 and JEOL JSM-7500FA, to characterize the microstructural changes of the powders during milling and the fracture behaviour of the fabricated composites. Tensile test was carried out using a Hounsfield universal test machine at a cross-head speed of 0.5 mm s^{-1}. The dog-bone shaped tensile specimens had a gauge size of 6 mm in diameter and 30 mm in length, according to ASTM: B557M-10.

3. Results and discussion

3.1. Morphological characterisation of powders

Fig. 1 demonstrates the (a) TEM image of composite powders of NT-SiC sample, (b) AR-SiC sample, and (c) HRTEM image of SiC

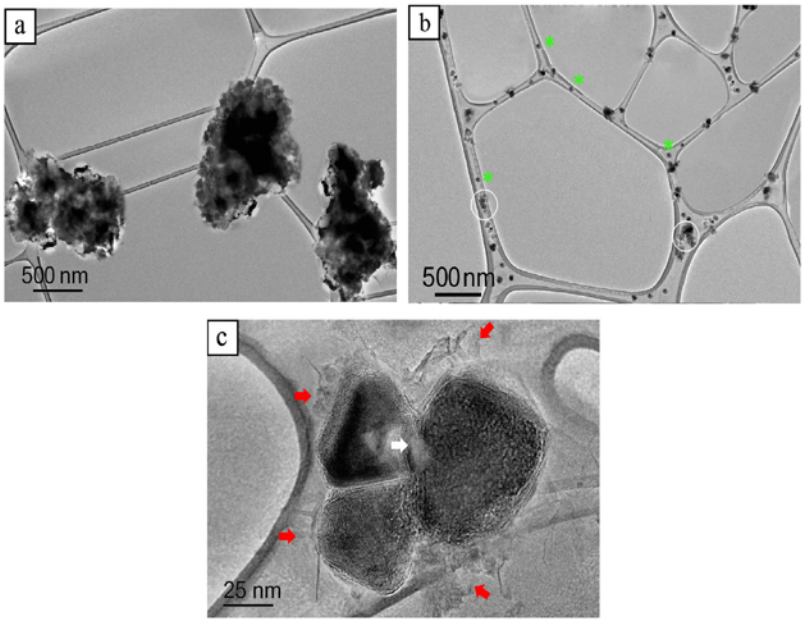

Fig. 1. TEM micrographs of (a) NT-SiC sample, (b) AR-SiC sample and (c) high magnification image of (b). (For interpretation of the references to colour in this figure, the reader is referred to the web version of this article.)

nanoparticles in AR-SiC sample. SiC nanoparticles in NT-SiC sample, as shown in Fig. 1(a), are susceptible to agglomeration resulted in formation of micron-sized clusters of SiC nanoparticles. In AR-SiC sample, however, SiC nanoparticles have a lower tendency for agglomeration, as shown in Fig. 1(b), ensued from a unique characteristic of solvothermal process for producing onion-liked graphene sheets (OLGS) encapsulating the SiC nanoparticles (Fig. 1 (c)). The formation of OLGS around the SiC nanoparticles is attributed to the reduction process of GO during the solvothermal process. As shown in Fig. 1(b) by green stars, most SiC nanoparticles in AR-SiC sample are formed without any agglomeration, but there is still some evidence that SiC nanoparticles have been agglomerated to form sub-micron sized clusters (white circles).

The formation of these clusters can be related to the wrinkling brought about by the force generated due to evaporation of droplets containing SiC nanoparticles [27], resulting in formation of some pores on the surface of SiC nanoparticles (white arrow in Fig. 1(c)) [28]. This makes the effect of attractive van der Waals forces (vdW) of substrate, i.e. SiC nanoparticles, more predominant by alleviating the opacity of graphene sheets coating SiC nanoparticles [14], thereby resulting in agglomeration.

As shown in Fig. 1(c), OLGS encapsulating SiC nanoparticle have a higher tendency to follow the surface curvature of these particles in order to minimise surface energy of system including particles and graphene shells. Basically, the force produced during the initial step of evaporation is what bends the sp^2 around the SiC nanoparticles [27], thus forming these OLGS.

From chemical bonding aspect, SiC nanoparticles are assembled into GO sheets due to the attachment of terminal NH_2 groups on APS–SiC nanoparticles with COOH groups on GO. These assemblies then underwent thermal heat treatment stimulating the reduction of GO into the graphene sheets with an onion shape. The formation of these OLGS is preferable from energetic perspective, as onion-like morphology is the most stable form of carbon particles [29].

As can be seen in Fig. 1(c), there are some graphene sheets (red arrows), which are not involved in the encapsulation process of SiC nanoparticles, and can be embedded between aluminium flakes during initial step of ball milling process [18], thereby inhibiting further agglomeration of SiC nanoparticles clusters.

3.2. Composite microstructure

3.2.1. FE-SEM results

Fig. 2 shows FE-SEM microstructures of NT-SiC (Fig. 2(a)) and AR-SiC (Fig. 2(b)) samples, respectively. There are some major discrepancies between these microstructures. First, as can be seen from Fig. 2(a), SiC nanoparticles in NT-SiC sample are formed with agglomerated morphology (black circle), but these particles have been uniformly distributed within the matrix of AR-SiC sample (Fig. 2(b)) apart from formation of some agglomerated SiC nanoparticles (white arrow in Fig. 2(b)). Second, SiC nanoparticles in NT-SiC sample are more prone to be agglomerated with some microvoids formed at the interface of these particles and surrounding matrix, deteriorating tensile properties. Third, the incorporation of agglomerated SiC nanoparticles is more considerable in NT-SiC sample compared to the AR-SiC sample. Finally, there is some evidence of formation of air gap in the agglomerated ceramic particles and presence of solidification shrinkages around these agglomerated particles, as demonstrated by white arrow in Fig. 2(a).

The formation of agglomerated SiC nanoparticles in the NT-SiC sample can be related to this fact these particles are agglomerated in the feeding composite powder, so they cannot be deagglomerated during releasing in the melt after injection in the liquid aluminium.

3.2.2. TEM results

Fig. 3 demonstrates TEM images of NT-SiC (Fig. 3(a)), AR-SiC (Fig. 3(c) and (e)) accompanied with schematic illustrations of the

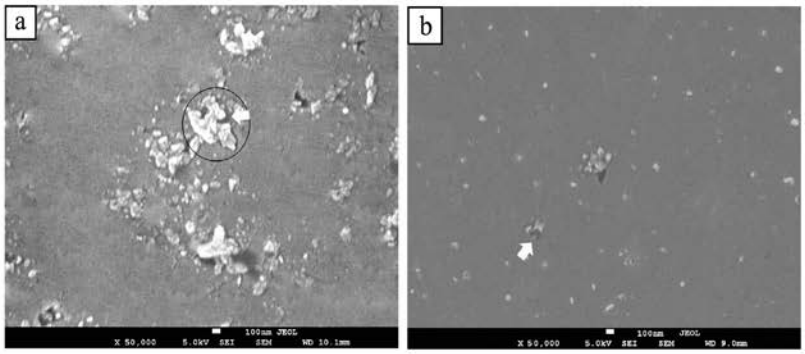

Fig. 2. FE-SEM micrograph of (a) NT-SiC and (b) AR-SiC samples.

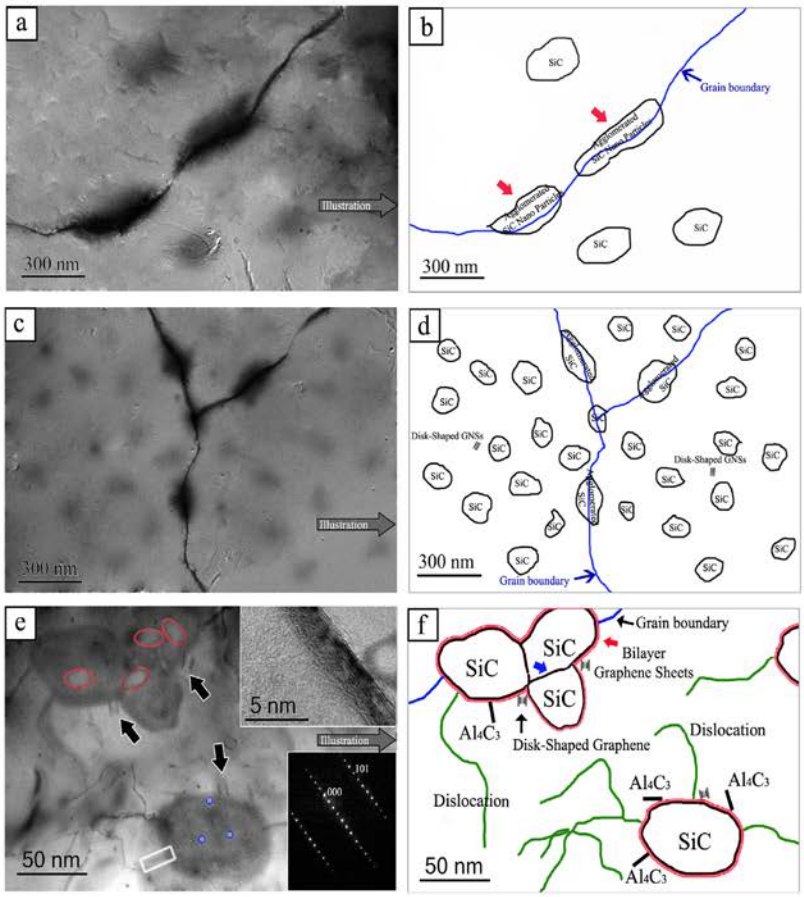

Fig. 3. TEM micrographs of (a) NT-SiC sample, (b) schematic representation of (a), (c) AR-SiC sample, (d) schematic representation of (c), (e) high magnification image of AR-SiC sample associated with selected area diffraction (SAD) pattern of specified region, and (f) schematic representation of (e). (For interpretation of the references to colour in this figure, the reader is referred to the web version of this article.)

former (Fig. 3(b)) and latter (Fig. 3(d) and (f)) to have a better clarification about nanostructural effects of graphene sheets produced during the solvothermal process. The effect of these graphene sheets on the solidifications mechanisms of produced composites, bringing about these nanostructural evolutions, is going to be discussed in Section 3.2.3.

As demonstrated in Fig. 3(a), SiC nanoparticles are formed as agglomerated particles in NT-SiCsample with a high propensity to be agglomerated at the grain boundaries rather than the grain interiors, ascribed to particle pushing mechanism during solidification, as demonstrated by red arrows in Fig. 3(b). Regarding AR-SiC sample, in contrast, as shown in Fig. 3(c), most SiC nanoparticles have been dispersed uniformly within the grain interior rather than at the grain boundaries, attributed to the particle engulfment mechanism controlling the solidification.

This discrepancy in agglomeration behaviour of SiC nanoparticles between NT-SiC and AR-SiC samples is related to the effect of OLGS wrapping SiC nanoparticles in AR-SiC sample. This effect, as discussed later in Section 3.2.3, prevents the agglomeration of SiC nanoparticles in the solid and liquid processing routes, as shown in Fig. 3(c)–(f). The uniform distribution of SiC nanoparticles is also brought about by beneficial effect of implementing the semi-solid processing route.

Indeed, stirring generated during semi-solid processing refines the dendrite morphology of the primary aluminium phase at 605 °C due to higher friction between the SiC nanoparticles and the aluminium alloy matrix, resulted in uniform dispersion of these particles within the matrix of the solidified composite. Additionally, there is a profound decrease in the sedimentation of the SiC nanoparticles at the semi-solid state stirring temperature [30], which can also result in a homogeneous distribution of these particles because of the presence of a solid phase [31]. More importantly, it is believed that OLGS can also manipulate the thermophysical properties of SiC nanoparticles, rendering higher propensity to these particles to be engulfed rather than be rejected from advancing solid/liquid interface, expounded more in the next section.

Fig. 3(e) demonstrates the HRTEM image of AR-SiC sample, representing the accumulation of thermal activated dislocation around SiC nanoparticles, attributed to the considerable mismatch between the negative thermal expansion coefficient of graphene (-6×10^{-6}/K at 300 K [32]) and A357 aluminium matrix ($\alpha_{A357}=21.6\times10^{-6}$/K [33]). Additionally, as specified in Fig. 3(e) by the blue circles, there is also more likely for OLGS encapsulating SiC nanoparticles to contain some ultra-small pores in some regions during the solvothermal process due to the evaporation-driven force triggering wrinkling of graphene sheets [27]. As shown in Fig. 3(e), SiC nanoparticles encapsulated by OLGS containing small pores (blue circles) have a higher propensity to be agglomerated within the grain interior, i.e. particle engulfment, but those encompassing larger pores (red ellipses) are susceptible to be agglomerated at the grain boundaries. This discrepancy in the solidification behaviour of SiC nanoparticles is attributed to the profound effect of large pores (red ellipses) on the opacity of graphene sheets, as the thinner graphene sheets form, the more transparent they are in transmitting van der Waals forces (vdW) of the substrate [14], thereby producing some degree of agglomeration in SiC nanoparticles after the powder (Fig. 1(c)) and liquid processes (Fig. 3(e) and (f)).

The homogeneity in number of graphene sheets wrapping SiC nanoparticles, however, is more prevalent in composites produced by the solvothermal process, as shown in Fig. 3(f), setting the composite produced in this study apart from those manufactured using ball-milling assisted graphene encapsulating process [20].

As can be seen in Fig. 3(f), there is also some evidence for the formation of nano-sized rod-shaped aluminium carbide (NRAC) at the interface of SiC nanoparticles and aluminium matrix. The inset in Fig. 3(e) shows the selected area diffraction (SAD) pattern of the white rectangular-shaped region in Fig. 3(e), confirming the formation of NRAC at the graphene/aluminium interface. The formation of NRAC can be attributed to the possible reaction of unfolded graphene sheets, detected around SiC nanoparticles (red arrows in Fig. 1(c)), at defect sites with liquid aluminium during the liquid processing, prompting the pinning of SiC nanoparticles into the surrounding aluminium matrix [34]. This pining can also be fortified due to the exceptional negative thermal expansion coefficient of graphene (-6×10^{-6}/K at 300 K [32]).

The another promising feature of unfolded graphene sheets (red arrows in Fig. 1(c)), detected over the regime of HRTEM investigations in AR-SiC sample, is facilitating the formation of disk-shaped graphene sheets (DSGS), as shown by black arrows in Fig. 3(e) and (f). The formation of DSGS is ascribed to the fragmentation unfolded graphene sheets during the ball milling process.

3.2.3. *Solidification mechanisms*

The interactions between solid/liquid interfaces and particles have been extensively investigated by different models [35–37]. Thermodynamic models consider thermodynamic free energy change during encapturing the particle by the solid/liquid interface, provided that the interface velocities are very small. Kinetic models consider critical interface velocities above which the particles are engulfed regardless of the thermodynamic criterion. Thermophysical models are built upon calculation of the thermal conductivity and the thermal diffusivity ratio between the particle and the liquid.

This study takes into account the thermophysical criterion to devise the following model to predict interaction of nanoparticles encapsulated by OLGS with an advancing macroscopically planar solid/liquid interface (V_{int}), as shown in Fig. 4.

Having considered the thermal conductivity ratio of nanoparticles and matrix, this model is of interest for this study to envisage the engulfment or pushing in a configuration where the nanoparticles encapsulated by OLGS are approaching to an advancing solid/liquid interface.

In the devised model, the heat flow is considered to be transferred only by conduction; therefore, other heat transfer mechanisms such as convection and viscous dissipation are not considered during calculation. In addition, latent heat which can be released at the solid/liquid interface is not considered in

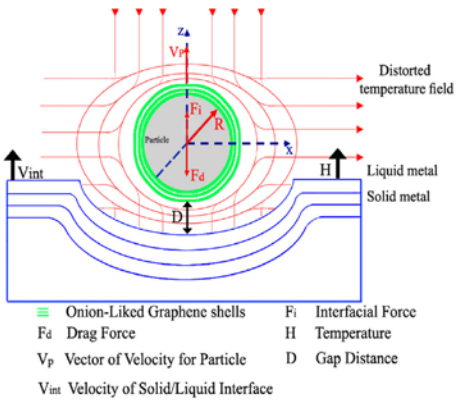

Fig. 4. Schematic image of an advancing solid/liquid interface approaching to the nanoparticle encapsulated by OLGS associated with the distortion of thermal fields and the forces acting on the nanoparticle.

calculations. The temperature gradient (H) was assumed along the growth direction far away from the nanoparticle. In addition, it was supposed that the thermal conductivity of solid and liquid phases is the same as the matrix (λ_m), but the thermal conductivity of nanoparticle was set to λ_p, provided that other material properties are considered to be independent of temperature, and the matrix is assumed to be an isotropic medium.

Having considered the azimuthal symmetry, the heat conduction in spherical co-ordinates (Fig. 4) can be approximated using Fourier's law based on Eq. (1) by considering the following boundary conditions ((Eqs. (2)–4)):

$$\frac{1}{r^2}\frac{\partial}{\partial r}\left(r^2\frac{\partial T}{\partial r}\right)+\frac{1}{r^2\sin\theta}\frac{\partial}{\partial\theta}(\sin\theta\frac{\partial T}{\partial\theta})=0 \tag{1}$$

1. The temperature gradient (H) in the Z direction should be considered constant in the larger distances from the nanoparticle, namely,

$$\left(\frac{\partial T}{\partial Z}\right)_{r\to\infty}=H \tag{2}$$

2. The temperature should be the same across the nanoparticle (T_P) and matrix interface (T_M), i.e.,

$$T_M^{r=R}=T_P^{r=R} \tag{3}$$

3. There is a close contact between the nanoparticle and the matrix so that there is no any local accumulation of heat at their interface; that is,

$$\lambda_m\left(\frac{\partial T_M}{\partial r}\right)_{r=R}=\lambda_p\left(\frac{\partial T_p}{\partial r}\right)_{r=R} \tag{4}$$

The reference temperature is considered to be T_{CTE}; that is,

$$(T_M)_{Z=0}^{r\to\infty}=T_{CTE} \tag{5}$$

The temperature distribution in the matrix (T_M) and nanoparticle (T_P) can be calculated by solving Eq. (1) using the given boundaries conditions ((Eqs. (2)–5)) as follows:

$$T_M=T_{CTE}-\left[1+\frac{1-\omega}{2+\omega}\left(\frac{R}{r}\right)^3\right]Hr\cos\theta \tag{6}$$

$$T_P=T_{CTE}-\left(\frac{3}{\omega+2}\right)Hr\cos\theta \tag{7}$$

In (Eqs. (6) and 7), the ω represents the thermal conductivity ratio, i.e.,

$$\omega=\frac{\lambda_P}{\lambda_m} \tag{8}$$

It is envisaged that by enhancing the thermal conductivity of particles incorporated into the liquid matrix compared to the matrix, i.e. increasing the ω value, the propensity of nanoparticles to be engulfed within the grain is enhanced due to the change of the interface shape from convex to concave [8,9,38,39]. Indeed, nanoparticles with lower thermal conductivity can blockade the removal of heat crucial for further solidification and consequently inhibits particle engulfment.

As shown in Fig. 4, there is a distortion in the temperature fields surrounding the particle, attributed to difference that can be generated between the thermal conductivity of the particle and the melt. It has been proven that for particles with high thermal conductivity ratios ($K_P/K_I>1$), the temperature field diverges near the particle, resulting in the particle having a lower temperature than the surrounding liquid [9].

It is anticipated that thermal conductivity of SiC nanoparticles encapsulated by OLGS outperforms intrinsic one of these particles, attributed to the high thermal conductivity of OLGS wrapping these particles [16,17,20]. This enhanced thermal conductivity of SiC nanoparticles stems from the fact that graphene shells encapsulating SiC particles are better conserved in bilayer and trilayer graphene sheets than that in single layer graphene sheet [40]. This, in turn, results in enhancing the thermal conductivity of SiC nanoparticles encapsulated by graphene sheets [17] compared to the liquid aluminium [41], i.e. higher ω value, bringing about the engulfment of these particles.

As illustrated in Fig. 4, regarding interaction forces generated between SiC nanoparticles and advancing solid/liquid interface, it has been asserted that graphene sheets can diminish the effect of the repulsive interfacial forces (F_i) generated from the substrate, i.e. SiC nanoparticle, at low gap distance (D), ascribed to the opaque characteristic of graphene sheets in transmitting the repulsive van der Waals forces (vdW) of the substrate [14]. So, this diminished F_i accompanied with drag force (F_D) can facilitate an engulfment condition for SiC nanoparticles encapsulated by OLGS.

Regarding AR-SiC sample, therefore, this is more likely for SiC nanoparticles encapsulated by OLGS to be engulfed within the grain interiors, as shown in Fig. 3(c)–(f), but these particles are most likely to be agglomerated at the grain boundaries in NT-SiC sample, as shown in Fig. 3(a) and (b).

3.3. Mechanical properties and strengthening mechanisms

Table 2 shows the tensile properties of the A357, NT-SiC and AR-SiC samples. As can be seen in Table 2, there is about 80% and 108% enhancement in the tensile yield strength and elongation of AR-SiC sample, respectively, compared to the ones of NT-SiC sample.

As shown in Fig. 3(f), graphene sheets in AR-SiC sample have been manifested in the form of OLGS encapsulating the SiC nanoparticles, thereby diminishing the threshold stress limit needed for cracking of these particles, resulting in higher tensile properties especially elongation of the AR-SiC sample. Additionally, OLGS encapsulating SiC nanoparticles make these particles less susceptible to interfacial decohesion due to the higher levels of plastic constraint imposed by the NRAC formed at the interface of these sheets with aluminium, as shown in Fig. 3(f) and in the top inset of Fig. 3(e).

The another reason for the higher tensile properties of the AR-SiC sample compared with the NT-SiC sample is ascribed to the lower porosity content (1.10 ± 0.15) introduced in the former compared to the latter (3.60 ± 0.20). This lower porosity content of the AR-SiC sample can be attributed to the lower agglomeration of SiC nanoparticles due to close contact between these nanoparticles before incorporation into the liquid aluminium matrix, thereby removing the air gap between them.

The enhanced tensile properties of the AR-SiC sample can be explained based on the some strengthening mechanisms including: (i) load-bearing effects due to the presence of SiC nanoparticles; (ii) thermally-activated dislocations manifested to

Table 2
The average values of yield stress (σ_{YS}), ultimate tensile strength (σ_{UTS}), total elongation (E %) and porosity content of samples.

Sample	Yield strength (MPa)	Ultimate tensile strength (MPa)	Elongation (E %)	Porosity (%)
A357	75 ± 2	125 ± 3	2 ± 0.30	3 ± 0.10
NT-SiC	155 ± 7	225 ± 10	4.80 ± 0.31	3.60 ± 0.20
AR-SiC	280 ± 9	410 ± 13	10 ± 0.52	1.10 ± 0.15

± Represents 95 pct. confidence interval.

accommodate considerable mismatch between the thermal expansion coefficient of graphene sheets and the aluminium matrix; (iii) Orowan strengthening mechanisms and (iv) geometrically necessary dislocations to compensate the strain incompatibility generated between the aluminium matrix and SiC nanoparticles encapsulated by OLGS.

To investigate the potential effect of aforementioned strengthening mechanisms on tensile properties, an analytical model (Eq. (9)) devised based on incorporation of a modified shear-lag (continuum mechanics approach), enhanced dislocation density (micromechanics strengthening approach), and geometrically necessary dislocations models into the model proposed by Ramakrishnan [42], as the latter generally is used for micron-sized particles.

$$\sigma_y^{AR-SiC}=\sigma_y^{NT-SiC}\left(1+\omega_L^{DSGS}\right)\left(1+\omega_T\right)\left(1+\omega_{Orowan}^{OLGS}\right)(1+\omega_{GNDs}) \tag{9}$$

In Eq. (9), the strengthening effect of graphene sheets in AR-SiC sample, manifested by two different morphologies including disk-shaped graphene sheets (*DSGS*) and onion-liked graphene sheets (*OLGS*), was investigated using load bearing (ω_l), thermal activated dislocation (ω_T), Orowan strengthening mechanisms (ω_{Orowan}) and geometrically necessary dislocations (ω_{GNDs}).

Nardone and Prewo [43] suggested a modified shear lag (MSL) model attributing the entire strengthening effect to the load bearing feature of the hard reinforcement. The classical shear lag model [44] was utilised to implement the MSL theory on the MMCs reinforced with graphene. Based on this, the shear stress that can be transferred from matrix to the graphene sheets is calculated using Eq. (10) [45].

$$\tau_P=nE_f e_m\left[\frac{\sin h(ns\frac{x}{L})}{\cos h(\frac{ns}{2})}\right] \tag{10}$$

To reach Eq. (10), the two-dimensional elastic configuration was considered for a platelet of graphene sheet with length L, thickness t, elastic modulus E and the aspect ratio of the s (let $s=L/t$), which is bonded to a matrix material of thickness λ.

In Eq. (10), n can be defined as $n=\sqrt{\frac{2G}{E_f}(\frac{t}{\lambda})}$ in which G represents the shear modulus of the matrix. According to Eq. (10), higher value of ns results in enhancing the maximum load that can be transferred from the matrix to the graphene platelet. To this end, it is essential to diminish the distance between the graphene platelets (λ) and simultaneously diminish their thickness, as thickness (t) affects the n with square root but it has an inverse relationship with S ($S=L/t$). To shed light the effect of ns on the load-bearing improvement factor (ω_l), affected mainly by the volume fraction of the reinforcements [42], Eq. (11) is introduced as follows [45].

$$\omega_l=\sqrt{\frac{2GL^2}{E_f\lambda_{eff}t}} \tag{11}$$

where λ_{eff} is an effective inter-particle spacing between the graphene sheets within the matrix that can be calculated using Eq. (12) [46]:

$$\lambda_{eff}^{DSGS}=0.931\sqrt{\frac{0.306\pi dt}{V_{Gr}^{DSGS}}}-\frac{\pi d}{8}-1.061t \tag{12}$$

Putting the values of $G_m=27$ GPa [47], $L=10$ nm, $t=5$ nm, $E_f=1000$ GPa and $\lambda_{eff}=194.83$ nm, calculated using Eq. (12), into Eq. (11) results in a ω_l value of 0.07 for the DSGS. It should be noted that the V_{Gr}^{DSGS} has been set to 0.1% of the total volume of the graphene ($V_{Gr}=0.01$) added as a raw material, and is measured along with other microstructural features such as L and t using image analysis of at least 20 HRTEM micrographs.

The enhancement in yield strength of AR-SiC sample due to the considerable mismatch between OLGS, encapsulating SiC nanoparticles, and aluminium matrix can be devised using Eq. (13) based on the Taylor dislocation strengthening equation [48].

$$\omega_T=\frac{\sqrt{3}\beta Gb}{\sigma_y^{NT-SiC}}\sqrt{\frac{12V_p\Delta\alpha\Delta T}{bd_p}} \tag{13}$$

In Eq. (13), β represents the strengthening coefficient which can be considered to be 1.25. Other parameters such as G, b, V_P, $\Delta\alpha$, ΔT and d_P represent the shear modulus of the aluminium matrix, b (2.84×10^{-10} m) [47] is the magnitude of the Burgers vector of dislocation, V_P is the total volume fraction of SiC nanoparticles (0.03), $\Delta\alpha$ is the difference between the thermal expansion coefficient of the aluminium and the graphene, ($\alpha_{Al}=21.6\times10^{-6}/^{\circ}$C [33], $\alpha_{graphene}=-6\times10^{-6}/^{\circ}$C at 300 K [32]), respectively, ΔT is the difference between the fabrication temperature (605 °C) and the room temperature (25 °C), and d_p is related to the average diameter of SiC nanoparticles within the aluminium matrix (100 nm), calculated using the average of at least 100 SiC nanoparticles in the HRTEM images. By inserting the noted values into Eq. (13), the thermal strengthening contributor factor (ω_T) is calculated to be 1.52.

In general, Orowan strengthening mechanism can be used when the matrix of composite encompasses fine particle with a uniform distribution. To delineate the contribution of the well-dispersed SiC nanoparticles in strengthening of AR-SiC sample in this study, Orowan strengthening mechanism was utilised using Eq. (14) [46].

$$\omega_{Orowan}^{OLGS}=\frac{MGb}{2\pi\sqrt{1-\vartheta}\,\sigma_y^{NT-SiC}\left(\frac{0.779}{\sqrt{V_P}}-0.785\right)d}\ln\frac{0.785d_P}{b} \tag{14}$$

In this equation, M (3) is the Taylor factor for polycrystalline FCC alloys, G (27 GPa) is the shear modulus of the aluminium matrix [47], b (2.84×10^{-10} m) is the magnitude of the Burgers vector of dislocation [47], ϑ (0.34) is Poisson's ratio [49], V_P (0.03) is the volume fraction of the SiC nanoparticles, d_P (100 nm) is the average diameter of at least 100 SiC nanoparticles measured using HRTEM analysis.

Putting the aforementioned values into Eq. (14) has shown that the Orowan strengthening contributor of about 0.44 attributed to the reduced agglomeration of SiC nanoparticles in AR-SiC sample by implementation of graphene encapsulating approach.

Additionally, geometrically necessary dislocations (GNDs) can also be manifested at the interface of SiC nanoparticles encapsulated by OLGS when the AR-SiC sample subjected to the external tensile load, attributed to the considerable mismatch between the elastic modulus of graphene sheets and aluminium matrix [50].

It has been approved that the formation of GNDs around dispersed nanoparticles can enhance the dislocation density trough the composite by increasing the density of obstacles in front of statistically distorted dislocations (SDDs) far beyond the one generated by primary SiC nanoparticles, thereby augmenting the tensile strength [50]. The strengthening effect of GNDs in AR-SiC sample can be calculated by the following equation [50].

$$\omega_{GND}=\frac{\alpha Gb}{\sigma_y^{NT-SiC}}\sqrt{\frac{8V_p\varepsilon_y}{bd_p}} \tag{15}$$

where α is the constant that is equal to 1.25, G is considered as the shear modulus of the aluminium matrix (27 GPa) [47], b the Burgers vector (2.84×10^{-10} m) [47], V_P the volume fraction of reinforcement (0.03), d_P the diameter of the prismatic dislocation loop around the reinforcement particles which can be considered

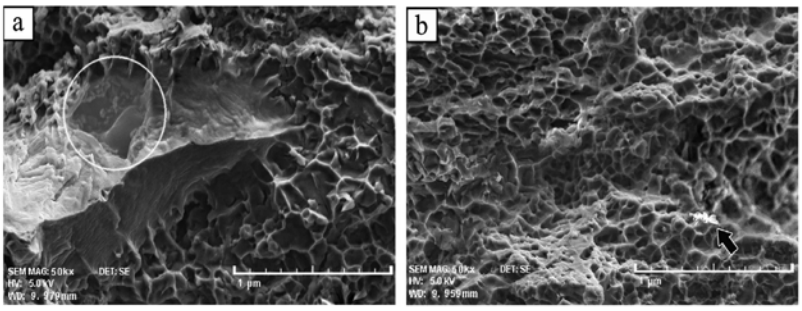

Fig. 5. Fracture surfaces of (a) NT-SiC and (b) AR-SiC samples.

approximately as particle diameter (100 nm), and ε_y the yield strain (0.2%). Investigation of Eq. (15) using the noted values represents the strengthening contributor of about 0.25 for GNDs (ω_{GNDs}).

Inserting the values achieved by (Eqs. (11)–15) into Eq. (9) approximates about 453.76 MPa increment in the yield stress of AR-SiC sample compared to the NT-SiC sample due to incorporation of SiC nanoparticles encapsulated by graphene sheets into the composite matrix. The lower yield strength of the AR-SiC sample compared to the one envisaged by Eq. (9) is attributed to some reasons:

First, it was considered in the presented model (Eq. (9)) that the habit planes of SiC nanoparticles are intersecting with the active slip plane of the aluminium matrix (111) with a perpendicular configuration. In practice, however, there is a possibility for OLGS to intersect with slip planes with an angled configuration, resulted in lower interaction between them and dislocations gliding on the matrix slip plane, thereby reducing the efficiency of Orowan strengthening mechanism.

Second, there is also some evidence of formation of large pores in OLGS encapsulating SiC nanoparticles, deteriorating significantly the bonding between these particles and aluminium matrix and capacity of them in emitting the thermal-activated dislocation through matrix, thereby levelling off the ω_{Orowan} and ω_T, respectively.

Third, there is still some degree of agglomeration for SiC nanoparticles in AR-SiC sample, brought about by the SiC nanoparticles not wrapped by OLGS. This is attributed to the possibility of incomplete graphene encapsulation for SiC nanoparticles during solvothermal process, augmenting the affinity of these particles to agglomerate at grain boundaries rather than engulfment within grain interior.

3.4. Fracture behaviour

Fig. 5(a) and (b) shows the fractographic images of the NT-SiC and AR-SiC samples after tensile tests, respectively. NT-SiC sample, as shown in Fig. 5(a), contains cleavage surfaces associated with some regions encompassing agglomerated SiC nanoparticles.

In essence, SiC nanoparticles pushed during solidification of NT-SiC sample results in agglomeration of these particles at the grain boundaries. This, in turn, facilitates cracking of these nanoparticles, i.e. micro-sized cluster (Fig. 2(a)), under lower stresses associated with a low energy path for crack propagation [51,52], thereby diminishing the tensile ductility of NT-SiC sample. Indeed, it is more likely for damage to be initiated at regions with high concentration of nanoparticles due to load transfer from particles-depleted zones to the former which are the suitable sites for crack nucleation [31].

AR-SiC sample, in contrast, as shown in Fig. 5(b), demonstrates nano-void coalescence fracture mechanism which is the main signature for occurrence the ductile fracture [53,54] with no evidence of cleavage surfaces, thereby increasing the ductility [55]. In addition, as shown by black arrow in Fig. 5(b), DSGS in AR-SiC sample (black arrows in Fig. 3(e)) exhibit unprecedented feature in harnessing the crack propagation trough matrix realized by the fibre pull-out toughening mechanism. Under these extenuating circumstances for crack propagation, the energy needed for crack to pass through the matrix augments significantly, thereby enhancing the ductility.

4. Conclusions

In this work, a solvothermal process was utilised to produce SiC nanoparticles encapsulated by graphene shells, alleviating the agglomeration of these particles. This was accomplished due to the enhanced thermal conductivity of SiC nanoparticles encapsulated by graphene sheets, alternating the solidification mechanism of these particles to be engulfed rather than being rejected from advancing solid/liquid interface, prompting uniform distribution of SiC nanoparticles. A devised strengthening model has revealed the substantial effect of thermal activated dislocation and Orowan strengthening mechanisms in enhancing the tensile yield strength. The fractographic investigations have also disclosed predominant nano-void coalescence fracture mechanism due to the uniform dispersion of SiC nanoparticles encapsulated by onion-liked graphene shells associated with the higher tensile ductility. Despite these promising features of graphene sheets in deagglomeration of SiC nanoparticles, the solvothermal process used in this study is still in its infancy and should be addressed in details the correlations between the process parameters such as concentration of nanoparticles in the solution and the process temperature affecting the evaporation rate and accordingly formation of pores, thereby controlling the degree of agglomeration.

Acknowledgements

The authors would like to acknowledge the use of facilities (ARC-LE0237478) within the University of Wollongong (UOW) Electron Microscopy Centre and especially the great assistance of Dr. Gilberto Casillas. Authors also thank Dr. David Mitchel and Dr. Mitchel Nancarrow for their valuable support.

References

[1] M.J. Tan, X. Zhang, Mater. Sci. Eng. A 244 (1998) 80–85.
[2] D. Miracle, Compos. Sci. Technol. 65 (2005) 2526–2540.
[3] C.A. León, G. Mendoza-Suarez, R.L. Drew, J. Mater. Sci. 41 (2006) 5081–5087.
[4] I. El-Mahallawi, H. Abdelkader, L. Yousef, A. Amer, J. Mayer, A. Schwedt, Mater. Sci. Eng. A 556 (2012) 76–87.
[5] J.A. Garcia-Hinojosa, C.G. R, J.A.J. I, M.K. Surrapa, Mater. Sci. Eng. A 386 (2004) 54–60.
[6] J. Hashim, L. Looney, M.S.J. Hashmi, J. Mater. Process. Technol. 92–93 (1999) 1–7.
[7] M. Kok, J. Mater. Process. Technol. 161 (2005) 381–387.
[8] E.M. Agaliotis, M.R. Rosenberger, A.E. Ares, C.E. Schvezov, Procedia Mater. Sci. 1 (2012) 58–63.
[9] M.A. Khan, P.K. Rohatgi, Compos. Eng. 3 (1993) 995–1006.
[10] S. Tahamtan, A. Halvaee, M. Emamy, Z.Y. Jiang, A. Fadavi Boostani, Mater. Sci. Eng. A 619 (2014) 190–198.
[11] M. Mohammadpour, R.A. Khosroshahi, R.T. Mousavian, D. Brabazon, Metall. Mater. Trans. B 46 (2015) 12–19.
[12] I.V. Lightcap, T.H. Kosel, P.V. Kamat, Nano Lett. 10 (2010) 577–583.
[13] V.H. Pham, T.T. Dang, S.H. Hur, E.J. Kim, J.S. Chung, ACS Appl. Mater. Interfaces 4 (2012) 2630–2636.
[14] F. Mugele, Nat. Mater. 11 (2012) 182–183.
[15] A. Fadavi Boostani, S. Tahamtan, Z.Y. Jiang, D. Wei, S. Yazdani, R. Azari Khosroshahi, R. Taherzadeh Mousavian, J. Xu, X. Zhang, D. Gong, Compos. Part A Appl. Sci. Manuf. 68 (2015) 155–163.
[16] R.P. Joshi, P.G. Neudeck, C. Fazi, J. Appl. Phys. 88 (2000) 265–269.
[17] C. Faugeras, B. Faugeras, M. Orlita, M. Potemski, R.R. Nair, A.K. Geim, ACS Nano 4 (2010) 1889–1892.
[18] M. Bastwros, G.-Y. Kim, C. Zhu, K. Zhang, S. Wang, X. Tang, X. Wang, Compos. Part B Eng. 60 (2014) 111–118.
[19] R. Pérez-Bustamante, D. Bolaños-Morales, J. Bonilla-Martínez, I. Estrada-Guel, R. Martínez-Sánchez, J. Alloy. Compd. 615 (Supplement 1) (2014) S578–S582.
[20] A. Fadavi Boostani, R.T. Mousavian, S. Tahamtan, S. Yazdani, R.A. Khosroshahi, D. Wei, J.Z. Xu, D. Gong, X.M. Zhang, Z.Y. Jiang, Mater. Sci. Eng. A 648 (2015) 92–103.
[21] H. Wang, J.T. Robinson, X. Li, H. Dai, J. Am. Chem. Soc. 131 (2009) 9910–9911.
[22] Q. Kuang, S.-Y. Xie, Z.-Y. Jiang, X.-H. Zhang, Z.-X. Xie, R.-B. Huang, L.-S. Zheng, Carbon 42 (2004) 1737–1741.
[23] S. Stankovich, D.A. Dikin, G.H.B. Dommett, K.M. Kohlhaas, E.J. Zimney, E. A. Stach, R.D. Piner, S.T. Nguyen, R.S. Ruoff, Nature 442 (2006) 282–286.
[24] P.V. Kamat, J. Phys. Chem. Lett. 2 (2011) 242–251.
[25] Y.H. Ng, I.V. Lightcap, K. Goodwin, M. Matsumura, P.V. Kamat, J. Phys. Chem. Lett. 1 (2010) 2222–2227.
[26] S. Naher, D. Brabazon, L. Looney, J. Mater. Process. Technol. 166 (2005) 430–439.
[27] X. Ma, M.R. Zachariah, C.D. Zangmeister, Nano Lett. 12 (2012) 486–489.
[28] D. Wu, R. Fu, M.S. Dresselhaus, G. Dresselhaus, Carbon 44 (2006) 675–681.
[29] D. Ugarte, Nature 359 (1992) 707–709.
[30] H. Zhang, L. Geng, L. Guan, L. Huang, Mater. Sci. Eng. A 528 (2010) 513–518.
[31] Z. Xu, J. Yan, W. Chen, S. Yang, Mater. Lett. 62 (2008) 2615–2618.
[32] W. Bao, F. Miao, Z. Chen, H. Zhang, W. Jang, C. Dames, C.N. Lau, Nat. Nano 4 (2009) 562–566.
[33] J.R. Davis, Aluminum and Aluminum Alloys, ASM International, Ohio, USA, 1993.
[34] L. Ci, Z. Ryu, N.Y. Jin-Phillipp, M. Rühle, Acta Mater. 54 (2006) 5367–5375.
[35] J. Hashim, L. Looney, M.S.J. Hashmi, J. Mater. Process. Technol. 123 (2002) 251–257.
[36] L. Hadji, Math. Comput. Model. 36 (2002) 147–156.
[37] M. Gelbstein, I. Edry, N. Froumin, N. Frage, Metall. Mater. Trans. A 40 (2009) 932–936.
[38] G.F. Bolling, J. Cissé, J. Cryst. Growth 10 (1971) 56–66.
[39] M.K. Surappa, P.K. Rohatgi, J. Mater. Sci. 16 (1981) 562–564.
[40] E. Muñoz, J. Lu, B.I. Yakobson, Nano Lett. 10 (2010) 1652–1656.
[41] S. Ho, A. Saigal, Scr. Metall. Mater. 31 (1994) 351–356.
[42] N. Ramakrishnan, Acta Mater. 44 (1996) 69–77.
[43] V.C. Nardone, K.M. Prewo, Scri. Metall. 20 (1986) 43–48.
[44] T. Jiang, R. Huang, Y. Zhu, Adv. Funct. Mater. 24 (2014) 396–402.
[45] A. Fadavi Boostani, S. Yazdani, R. Taherzadeh Mousavian, S. Tahamtan, R. Azari Khosroshahi, D. Wei, D. Brabazon, J.Z. Xu, X.M. Zhang, Z.Y. Jiang, Mater. Des. 88 (2015) 983–989.
[46] J.F. Nie, Scr. Mater. 48 (2003) 1009–1015.
[47] I. Gutierrez-Urrutia, M.A. Muñoz-Morris, I. Puertas, C. Luis, D.G. Morris, Mater. Sci. Eng. A 475 (2008) 268–278.
[48] C.S. Goh, J. Wei, L.C. Lee, M. Gupta, Acta Mater. 55 (2007) 5115–5121.
[49] Y.T. Zhao, S.L. Zhang, G. Chen, X.N. Cheng, C.Q. Wang, Compos. Sci. Technol. 68 (2008) 1463–1470.
[50] M. MA, K. CHAWLA, Prentice-Hall, Englewood Cliffs, New Jersey, 1984.
[51] A. Fadavi Boostani, S. Tahamtan, J. Alloy. Compd. 481 (2009) 220–227.
[52] S. Tahamtan, A. Fadavi Boostani, H. Nazemi, J. Alloy. Compd. 468 (2009) 107–114.
[53] A. Fadavi Boostani, S. Tahamtan, Mater. Des. 31 (2010) 3769–3776.
[54] S. Tahamtan, A. Fadavi Boostani, Trans. Nonferrous Met. Soc. China 20 (Supplement 3) (2010) S781–S787.
[55] A. Fadavi Boostani, S. Tahamtan, Trans. Nonferrous Met. Soc. China 20 (2010) 1608–1614.

Chapter 6 Graphene tweaking Hamaker constant of SiC nanoparticles: A new horizon to solve the conflict between strengthening and toughening

6.1 Statement

Although the results presented in Chapters 3-5 have shown the profound effect of graphene sheets on enhancing the propensity of SiC nanoparticles to be engulfed within advancing solid/liquid aluminium, the mechanism by which this capturing is stimulated has not been explained so far. This chapter, therefore, aims to delineate the effect of graphene sheets on manipulating the Hamaker constant of SiC nanoparticles as an intrinsic property of these particles, playing an important role in engulfment or agglomeration of not only SiC, but other nanoparticles confronting with advancing solid/liquid interface. This was accomplished by devising a novel theoretical approach, addressing the effect of graphene sheets on manipulating the Hamaker constant of SiC nanoparticles. Experimental approaches used in this chapter include the production of SiC nanoparticles encapsulated by graphene sheets using the solvothermal process, as introduced in Chapter 5, associated by incorporation of these nanoparticles within the aluminium matrix accomplished by semi-solid powder forming process. This manufacturing process utilized in this chapter has the advantage of liquid state processing routes used in the past Chapters 3-5 due to the formation of liquid during sintering process of milled powder, but it is not resulted in adverse rearrangement of SiC nanoparticles, i.e. agglomeration, during manufacturing attributed to the lower liquid content associated with semi-solid powder forming processes. Micro/nanostructural investigation using high resolution transmission electron microscopy (HRTEM) and Field emission scanning electron microscopy (FE-SEM) has shown the significant effect of graphene sheets in conferring multi-scaled sized grains including nano and micro-sized grains within aluminium matrix. Results achieved by the tensile tests have represented the 181% and 171% enhancement in yield and ultimate tensile strengths of the produced composites compared to the unreinforced ones, respectively.

Scripta Materialia 118 (2016) 65–69

Contents lists available at ScienceDirect

Scripta Materialia

journal homepage: www.elsevier.com/locate/scriptamat

Graphene tweaking Hamaker constant of SiC nanoparticles: A new horizon to solve the conflict between strengthening and toughening

A. Fadavi Boostani [a,b], S. Tahamtan [c], S. Yazdani [b], R. Azari Khosroshahi [b], D. Wei [d], H. Sahamirad [e], X.M. Zhang [c], Z.Y. Jiang [a,*]

[a] School of Mechanical, Materials and Mechatronic Engineering, University of Wollongong, NSW 2522, Australia
[b] Faculty of Materials Engineering, Sahand University of Technology, Tabriz, Iran
[c] State Key Laboratory of Rolling and Automation, Northeastern University, Shenyang, Liaoning 110004, China
[d] School of Electrical, Mechanical and Mechatronic Systems, University of Technology, Sydney, NSW 2007, Australia
[e] Department of Mechanical Engineering, University of Ottawa, Ottawa, Ontario, K1N 6N5, Canada

ARTICLE INFO

Article history:
Received 15 December 2015
Received in revised form 22 February 2016
Accepted 24 February 2016
Available online xxxx

Keywords:
Hamaker constant
Semi-solid processing
Nanocomposites
Fracture
Ductility

ABSTRACT

This study reveals a promising feature of graphene encapsulating process to significantly enhance the mutually inclusive tensile strength and ductility of aluminium based composites using the semi-solid powder forming process. It was corroborated based on van der Waals–Casimir interaction free energy that graphene sheets have an unprecedented capacity to manipulate the Hamaker constant of SiC nanoparticles, prompting formation of nano/micro-sized grains. Authenticating by the strengthening model, fractographic observations have also demonstrated the unique functionality of graphene sheets in strengthening via grain refining, thermally enhanced dislocations, shear-lag, geometrically necessary dislocations, crack bridging and fibre pull out mechanisms.

Conferring concurrent superior tensile strength and elongation on metal matrix nanocomposites reinforced with nanoparticles is a challenging task [1–3] due to the high propensity of these particles for agglomeration in the most solid and liquid processing routes [4]. Some studies were conducted to tackle this problem making use of casting [5,6] and semi-solid powder processing [7], i.e. semi-solid forming of milled powder. To date, however, there is no in-depth study considering the effect of tweaking Hamaker constant of nanoparticles to attenuate the agglomeration of these particles. The Hamaker constant (A) is an intrinsic characteristic of materials measuring the quality and quantity of the interaction forces between two surfaces, playing an important role in engulfment or pushing, i.e. agglomeration, of nanoparticles where they confront with approaching solid/liquid interface [8].

Following the rise of graphene with a combination of outstanding electrical, thermal, and mechanical characteristics as atom-thick filler in polymer [9,10] and metal matrix composites [7], graphene can also be employed more functionally as nano-sized building blocks to coat other surfaces, thereby manipulating some intrinsic properties of materials such as wetting [11,12].

* Corresponding author.
E-mail addresses: afb496@uowmail.edu.au (A. Fadavi Boostani), jiang@uow.edu.au (Z.Y. Jiang).

Albeit authors have recently characterized that SiC nanoparticles, encapsulated by graphene sheets, have more propensity to be engulfed within the advancing solid/liquid interface [13], the mechanism by which this capturing has been stimulated was not clear so far.

To this end, a theoretical approach was implemented in this study, for the first time, to address the effect of graphene sheets on manipulating the Hamaker constant of SiC nanoparticles, thereby enhancing the engulfment of these particles within advancing solid/liquid interface during solidification to attain concurrent augmentation in tensile strength and ductility. SiC nanoparticles, 45 nm, supplied by Nanostructured & Amorphous Materials, were encapsulated by onion-liked graphene sheets (OLGS) using the new solvothermal approach introduced elsewhere (Fig. 1(a)) [14]. These particles and as-received ones (5 vol.%) were then ball milled for 2 h with a mixed powder containing high purity aluminium (45 μm), silicon (45 μm) and Mg (45 μm) powders, supplied from Alpha Aesar Company with 99.5% purity, in the desired composition (Al–7 wt.%Si–0.3%Mg) based on the cryomilling method [13], called as GE-SiC and AR-SiC samples, respectively. Fig. 1(b) shows well-dispersed SiC nanoparticles (red arrow) in GE-SiC compared to the agglomerated ones (green arrows) in AR-SiC sample (Fig. 1(c)).

These powders (Fig. 1(b–c)) were then placed into a high temperature steel mould with a diameter of 50 mm and 60 mm height in inert atmosphere (argon), and then uniaxially cold pressed using the applied

http://dx.doi.org/10.1016/j.scriptamat.2016.02.028
1359-6462/

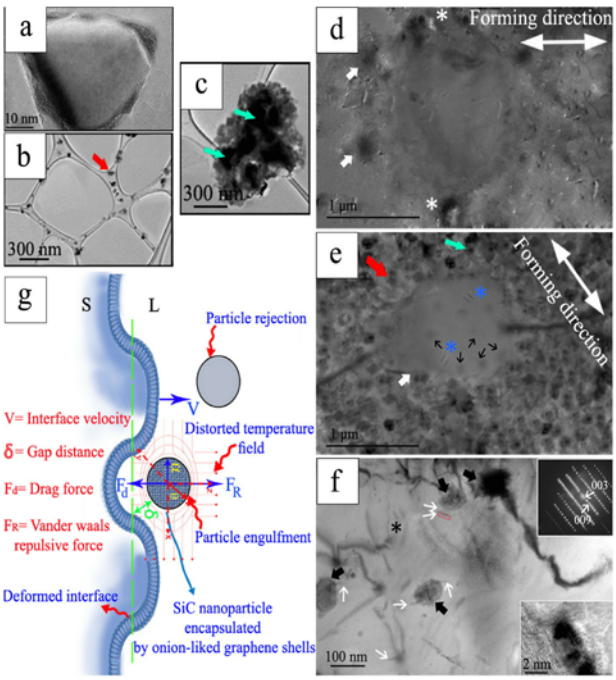

Fig. 1. TEM micrographs of (a) SiC nanoparticle encapsulated by graphene shells, (b) GE-SiC sample (c) AR-SiC sample, (d) SPF sample, (e) SPFG sample, (f) high magnification image of CG region in SPFG sample, and (g) solidification mechanism of SPF and SPFG samples.

pressure of 100 MPa to produce green cylindrical bulk samples. These samples were placed into a H13 tool steel die in the argon-gas protected glove box. The assembly was then heated to a targeted semi-solid powder forming (SPF) temperature of 564 °C corresponding to the liquid fraction of 0.25 for the holding time of 40 min with the heating rate of 40 °C/min under the fixed SPF pressure of 63 MPa in a chamber of uniaxial press protected by high purity argon gas (99.99%).

The nanocomposites manufactured by AR-SiC powder are named as SPF samples (Fig. 1(d)) and those fabricated using GE-SiC powder are called as SPFG samples (Fig. 1(e)).

The density of the samples was measured by the Archimedes method and reported based on comparison with the theoretical density. TEM analysis was performed using Philips CM200 and JEOL JEM-2011 at an accelerating voltage of 200 kV. Fractographic investigations were conducted using field emission scanning electron microscopy (FE-SEM) performed in a JEOL JSM-7500FA. Tensile properties were measured using a Hounsfield universal test machine at a cross-head speed of 0.5 mms^{-1}.

As demonstrated in Fig. 1(d) by white arrows, SiC nanoparticles in the SPF sample are more susceptible to be agglomerated at grain boundaries resulted in a higher grain size (3.2 μm) accompanied by high degree of porosities (white stars). SPFG sample, however, contains SiC nanoparticles preferentially more engulfed within grain interior, as shown in Fig. 1(e) by black arrows, prompting two distinct regions including coarse grains (white arrow) with high-angle boundaries and nanocrystalline grains (red arrow).

The formation of coarse grains (CG) is ascribed to the grain growth occurred at local contact points of milled particles during SPF process, while the nanocrystalline grains (NG) are manifested due to the synergic effect of cryomilling and graphene sheets in the milling process. The produced CG–NG structure was also stabilized during SPF process due to the uniform distribution of SiC nanoparticles within NG regions and engulfment of them with network configuration in the CG regions (black arrows in Fig. 1(e)) rather than being agglomerated at grain boundaries which is prevalent in the SPF sample (white stars in Fig. 1(d)), resulted in a higher density of SPFG sample (98%) compared to a lower value reported for SPF sample (94%).

The network structure of SiC nanoparticles (black arrows in Fig. 1(e)) is ascribed to the semi-solid-assisted rearrangement of these nanoparticles after engulfment in the CG regions, brought about by the SPF forming force. As demonstrated in Fig. 1(f), graphene sheets can be distinguished in the SPFG sample with two different appearances including OLGS, as shown by black arrows and disc-shaped graphene sheets (DSGS), as demonstrated by a black star. The preferential engulfment of SiC nanoparticles within CG interior in SPFG sample can be attributed to the enhanced thermal conductivity of SiC nanoparticles encapsulated by OLGS compared to those pushed away into the interparticle aluminium regions in SPF sample, as shown by white stars in Fig. 1(d) [13,15,16].

Eq. (1) [17] envisages that particles with a lower thermal conductivity than the liquid, prompt convex bending of the interface advancing towards the particles (particle rejection), but those particles inheriting a higher thermal conductivity than that of liquid ($K_P > K_l$) cause a concave deformation of the interface away from it (particle engulfment), as shown in Fig. 1(g) [17–19].

$$K_P > K_l \text{ for engulfment} \quad (1)$$

Fig. 1(g) shows the suggested solidification mechanism of composites studied. Based on the thermodynamic perspective, van der Waals

potential can inhibit SiC nanoparticles to be engulfed within advancing solid/liquid interface due to the repulsive forces (F_R in Fig. 1(g)).

Eq. (2) [20] approximates the van der Waals potential generated between SiC nanoparticles with radius of α and approaching solid/liquid interface in the closest possible distance (δ), as shown in Fig. 1(g).

$$W_{VdW} = \frac{-A}{6}\left(\frac{\alpha}{\delta} + \frac{\alpha}{2\alpha+\delta} + \ln\frac{\delta}{2\alpha+\delta}\right) \quad (2)$$

In Eq. (2), A represents the Hamaker constant. Having considered the small value of δ, Eq. (2) can be rearranged in the following form [21]:

$$W_{VdW} = \frac{-A\alpha}{6\delta} \quad (3)$$

It is then crucial to calculate the non-retarded Hamaker constant of a system (A_{SYS}) encompassing SiC nanoparticles encapsulated by OLGS facing with the advancing solid/liquid (S) interface within liquid aluminium (L), as depicted in Fig. 1(g)), as follows [22]:

$$A_{SYS} = \left(\sqrt{A_{SA}} - \sqrt{A_{LA}}\right)\left(\sqrt{A_{SiC}^{OLGS}} - \sqrt{A_{LA}}\right) \quad (4)$$

Eq. (4) makes it possible to envisage the engulfment or rejection of the nanoparticles approaching to the advancing solid/liquid (SA) interface based on the A_{SYS}. It has been proven before that the liquid metal mostly has a lower plasma frequency than that of solid metal [23], resulting in a higher Hamaker constant for solid metals (A_{SA}) compared to the liquid metals (A_{LA}). So, the higher engulfment of SiC nanoparticles in SPFG sample should be related to the higher Hamaker constant of them due to the graphene encapsulating process.

In this regard, it has been approved that coating a surface of a particle with another material can change the type of its interaction with surrounding surfaces, thereby reversing the sign of the interaction (i.e., to convert a repulsive interaction into an attractive one) [24]. So, in order to achieve a better insight into the effect of graphene sheets on manipulating the Hamaker constant of SiC nanoparticles, A_{SYS} was calculated based on the Lifshitz theory using Eq. (5) [25].

$$A = \frac{3}{4}KT\left(\frac{\varepsilon_{SiC}^{OLGS} - \varepsilon_{LA}}{\varepsilon_{SiC}^{OLGS} + \varepsilon_{LA}}\right)\left(\frac{\varepsilon_{SA} - \varepsilon_{LA}}{\varepsilon_{SA} - \varepsilon_{LA}}\right) + \frac{3h}{4\pi}\int_{\vartheta_{SiC}}^{\infty}\left(\frac{\varepsilon_{SiC}^{OLGS}(i\vartheta_n) - \varepsilon_{LA}(i\vartheta_n)}{\varepsilon_{SiC}^{OLGS}(i\vartheta_n) + \varepsilon_{LA}(i\vartheta_n)}\right)\left(\frac{\varepsilon_{SiC}^{OLGS}(i\vartheta_n) - \varepsilon_{LA}(i\vartheta_n)}{\varepsilon_{SiC}^{OLGS}(i\vartheta_n) + \varepsilon_{LA}(i\vartheta_n)}\right) \quad (5)$$

where ε is the static dielectric constants of the composite elements, (ε(iϑ)) is the value for ε at imaginary frequencies, and $\vartheta_n = (\frac{2\pi KT}{h})n$. As shown in Eq. (5), the static dielectric constant of pure SiC nanoparticles is not governing anymore in the Hamaker constant formulation, attributed to the fact that these particles were encapsulated by OLGS.

To calculate the Hamaker constant of SiC nanoparticles encapsulated by OLGS, the Hamaker constant was calculated for a system composing two graphene sheets with the specified thickness (δ) as a function of their distance (λ), when retardation effects are ignored, based on van der Waals–Casimir interaction [26,27] as follows:

$$A_{SiC}^{OLGS} = \frac{12\pi\lambda^2\varphi}{1 - \left(\frac{2\lambda^2}{(\lambda+\delta)^2} + \frac{\lambda^2}{(\lambda+2\delta)^2}\right)} \quad (6)$$

where φ is considered as the van der Waals–Casimir interaction free energy per unit area between two graphene sheets with the thickness of δ located on each other with separation distance of λ. Recent studies have demonstrated that graphene sheets have an opaque characteristic, alleviating the van der Waals forces (vdW) generated between nanoparticles and substrates, and the amount of this opacity can be increased by increasing the number of graphene sheets covering the substrate [11,12]. To this end, given the graphene thickness of 1 A°, $\varphi = 10^{17}$ (evm^{-2}) [28], and the separation distance of 0.35 nm, Eq. (6) registers value about 2.82 ev (387 zJ) for A_{SiC}^{OLGS} which is larger than 266 (zJ) pertinent to the Hamaker constant of the liquid aluminium [29], stimulating the engulfment of these particles within the advancing solid/liquid aluminium.

As shown in Fig. 2, yield (430 ± 3.2 MPa) and ultimate tensile strengths (556 ± 5.6 MPa) of the SPFG sample are significantly higher than those of the SPF sample by 181% (152 MPa ± 2.6) and 171% (205 MPa ± 4.7), respectively, ascribed to the unique formation of CG and NG regions within SPFG sample, as confirmed in Fig. 1(e–f), and the higher density of the SPFG sample (98%) compared to the lower value of the SPF sample (94%). Indeed, the enhanced tensile strength of the SPFG sample is attributed to the high densities of defects and cold deformation energy stored during cryomilling process, providing plentiful nucleation sites during reheating process to maintain the vast majority of grain in the NG regime, as shown in Fig. 1(e).

As shown in Fig. 2, elongation of the SPFG sample outperforms the one of the SPF sample, attributed to the CG regions prompting the higher strain hardening and prolonged ductility for uniform deformation at large strains. The excessive growth of CG regions, however, is inhibited by the formation of the network structure of the engulfed SiC nanoparticle within CG interior (black arrows in Fig. 1(e)).

The enhanced yield strength of the SPFG sample can be explained using the strengthening model (Eq. (7)) developed by the authors [30] via incorporating (1) Orowan strengthening by SiC nanoparticles encapsulated by OLGS (ω_{Orowan}^{OLGS}), (2) thermal enhanced dislocation density (ω_T), (3) geometrically necessary dislocations (GNDs) (ω_{GNDs}), (4) a modified shear-lag and (5) accumulative Hall–Petch effect ($\sigma_{Accumulative}^{Hall-Petch}$) into the model presented by Ramakrishnan [31].

$$\sigma_y^{SPFG} = \sigma_y^{SPF}(1+\omega_{Orowan}^{OLGS})(1+\omega_T)(1+\omega_{GNDs})(1+\omega_{NRAC}) + \sigma_{Accumulative}^{Hall-Petch}\left(\sigma_i + \frac{k}{\sqrt{D}}\right) \quad (7)$$

Putting M = 3, representing the Taylor factor for polycrystalline FCC alloys, G = 27 GPa [32], ϑ = 0.34 is Poisson's ratio [33], b the Burgers vector (2.84×10^{-10} m) [32], V_P the volume fraction of SiC nanoparticles (0.05) and d (45 nm) as a diameter of SiC nanoparticle, calculated using the average of at least 100 SiC nanoparticles in the HRTEM images, into Eq. (8) [34] results in $\omega_{Orowan}^{OLGS} = 1.18$.

$$\omega_{Orowan}^{OLGS} = \frac{MGb}{2\pi\sqrt{1-\vartheta}\,\sigma_y^{SPF}\left(\frac{0.779}{\sqrt{V_P}} - 0.785\right)d}\ln\frac{0.785\,d}{b} \quad (8)$$

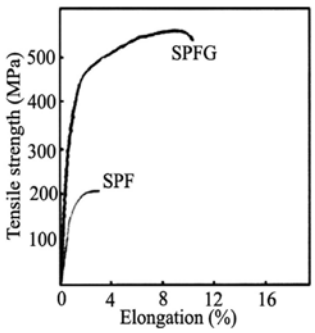

Fig. 2. Stress–strain curves of SPF and SPFG samples.

To determine the ω_T, the following model, devised based on the Taylor dislocation strengthening, was used [35].

$$\omega_T = \frac{\sqrt{3}\beta Gb}{\sigma_y^{SPF}}\sqrt{\frac{12V_p\Delta\alpha\Delta T}{bd}} \quad (9)$$

where $\beta(1.25)$ demonstrates the strengthening coefficient. $\Delta\alpha$ shows the difference between the thermal expansion coefficient of the aluminium and the graphene, ($\alpha_{Al} = 21.6 \times 10^{-6}/°C$ [36], $\alpha_{graphene} = -6 \times 10^{-6}/°C$ at 300 k [37]), and ΔT represents the difference between the fabrication temperature (564 °C) and the room temperature (25 °C). Replacing the noted values into Eq. (9) results in $\omega_T = 2.18$.

Eq. (10) was used to delineate the ω_{GND}, representing the effect of incompatibility between elastic modulus of the OLGS wrapping SiC nanoparticles and the aluminium matrix to produce geometrically necessary dislocations (GNDs) in front of statistically stored dislocations (SDDs), thereby augmenting the yield strength.

$$\omega_{GND} = \frac{\alpha Gb}{\sigma_y^{SPF}}\sqrt{\frac{8V_p\varepsilon_y}{bd}} \quad (10)$$

where α is the constant (1.25) and ε_y the yield strain (0.2%). Investigation of Eq. (10) using the aforementioned values demonstrates the strengthening contributor of about 0.49 for GNDs (ω_{GNDs}).

Fig. 3(a) demonstrates the cleavage fracture pattern manifested by propagation of crack through porous regions occupied by agglomerated SiC nanoparticles (white arrows), thereby deteriorating the tensile ductility of the SPF sample [38,39]. Given the uniform dispersion of SiC nanoparticles in the SPFG sample, however, the probability for cracking or interfacial decohesion of SiC nanoparticles is diminished, as shown in Fig. 3(b).

Additionally, the formation of nano-sized rod-shaped aluminium carbide (NRAC), i.e. Al_4C_3, at the interface of OLGS and DSGS was also detected, as illustrated by white arrows in Fig. 1(f), substantiated by selected area electron diffraction (SAED) pattern of specified region (upper inset) and high resolution TEM (HRTEM) picture, as shown in the bottom inset of Fig. 1(f).

The strengthening contribution manifested by the NRAC (ω_{NRAC}) can be measured using the following modified shear lag model [30,40].

$$\omega_l = \sqrt{\frac{2GL^2}{E_f\lambda_{eff}t}} \quad (11)$$

where λ_{eff} is an effective inter-particle spacing between the NRAC that can be replaced by the space between SiC nanoparticles encapsulated by OLGS using Eq. (12) [34], E_f and t are the young's modulus and thickness of NRAC, respectively.

$$d = \left(\frac{0.779}{\sqrt{V_P}} - 0.785\right)d \quad (12)$$

Putting the values of $G_m = 27$ GPa [32], L = 8 nm, t = 3 nm, $E_f = 1000$ GPa and $\lambda_{eff} = 121.44$ nm, calculated using Eq. (12), into Eq. (11) results in a ω_l value of 0.097 for the NRAC.

To calculate the $\sigma^{Hall-Petch}_{Accumulative}$ in Eq. (7), the σ_i, k and D define the intrinsic stress of the material ($\sigma_i = 15.7$ MPa), the material constant ($k = 0.068$ MPa$\sqrt{m}$) and grain size of NC (150 nm) and CG (1 μm) regions [41]. The calculated $\sigma^{Hall-Petch}$ for NC (191.2 MPa) and CG (83.7 MPa) regions was accumulated using the rule of mixtures based on the volume percentages of CG (23.2%) and NG (76.8%) regions, calculated using investigation of 50 TEM pictures of the SPFG sample. The calculated $\sigma^{Hall-Petch}_{Accumulative}$ has therefore shown 166.25 MPa augmentation in the yield strength of the SPFG sample due to grain size strengthening of the NC and CG regions.

Inserting the values achieved by Eqs. (8)–(11) into Eq. (7) approximates the yield strength of about 1846.2 MPa for the SPFG sample, which is significantly higher than the experimental result (430 ± 3.2 MPa).This can be attributed to the combination effect of the porosity, agglomeration of SiC nanoparticles not covered entirely by OLGS and a lower efficiency of Orowan strengthening in nano-sized grains.

The perfect bonding between SiC nanoparticles and matrix in the SPFG sample is attributed to the higher levels of plastic constraint that can be exerted by the NRAC, attributed to the exceptional negative thermal expansion coefficient of graphene ($-6 \times 10^{-6}/°C$ at 300 k [37]), thereby effectively prompting mechanical bonding, i.e. pinning, of the SiC nanoparticles to the matrix. This stimulates formation of microcracks in the matrix that can be deflected and hindered by a fibre (graphene) pull-out mechanism activated by the DSGS, as shown by white arrows in Fig. 3(b) and its upper-high magnification inset. Following the network structure of SiC nanoparticles (black arrows in Fig. 1(e)), the cracks propagated from NG regions can be inhibited by the CG region. The narrow and elongated CG regions (white circles in Fig. 3(b)) compared to the wider one in the as-fabricated state (white arrow in Fig. 1(e)) are due to the extensive plastic deformation exerted on these regions during tensile tests and higher capacity of these regions for strain hardening, sustaining the effective uniform deformation to large strains, as shown in Fig. 2.

As shown in the bottom inset of Fig. 3(b), DSGS surprisingly have unique functionalities not only in strengthening but also hampering the grain growth of the CG regions. Indeed, DSGS are more likely to be engulfed within CG regions, as shown by blue stars in Fig. 1(e), due to the large size of the CG regions compared to the NG regions. This, in turn, is resulted in crack bridging (white arrow in the bottom inset of Fig. 3(b)) activated mainly on the wake of the crack, and can be assisted by formation of carbon nanotubes as shown by green star in the bottom

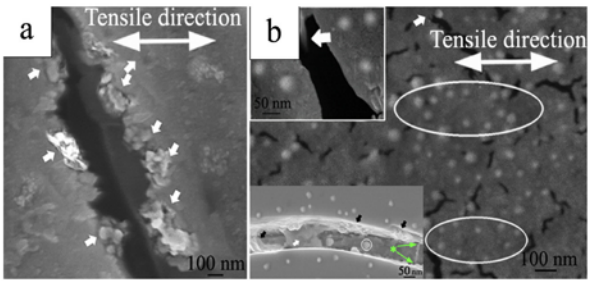

Fig. 3. Fracture-side view of (a) SPF and (b) SPFG samples.

inset of Fig. 3(b), to diminish the local stresses and strains essentially imparted at the crack tip, thereby reducing the crack propagation rate.

It has been approved that the formation of DSGS along with astonishing assembly of SiC nanoparticles encapsulated by inter-connected OLGS (white circle in the bottom inset of Fig. 3(b)) can also play an important role in imparting more restriction on the grain growth of aluminium grains by providing a diffusion barrier within grains [42]. Interestingly, as shown by black arrows in the bottom inset of Fig. 3(b), different slipping systems have been activated in the SPFG sample subjected to the axial tensile stress, attributed to the effect of graphene sheets in hampering the penetration of gliding dislocations within the matrix. These accumulated-blocked dislocations, however, can also pile up to another gliding system due to interfacial sliding, thereby significantly enhancing the ductility [43].

To recapitulate, this study reveals an unprecedented functionality of graphene sheets to manipulate the Hamaker constant of SiC nanoparticles, prompting higher engulfment of these particles within solidifying matrix. This, in turn, pieces together the superior tensile strength and ductility by conferring nano/micro grains on the microstructure, paving the way for manufacturing advanced metal matrix composites.

The authors would like to acknowledge the use of facilities within the University of Wollongong (UOW) Electron Microscopy Centre and especially the great assistance of Dr. Gilberto Casillas and Dr. Madeleine Strong Cincotta.

References

[1] R. George, K.T. Kashyap, R. Rahul, S. Yamdagni, Scr. Mater. 53 (2005) 1159–1163.
[2] R.Z. Valiev, M.Y. Murashkin, I. Sabirov, Scr. Mater. 76 (2014) 13–16.
[3] R.Z. Valiev, N.A. Enikeev, M.Y. Murashkin, V.U. Kazykhanov, X. Sauvage, Scr. Mater. 63 (2010) 949–952.
[4] C.W. Schmidt, C. Knieke, V. Maier, H.W. Höppel, W. Peukert, M. Göken, Scr. Mater. 64 (2011) 245–248.
[5] S. Tahamtan, A. Halvaee, M. Emamy, Z.Y. Jiang, A. Fadavi Boostani, Mater. Sci. Eng. A 619 (2014) 190–198.
[6] I. El-Mahallawi, H. Abdelkader, L. Yousef, A. Amer, J. Mayer, A. Schwedt, Mater. Sci. Eng. A 556 (2012) 76–87.
[7] M. Bastwros, G.-Y. Kim, C. Zhu, K. Zhang, S. Wang, X. Tang, X. Wang, Compos. Part B 60 (2014) 111–118.
[8] J. Visser, Adv. Colloid Interf. Sci. 3 (1972) 331–363.
[9] R.S. Edwards, K.S. Coleman, Nanoscale 5 (2013) 38–51.
[10] K.S. Novoselov, V.I. Falko, L. Colombo, P.R. Gellert, M.G. Schwab, K. Kim, Nature 490 (2012) 192–200.
[11] F. Mugele, Nat. Mater. 11 (2012) 182–183.
[12] A. Fadavi Boostani, R.T. Mousavian, S. Tahamtan, S. Yazdani, R.A. Khosroshahi, D. Wei, J.Z. Xu, D. Gong, X.M. Zhang, Z.Y. Jiang, Mater. Sci. Eng. A 648 (2015) 92–103.
[13] A. Fadavi Boostani, S. Tahamtan, Z.Y. Jiang, D. Wei, S. Yazdani, R. Azari Khosroshahi, R. Taherzadeh Mousavian, J. Xu, X. Zhang, D. Gong, Compos. A: Appl. Sci. Manuf. 68 (2015) 155–163.
[14] A. Fadavi Boostani, R. Taherzadeh Mousavian, S. Tahamtan, S. Yazdani, R. Azari Khosroshahi, D. Wei, J. Xu, X. Zhang, Z.Y. Jiang, Mater. Sci. Eng. A 653 (2016) 99–107.
[15] C. Faugeras, B. Faugeras, M. Orlita, M. Potemski, R.R. Nair, A.K. Geim, ACS Nano 4 (2010) 1889–1892.
[16] R.P. Joshi, P.G. Neudeck, C. Fazi, J. Appl. Phys. 88 (2000) 265–269.
[17] G.F. Bolling, J. Cissé, J. Cryst. Growth 10 (1971) 56–66.
[18] E.M. Agaliotis, M.R. Rosenberger, A.E. Ares, C.E. Schvezov, Procedia Mater. Sci. 1 (2012) 58–63.
[19] M.A. Khan, P.K. Rohatgi, Compos. Eng. 3 (1993) 995–1006.
[20] H. Hamaker, Physica 4 (1937) 1058–1072.
[21] J.N. Israelachvili, Intermolecular and Surface Forces: Revised Third Edition, Academic press, CA, 2011.
[22] G. Lefevre, A. Jolivet, in: H. Müller-Steinhagen, M.R. Malayeri, A.P. Watkinson (Eds.),Proceedings of International Conference on Heat Exchanger Fouling and Cleaning 2009, pp. 120–124.
[23] R. Egerton, Electron Energy-Loss Spectroscopy in the Electron Microscope, Springer Science & Business Media, 2011.
[24] D.C. Prieve, W.B. Russel, J. Colloid Interface Sci. 125 (1988) 1–13.
[25] E. Lifshitz, Sov. Phys. JETP 2 (1956) 73–83.
[26] M. Bordag, G.L. Klimchitskaya, U. Mohideen, V.M. Mostepanenko, Advances in the Casimir Effect, Oxford University Press, Oxford, 2009.
[27] V.A. Parsegian, Van der Waals Forces: A Handbook for Biologists, Chemists, Engineers, and Physicists, Cambridge University Press, New York, 2005.
[28] J. Sarabadani, A. Naji, R. Asgari, R. Podgornik, Phys. Rev. B 84 (2011) 155407.
[29] X. Chen, A. Levi, E. Tosatti, Surf. Sci. 251 (1991) 641–644.
[30] A. Fadavi Boostani, S. Yazdani, R. Taherzadeh Mousavian, S. Tahamtan, R. Azari Khosroshahi, D. Wei, D. Brabazon, J.Z. Xu, X.M. Zhang, Z.Y. Jiang, Mater. Des. 88 (2015) 983–989.
[31] N. Ramakrishnan, Acta Mater. 44 (1996) 69–77.
[32] I. Gutierrez-Urrutia, M.A. Muñoz-Morris, I. Puertas, C. Luis, D.G. Morris, Mater. Sci. Eng. A 475 (2008) 268–278.
[33] Y.T. Zhao, S.L. Zhang, G. Chen, X.N. Cheng, C.Q. Wang, Compos. Sci. Technol. 68 (2008) 1463–1470.
[34] J.F. Nie, Scr. Mater. 48 (2003) 1009–1015.
[35] C.S. Goh, J. Wei, L.C. Lee, M. Gupta, Acta Mater. 55 (2007) 5115–5121.
[36] J.R. Davis, Aluminum and Aluminum Alloys, ASM international, OH, 1993.
[37] W. Bao, F. Miao, Z. Chen, H. Zhang, W. Jang, C. Dames, C.N. Lau, Nat. Nanotechnol. 4 (2009) 562–566.
[38] A. Fadavi Boostani, S. Tahamtan, Trans. Nonferrous Metals Soc. China 20 (2010) 1608–1614.
[39] A. Fadavi Boostani, S. Tahamtan, J. Alloys Compd. 481 (2009) 220–227.
[40] V.C. Nardone, K.M. Prewo, Scr. Metall. 20 (1986) 43–48.
[41] M. MA, K. CHAWLA, in, Prentice-Hall, Englewood Cliffs, New Jersey, 1984.
[42] D. Lahiri, E. Khaleghi, S.R. Bakshi, W. Li, E.A. Olevsky, A. Agarwal, Scr. Mater. 68 (2013) 285–288.
[43] Y. Kim, J. Lee, M.S. Yeom, J.W. Shin, H. Kim, Y. Cui, J.W. Kysar, J. Hone, Y. Jung, S. Jeon, Nat. Commun. 4 (2013) 1–7.

Chapter 7 Strengthening mechanisms of graphene sheets in aluminium matrix nanocomposites

7.1 Statement

As shown in the past Chapters 3-6, one of the most important aspects of utilizing graphene sheets within aluminium matrix composites is the capability of them in enhancing the mechanical properties, but theoretical approaches used to generate the strengthening mechanisms of graphene sheets in the last chapters have not been explained completely so far. This chapter, therefore, aims to provide a new insight into the theoretical calculations implemented to generate the aforementioned strengthening mechanisms making use of Orowan, Hall-Petch, shear lag and thermal enhanced dislocation strengthening mechanisms. To this end, the analytical model devised in this study, demonstrating the significant role of shear lag and thermally activated dislocation mechanisms in strengthening aluminium metal matrix composites due to the exceptional negative thermal expansion coefficient of graphene sheets. This triggers the pinning capacity of nano-sized rod-liked aluminium carbide, prompting strong interface bonding for SiC nanoparticles with the matrix, thereby enhancing tensile elongation. Regarding experimental procedure implemented in this chapter, SiC nanoparticles encapsulated by graphene sheets were ball milled with aluminium powder, and the milled powder was incorporated within liquid aluminium using stir casting process. The stirred aluminium melt was subjected to the deformation at semi-solid range, i.e. thixoforming, to produce balk composites with minimum porosity. This, in turn, provides a good opportunity to investigate the uncertainty of the devised strengthening model in predicting the mechanical properties of the produced composites. To have a better insight into the effect of graphene sheets in generation of strengthening dislocations such as thermal activated dislocations and distribution of SiC nanoparticles, micro/nano structure of the produced composites was investigated using high resolution transmission electron microscopy (HRTEM) and Field emission scanning electron microscopy (FE-SEM).

Materials and Design 88 (2015) 983–989

Contents lists available at ScienceDirect

Materials and Design

journal homepage: www.elsevier.com/locate/jmad

Strengthening mechanisms of graphene sheets in aluminium matrix nanocomposites

A. Fadavi Boostani [a], S. Yazdani [b], R. Taherzadeh Mousavian [b], S. Tahamtan [c], R. Azari Khosroshahi [b], D. Wei [d], D. Brabazon [e], J.Z. Xu [c], X.M. Zhang [c], Z.Y. Jiang [a,f,*]

[a] School of Mechanical, Materials and Mechatronic Engineering, University of Wollongong, NSW 2522, Australia
[b] Faculty of Materials Engineering, Sahand University of Technology, Tabriz, Iran
[c] State Key Laboratory of Rolling and Automation, Northeastern University, Shenyang, Liaoning 110004, China
[d] School of Electrical, Mechanical and Mechatronic Systems, University of Technology, Sydney, NSW 2007, Australia
[f] School of Materials and Metallurgy, University of Science and Technology, Liaoning, Anshan 114051, China
[e] Advanced Processing Technology Research Centre, School of Mechanical & Manufacturing Engineering, Dublin City University, Dublin 9, Ireland

ARTICLE INFO

Article history:
Received 27 May 2015
Received in revised form 10 September 2015
Accepted 11 September 2015
Available online 14 September 2015

Keywords:
Metal matrix composites
Graphene sheets
Strengthening mechanisms
Fracture
Ductility

ABSTRACT

Uniform dispersion of SiC nanoparticles with a high propensity to agglomerate within a thixoformed aluminium matrix was attained using a graphene encapsulating approach. The analytical model devised in this study has demonstrated the significant role of shear lag and thermally activated dislocation mechanisms in strengthening aluminium metal matrix composites due to the exceptional negative thermal expansion coefficient of graphene sheets. This, in turn, triggers the pinning capacity of nano-sized rod-liked aluminium carbide, prompting strong interface bonding for SiC nanoparticles with the matrix, thereby enhancing tensile elongation.

1. Introduction

Metal matrix nano-composites (MMNCs) strengthened with ceramic nanoparticles outperform the disadvantages associated with the conventional metal matrix composites (MMCs) because of the enhanced mechanical and electrical properties and the diminished coefficient of thermal expansion and friction [1]. This makes MMNCs an appropriate candidate to be employed in advanced industries such as automobile, aerospace and thermal management [1,2].

Enhancing the tensile elongation of aluminium metal matrix composites (AMMCs) reinforced with ceramic nanoparticles, however, is a challenging task via both solid and liquid processing routes. This is attributed to the large surface-to-volume ratio and poor wettability, prompting a high degree of particulate agglomeration and imperfect interface bonding of these nanoparticles with the surrounding matrix, respectively [3,4].

Different methods have been suggested to overcome this problem, including semi-solid stirring [5] and ball milling with ultrasonic treatment [6] but they have not been very successful. This is attributed to the fact that they have mainly concentrated on the deagglomeration of nanoparticles when they are mixing with the metallic alloy during the manufacturing process rather than in their as-received state, diminishing the efficiency of the process due to the lower wettability of these nanoparticles with most metal matrices [5,7,8]. Most importantly, these studies suffer from exploiting thermal models to predict the interaction of the nanoparticles with the solid/liquid interface during solidification.

Thixoforming is defined as a two-step process encompassing the preparation of a feed stock material with a thixotropic characteristic, followed by reheating the feed stock material to a semi-solid temperature in order to provide the semi-solid slurry which is then subjected to the deformation process [9–11]. This process, unlike the preceding ones, is better able to alleviate the agglomeration of the nanoparticles due to the lower mobility of these particles within the highly viscous metallic matrix during the manufacturing process, but this process by itself is still immature to effectively deagglomerate nanoparticles.

It has been reported that graphene sheets possess the unique feature of having a two-dimensional shell(s) which can nucleate and anchor nano-particles on the edges and surface [12,13]. Authors have shown [14] that graphene nanosheets (GNSs) can confer on nanoparticles the unique capacity to resist being repelled by the advancing solid/liquid interface during solid and liquid processing routes. The ability of graphene sheets to alleviate the agglomeration of nano-particles during solid and

* Corresponding author.
E-mail addresses: afb496@uowmail.edu.au (A. Fadavi Boostani), jiang@uow.edu.au (Z.Y. Jiang).

http://dx.doi.org/10.1016/j.matdes.2015.09.063
0264-1275/

liquid processing for the production of meal matrix composites, however, has hitherto not been reported.

Apart from this promising feature, to date, the actual enhancement in the thermal conductivity of SiC nanoparticles wrapped by graphene sheets and the strengthening mechanisms of graphene sheets are not well understood. This study, therefore, aims to investigate how the strengthening mechanisms of Orowan, Hall–Petch, shear lag and thermal enhanced dislocation relate to graphene reinforced AMMCs. To reach a more reliable strengthening model the thixoforming process, including forming an alloy in a semi-solid region with thixotropic behaviour, was utilized to diminish the detrimental effects of porosity associated with as-cast samples.

2. Materials and methods

In order to prepare composite powder, i.e. preform, used for the fabrication of A357 thixoformed samples, a powder metallurgy process was utilized. This was conducted using a mixture containing SiC nanoparticles (45 nm, supplied by Nanostructured & Amorphous Materials, Inc.), graphene nanosheets (GNSs) with the average lateral size of 550 nm (supplied by Graphene Supermarket) as reinforcements and high purity aluminium powder (45 μm, supplied by Alpha Aesar Company with 99.5% purity).

A Fritsch Pulverisette P5 planetary machine was used for ball milling without interruption under high purity (99.999%) argon gas in a liquid nitrogen environment (cryomilling) added constantly to compensate for evaporation. The stainless steel vial was sealed with an elastomeric O ring. The stainless steel balls to powder weight ratio was 15:1, and the rotation rate of the vial was 250 rpm under a total milling time of 2 h. The amount of GNSs and SiC nanoparticles was adjusted to 83 wt.% SiC and 17 wt.% graphene. These components were milled for 0.5 h without aluminium powder. Subsequently, the milling was continued for 1.5 h by adding aluminium powder to the mixture containing graphene and SiC, by setting the aluminium weight equal to 45 wt.% of the total SiC and graphene powders, in order to enhance the incorporation of the SiC nanoparticles into the molten aluminium. The prepared powder was then injected into molten A357 aluminium alloy in an atmosphere controlled with high purity (99.999%) argon gas (6 l/min) in the semi-solid state. Table 1 demonstrates the chemical composition of the A357 alloy used in this study.

SiC nanoparticles with two different processing histories were used including (i) as received SiC nanoparticles and (ii) SiC nanoparticles encapsulated by graphene sheets (prepared, as noted above, by the milling process). After the entire alloy in the crucible was melted, it was cooled to 605 °C and held at this temperature with a solid fraction of about 0.30 [15]. The stirring process was conducted on the semi-solid alloy (using a graphite impeller) at 400 rpm associated with uniform adding of prepared powders over a time period of approximately 5 min associated with adding 1 wt.% Mg as a wetting agent. A non-contact ultrasonic process was then implemented during casting using an ultrasonic chamber (Bandelin-Germany Make – Model: RK – 100 H), which can vibrate at a frequency of 35 kHz. After the completion of particle feeding, mixing was continued for an extra 1 min. Finally, the composite slurry was poured into a pre-heated cast iron mould using a bottom-pouring system to prepare the semi-solid billet. The thixoforming process was conducted on the prepared billets based on the procedure described by S. Kandemir at a fabrication temperature of 580 °C, i.e. $T_{Fabrication}$, with continuous application of thixoforming pressure to room temperature, i.e. $T_{test} = 25$ °C [16]. Table 2 represents a nomination system used to identify different specimens in the rest of this paper.

Table 1
Chemical composition of A357 alloy used in this study (wt.%).

Al	Si	Fe	Cu	Mn	Mg	Zn	Ti
Bal.	7.0	<0.2	<0.2	<0.1	<0.3	<0.1	<0.2

Table 2
Nomination system of the specimens.

Name used in the paper	Different treatment applied on samples		
	Thixoforming	Graphene	Incorporation of SiC
A357	–	–	–
Thix	*	–	*
GThix	*	*	*

The density of the samples was measured by the Archimedes method for at least three different samples in order to calculate the porosity of the samples. TEM analysis was performed using a Philips CM200 at an accelerating voltage of 200 kV. Fractographic investigations were conducted using field emission scanning electron microscopy (FE-SEM) performed in a JEOL JSM-7500FA. Tensile properties were measured using a Hounsfield universal test machine at a cross-

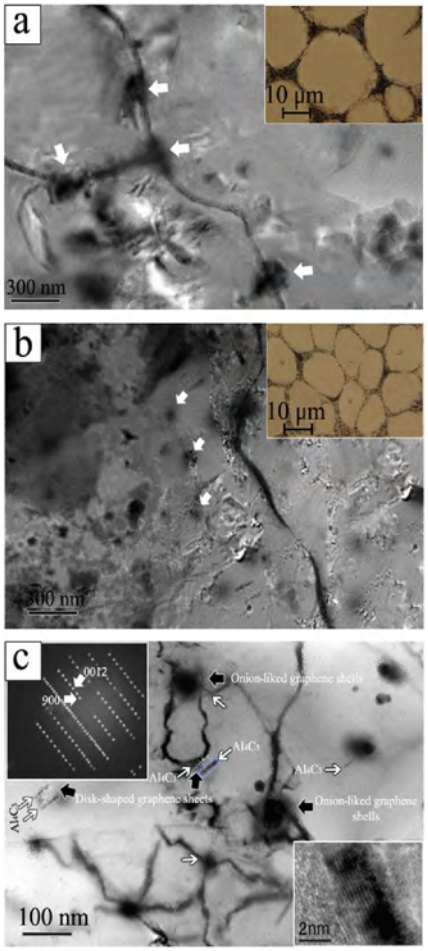

Fig. 1. TEM micrographs of (a) Thix sample, (b) GThix samples associated with corresponding optical images as insets and (c) the high magnification image of the GThix sample accompanied by the selected area diffraction (SAD) pattern of the rectangular area.

head speed of 0.5 mm s^{-1} for at least three samples in order to confirm the repeatability of the measurements.

3. Results and discussion

Fig. 1 demonstrates TEM images captured from the nanostructure of (a) Thix, (b) GThix and (c) the high magnification image of the GThix sample accompanied by the selected area diffraction (SAD) pattern of the rectangular area.

As shown by arrows in Fig. 1(a), although SiC nanoparticles in the Thix sample are agglomerated at the grain boundaries, they are mostly engulfed within the grain interior in the GThix sample, as demonstrated in Fig. 1(b).

In Fig. 1(c), graphene sheets appear in the GThix sample with two different morphologies: onion like graphene shells (OLGS) and disk-shaped graphene sheets (DSGS). There is also some evidence for the formation of nano-sized rod-shaped aluminium carbide (NRAC) at the interface of the OLGS and the DSGS with the aluminium matrix, as shown by white arrows in Fig. 1(c). This has also been confirmed by the selected area diffraction (SAD) pattern of the rectangular region in Fig. 1 (c) and high resolution TEM (HRTEM) picture as demonstrated in the bottom inset of Fig. 1(c).

The white arrows demonstrate the location where the reaction for the formation of NRAC is started at the damaged regions of the graphene sheets. The formation of NRAC is known to occur between the aluminium and the defective regions of the graphene sheets and can be expressed by the following chemical reaction scheme:

$$4Al_{(l)} + 3C_{(s)} \rightarrow Al_4C_3. \quad (1)$$

There is, however, no evidence for the formation of NRAC in the Thix sample and this is attributed to the lower temperature (580 °C) used for manufacturing this sample. It has been reported that without any external source of carbon, the reaction for the formation of Al_4C_3 can occur between SiC reinforcements and molten aluminium using the following reaction:

$$4Al_{(l)} + 3SiC_{(s)} \rightarrow Al_4C_3 + 3Si. \quad (2)$$

The change in free energy (ΔG) for this reaction is given by the following equation [17]:

$$\Delta G\left(J\ mol^{-1}\right) = 113{,}900 - 12.06T\ln T + 8.92 \times 10^{-3}T^2 + 7.53 \times 10^{-4}T^{-1} + 21.5T + 3RT\ln(a_{Si}) \quad (3)$$

where a_{Si} is the silicon chemical activity in molten aluminium, R the universal gas constant and T the absolute temperature (K). Eq. (3) registers a negative value for ΔG when the temperature exceeds 727 °C (1000 K) which is higher than the processing temperature of the Thix sample.

It has been asserted qualitatively that the SiC nanoparticles encapsulated by OLGS, as shown in Fig. 1(c), have a high tendency to be engulfed within the grain interior and this has been ascribed to the enhanced thermal conductivity of these particles [14].

The model presented in Eq. (4) predicts that particles with higher thermal conductivity are more prone to be engulfed within grains rather than being agglomerated at grain boundaries. The subscripts p and l refer to properties of the particles and the liquid, respectively.

$$K_P > K_l \text{ for engulfment} \quad (4)$$

The following model (Eq. (5)) was built based on heat diffusivity [18] characteristics using thermal conductivity (K), specific heat (c_p) and density (ρ):

$$\sqrt{\frac{K_P \cdot \rho_P \cdot C_P^P}{K_l \cdot \rho_l \cdot C_p^l}} > 1 \text{ for engulfment.} \quad (5)$$

The aforementioned model demonstrate that augmenting the thermal conductivity of particles results in increasing the possibility of their entrapment within grain boundaries due to the change of the interface shape from convex to concave [19–22].

It is also postulated that SiC nanoparticles encapsulated by graphene shells have higher thermal conductivity than the ones not wrapped by graphene shells [23,24]. This is attributed to the fact that the thermal conductivity of graphene shells on SiC nanoparticles is better conserved in bilayer and trilayer GNSs than in single layer GNSs [25].

The insets in Fig. 1 show the optical images of (a) Thix and (b) GThix samples, respectively. Image analysis results have shown a considerable reduction in the grain size of the GThix samples (D = 14 μm) compared with the Thix samples (D = 30 μm), substantiating the refining effect of well-dispersed SiC nanoparticles in the GThix sample rather than thixoforming pressure in the Thix sample. Fig. 2 shows the stress–strain curves of samples studied associated with schematic pictures representing their real microstructure. As can be seen from Fig. 2, the graphene encapsulating process has enhanced significantly the tensile properties of the PGT samples.

Table 3 represents the tensile properties and porosity content of the samples resulting from the analysis of different samples. According to Table 3, the yield strength (σ_{YS}) and ultimate tensile strength (σ_{UTS}) of the GThix sample are considerably higher than the Thix sample by 81% and 60%, respectively, and this is ascribed to the uniform distribution of SiC nanoparticles and the lower porosity of this sample.

Fig. 3(a) represents the cleavage fracture surface of the Thix sample which is attributed to the agglomeration of SiC nanoparticles in this sample, as shown by arrows.

This agglomeration increases the probability of particle cracking associated with a higher crack propagation rate due to the settlement of these particle at the grain boundaries, thereby diminishing the ductility.

Fig. 3(b), in contrast, shows that well-dispersed SiC nanoparticles in the GThix sample are not prone to cracking or interfacial decohesion. The former is attributed to the lower possibility of cracking associated with nanoparticles and the latter can be attributed to the higher levels of plastic constraint exerted by the NRAC formed at the interface of OLGS and DSGS with aluminium, as shown by arrows in Fig. 1(c) and in the bottom inset of Fig. 3(b), respectively. The aforementioned plastic constraint is fortified by the expansion of OLGS and DSGS during solidification due to the exceptional negative thermal expansion coefficient of graphene, thereby effectively prompting the mechanical bonding, i.e. pinning, of the SiC nanoparticles to the matrix.

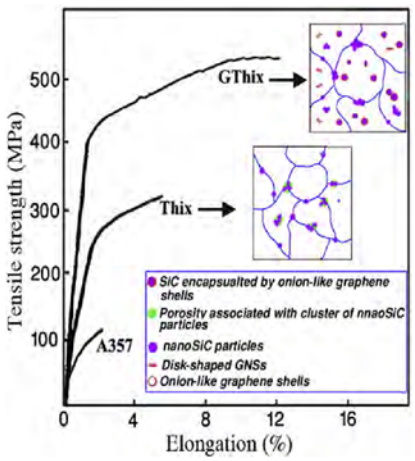

Fig. 2. Stress–strain curve of A357, Thix and GThix samples accompanied with schematic illustration of their nanostructures.

Table 3
The average values of yield stress (σ_{YS}), ultimate tensile strength (σ_{UTS}), total elongation (E%) and porosity content of samples.

Samples	σ_{YS}	σ_{UTS}	Elongation (E%)	Porosity (%)
A357	75 ± 2	125 ± 3	2 ± 0.3	3 ± 0.1
Thix	221 ± 7	326 ± 10	5.4 ± 0.3	0.9 ± 0.2
GThix	401 ± 11	523 ± 13	12.1 ± 0.5	0.5 ± 0.2

±: Represents 95% confidence interval.

Table 4
Physical and mechanical properties of materials [27–30].

Parameter	Unit	Al	SiC	Graphene
Burgers vector (b)	nm	0.25	–	Not fixed
Thermal expansion coefficient (α)	$\times 10^{-6}$/°C	21.4	4.3	−6
Shear modulus (G)	MPa	25	–	250
Young modulus (GPa)	GPa	70	427	1000
Poisson ratio	–	0.35	0.17	0.16
Taylor factor (M)	–	3	–	–

These, in turn, trigger matrix cavitation through the aluminium matrix, postponed to higher strain fields, i.e. prolonged ductility. To have a better insight into the degree of strain imposed on the NRAC nucleated at the interface of SiC nanoparticles encapsulate by graphene sheets and an aluminium matrix, Eq. (6) was developed by J. F. Nye [26] to calculate the strain value exerted on the interface due to the mismatch between the thermal coefficient expansion between the graphene and surrounding aluminium matrix:

$$\varepsilon^{T} = \int_{T_R}^{T_F} (\alpha_M - \alpha_G) dT \approx \Delta\alpha\Delta T \tag{6}$$

where T_F, T_R, ΔT, α_m and α_G represent the fabrication temperature (580 °C), room temperature (25 °C), difference between the fabrication temperature and room temperature, thermal expansion coefficient of matrix and graphene sheets, respectively. Table 4 lists the pertinent physical and mechanical properties of the composite constituents.

Having considered Eq. (6) using the values noted in Table 4, it is clear that SiC nanoparticles encapsulated by graphene sheets can impose more plastic strain on the NRAC, nucleated on the interface of graphene sheets and the aluminium matrix, compared to the SiC nanoparticles not wrapped by graphene sheets, thereby augmenting their pinning capacity.

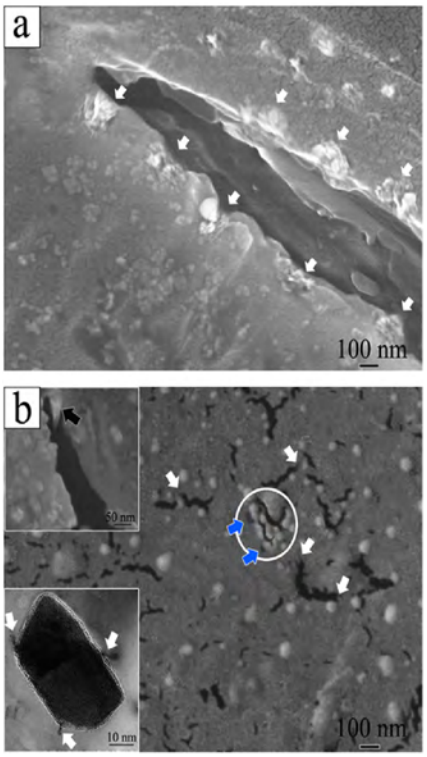

Fig. 3. Fracture side-view of (a) Thix and (b) GThix samples.

The progressive propagation of cracks via the microvoid coalescence mechanism is also deflected and hindered by a fibre (graphene) pull-out mechanism activated by the DSGS, as shown by white arrows in Fig. 3(b) and the top inset of Fig. 3(b). Some SiC nanoparticles in the GThix sample, however, are agglomerated with a high tendency to cracking, as shown by the white circle in Fig. 3(b), promoting cracking that can be blocked by the graphene pull-out mechanism.

This study aims at presenting a new analytical model (Eq. (7)) by incorporating a modified shear-lag model (continuum mechanics approach) and an enhanced dislocation density model (micromechanics strengthening approach) into the model proposed by Ramakrishnan [31], as the latter generally is used for micron-sized particles.

$$\sigma_y^{GThix} = \sigma_y^{Thix}\left(1+\omega_L^{DSGS}\right)\left(1+\omega_T\right)\left(1+\omega_{Orowan}^{DSGS}+\omega_{Orowan}^{OLGS}\right) + \sigma_y^{Hall-Petch}\left(\sigma_i + \frac{k}{\sqrt{D}}\right) \tag{7}$$

Eq. (7) takes into account the strengthening effects of graphene sheets, manifested in the form of load bearing (ω_L), thermal enhanced dislocation density (ω_T), and the Orowan (ω_{Orowan}), and Hall–Petch mechanisms, on the yield strength of the Thix sample (σ_y^{Thix}) in order to approximate the yield strength of the GThix sample (σ_y^{GThix}).

Regarding Hall–Petch strengthening, the σ_i, k and D define the intrinsic stress of the material (σ_i = 15.7 MPa) and k is the material constant (k = 0.068 MPa/$M^{0.5}$) for aluminium [32]. The Hall–Petch relationship has shown a 33.87 MPa enhancement in the yield strength of the GThix sample due to the refining effect of SiC nanoparticles encapsulated by graphene sheets. To have a subtle approximation of σ_y^{GThix}, it is crucial to determine strengthening contributors including ω_L, ω_T, ω_{Orowan}^{DSGS} and ω_{Orowan}^{OLGS} in Eq. (7).

It is generally agreed that the load transfer from the ductile matrix to the hard reinforcements (i.e. ceramic and graphene) under an applied external load contributes to the strengthening of the base material according to the modified shear lag model proposed by Nardone and Prewo [33]. To investigate the concept of load transfer from the composite matrix to the embedded DSGS and OLGS, the classical shear lag model [34] was used. For this reason the two-dimensional elastic configuration was considered for a platelet of length L, thickness t and elastic modulus E, bonded to a matrix material of thickness λ.

The stress–strain relation along the axial direction of the platelet is $\sigma_f = E\varepsilon_f$, where σ_f denotes the axial stress and ε_f the axial strain in the platelet. The equilibrium of the forces along the length of the platelet is achieved using Eqs. (8) and (9).

$$\tau_p dx = -td\sigma_f \tag{8}$$

$$\frac{\tau_p}{t} = -\frac{d\sigma_f}{dx} \tag{9}$$

It is supposed that the matrix surrounding the graphene platelet can be displaced (δ) in the z direction and the shear strain (γ) is calculated

using following Eq. (10).

$$\gamma = \frac{d\delta}{dz} \tag{10}$$

Having considered the shear stress modulus of the matrix, Eq. (10) can be rewritten in the form of Eq. (11) under the assumption that the shear stress of the matrix is transferred to the graphene platelet ($\tau = \tau_p$) via the graphene/matrix interface, as long as this interfacial bonding is perfect, which seems reasonable because of the negative thermal expansion coefficient of the graphene, as shown in Table 2.

$$\frac{d\delta}{dz} = \frac{\tau_p}{G_m} \tag{11}$$

where G_m represents the shear modulus of the matrix, i.e. aluminium. The integration of Eq. (11) using the boundary conditions of ($z = \frac{t}{2}$ at $\delta = \delta_f$) and ($z = \frac{\lambda}{2}$ at $\delta = \delta_\lambda$) results in Eq. (12).

$$\delta_\lambda - \delta_f = \left(\frac{\tau}{2G_m}\right)(\lambda - t) \tag{12}$$

To approximate the strain of the graphene platelet and the surrounding matrix, displacements in Eq. (12) can be converted to strain by considering that $e_f = \frac{d\delta_f}{dx}$ and $e_m = \frac{d\delta_m}{dx}$. So, differentiating Eq. (12) with respect to x, using Eq. (9) and the noted strains (e_f and e_m), results in Eq. (13):

$$e_f - e_m = \left(\frac{t\lambda}{2G_m}\right)\left(\frac{d^2\sigma_f}{dx^2}\right). \tag{13}$$

By considering that generally $\lambda >> t$ and multiplying Eq. (13) by E_f, Eq. (13) can be written in the form of Eq. (14):

$$\frac{d^2\sigma_f}{dx^2} = \left(\frac{n^2}{t^2}\right)(\sigma_f - e_m E_f). \tag{14}$$

In this equation, n can be defined as $n = \sqrt{\frac{2G_m}{E_f}\left(\frac{1}{\lambda}\right)}$. Then the general solution for this differential equation can be written as:

$$\sigma_f = E_f e_m + C\sinh\left(\frac{nx}{t}\right) + D\cosh\left(\frac{nx}{t}\right). \tag{15}$$

Using the boundary conditions that if $x = 0$, then $\sigma_f = E_f e_m$ and if $x = \pm\frac{L}{2}$, then $\sigma_f = 0$, the constants C and D for Eq. (15) are achieved. Hence, the final solution of Eq. (15) can give the stress distribution along the length of the graphene platelet as Eq. (16):

$$\sigma_f = E_f e_m\left[1 - \frac{\cosh\left(\frac{nx}{t}\right)}{\cosh\left(\frac{nL}{2t}\right)}\right]. \tag{16}$$

Additionally using Eq. (16) the interfacial shear stress for the graphene platelet can be calculated according to Eq. (17):

$$\tau_p = nE_f e_m\left[\frac{\sinh\left(\frac{nx}{t}\right)}{\cosh\left(\frac{nL}{2t}\right)}\right]. \tag{17}$$

Having considered the aspect ratio of the graphene plate and the matrix strain (e_m), let ($s = \frac{L}{t}$), Eq. (16) and (17) can be rewritten in the following forms [35]:

$$\sigma_f = E_f e_m\left[1 - \frac{\cosh\left(ns\frac{x}{L}\right)}{\cosh\left(\frac{ns}{2}\right)}\right] \tag{18}$$

$$\tau_p = nE_f e_m\left[\frac{\sinh\left(s\frac{x}{L}\right)}{\cosh\left(\frac{ns}{2}\right)}\right]. \tag{19}$$

Therefore, the maximum load transfer from the matrix to the graphene platelet is attainable for the composite with the higher value of ns. To reach this, it is necessary to reduce the distance between the graphene platelets (λ) and simultaneously diminish their thickness, as thickness (t) affects the n with square root but it has an inverse relationship with S ($S = L / t$). At this stage, it is also necessary to introduce a new parameter to correlate the ns value of the graphene platelet with the load-bearing improvement factor (ω_l) affected mainly by the volume fraction of the reinforcements [31]. To find the ω_l value, it is imperative to ascertain the inter-particle spacing, as a function of the total graphene volume fraction (V_{Gr}). Hence, the ω_l parameter is defined as:

$$\omega_l = \sqrt{\frac{2G_m L^2}{E_f \lambda_{eff} t}} \tag{20}$$

where λ_{eff} is an effective inter-particle spacing between the graphene sheets within the matrix, and can be calculated using Eqs. (21) and (22) [36]:

$$\lambda_{eff}^{DSGS} = 0.931\sqrt{\frac{0.306\pi dt}{V_{Gr}^{DSGS}}} - \frac{\pi d}{8} - 1.061t \tag{21}$$

where d, t and V_{Gr}^{DSGS} is the length, thickness and volume fraction of DSGS, respectively, and is measured by image analysis of at least 20 HRTEM micrographs.

Putting the values of $t = 10$ nm, $\lambda_{eff} = 427$ nm (calculated by Eq. (21)) and the values provided in Table 2 into Eq. (20) results in $\omega_l = 0.15$ for DSGS.

It should be noted that the V_{Gr}^{DSGS} and V_{Gr}^{OLGS} have been set to 0.18% and 0.82% of the total volume of the graphene ($V_{Gr} = 0.01$) added as a raw material, respectively, and is measured along with other microstructural features such as L and t using image analysis of at least 20 HRTEM micrographs. The aforementioned calculations represent the significant effect of OLGS on load transfer and the subsequent strengthening the aluminium matrix compared to DSGS due to the lower thickness and angled formation of the NRAC in the former, fortifying the pinning and thereby the load transfer from the matrix to the SiC nanoparticles.

According to Table 2, exceptional difference in the thermal expansion coefficient of graphene compared to aluminium can significantly strengthen the aluminium matrix by generating thermally induced dislocation, as shown in Fig. 1(c), reaffirmed by a high strengthening contributor (ω_T) calculated by Eq. (22) [37].

$$\omega_T = \frac{1.25G_m b}{\sigma_y^{Thix}}\sqrt{\frac{12(T_{Fabrication} - T_{test})(\alpha_m - \alpha_{Gr})V_{Gr}}{bd_{Gr}(1 - V_{Gr})}} \tag{22}$$

Eq. (22) can be solved based on the values presented in Table 2, V_{Gr} is the total volume fraction of the graphene encompassing the graphene sheets and the shells encapsulating the SiC nanoparticles (0.01), d_{Gr} is related to the average diameter of the graphene sheets and shells within the aluminium matrix (45 nm), and σ_y^{Thix} is the yield strength of the Thix sample (221 MPa), resulting in $\omega_T = 0.42$.

To determine the strengthening contribution of DSGS and the OLGS under the Orowan strengthening mechanism, two different models can be utilized [36].

$$\omega_{Orowan}^{DSGS} = \frac{MGb}{2\pi\sqrt{1-\vartheta}\sigma_y^{Thix}} \left(\frac{1}{0.931\sqrt{\frac{0.306\pi dt}{V_{Gr}^{Disc}}} - \frac{\pi d}{8} - 1.061t} \right) \ln \frac{1.225t}{b} \quad (23)$$

$$\omega_{Orowan}^{OLGS} = \frac{MGb}{2\pi\sqrt{1-\vartheta}\sigma_y^{Thix}\left(\frac{0.779}{\sqrt{V_{Gr}^{Onion}}} - 0.785 \right) d} \ln \frac{0.785d}{b} \quad (24)$$

The investigation of Eq. (23) and (24) using the values provided in Table 2, V_{Gr}^{DSGS} (0.0018), V_{Gr}^{OLGS} (0.0082), d (45 nm) and t (10 nm) which are the average diameter and thickness of at least 60 DSGS and OLGS measured using HRTEM analysis, respectively, gives the values of 0.13 and 0.23 for ω_{Orowan}^{DSGS} and ω_{Orowan}^{OLGS}, respectively. It should be noted that V_{Gr}^{DSGS} (0.0018) and V_{Gr}^{OLGS} (0.0082) are the effective volume fractions of the DSGS and the OLGS calculated based on image analysis of 20 HRTEM micrographs, respectively. This shows the greater role of the OLGS as compared to the DSGS. This discrepancy is attributed mainly to the orientation in which the DSGS interact with active slip planes during the deformation process. This can be ascribed to the fact that the DSGS are assumed to have a habit plane perpendicular to the slip plane of the aluminium (111) in Eq. (23). In practice, however, some DSGS lie on the slip plane of the aluminium matrix, resulting in lower interaction between the DSGS and dislocation gliding on the matrix slip plane.

Fig. 4 shows the strengthening contributor values corresponding to different strengthening mechanisms, as calculated in the preceding equations, demonstrating the major role of thermally activated dislocation mechanism in augmenting the yield strength compared to the other strengthening mechanisms. As shown in Fig. 4, OLGS are stronger in strengthening aluminium matrix compared to the DSGS, attributed to the circular morphologies of these graphene sheets, thereby increasing the density of dislocation more effectively compared to the DSGS.

By inserting the calculated values: $\omega_L^{DSGS} = 0.15$, $\omega_T = 0.42$, $\omega_{Orowan}^{DSGS} = 0.13$ and $\omega_{Orowan}^{OLGS} = 0.23$ into Eq. (7), σ_y^{GThix} is envisaged to be around 490 MPa, which is close to the value obtained experimentally (401 MPa). This suggests that the devised model is worth being considered to have a subtle approximation about the effect of incorporation of graphene sheets in enhancing the tensile properties of the metal matrix composites. The difference between the tensile properties envisaged by the models and the experimental ones is attributed to four possible

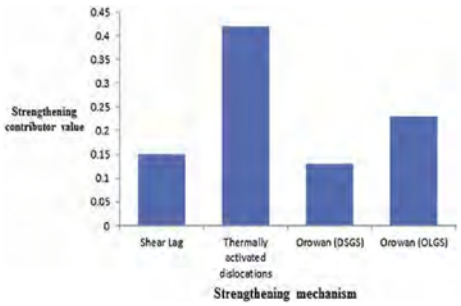

Fig. 4. Contribution of different strengthening mechanisms in enhancing the tensile yield strength of composite reinforced with graphene sheets.

reasons including (i) the total volume fraction of the DSGS is assumed to have a habit plane perpendicular to the slip plane of the aluminium (111) in the model presented, however, some of them could settle on the slip plane of the aluminium matrix resulting in lower interaction between them and resulting in gliding dislocations; (ii) graphitization through Van der Waals interactions between some graphene sheets during the manufacturing process, resulting in the formation of unwrapped-graphene and hence agglomerated SiC nanoparticles; (iii) the possibility of overwrapping SiC nanoparticles by OLGS, as the calculation relies on the existence of at least 5 OLGS and (iv) high SiC nanoparticles content stimulates the incomplete graphene encapsulation process and in turn the agglomeration of these particles, thereby levelling off the strengthening.

4. Conclusion

This study reveals the major strengthening mechanisms coming to practice by implementation of graphene sheets as reinforcement in metal matrix composites. In fact, this study demonstrates that the graphene encapsulating process not only has a unique capacity to attenuate the agglomeration of SiC nanoparticles but also has the exceptional feature in strengthening the aluminium metal matrix composites using thermally activated dislocation and pinning the SiC nanoparticles to the matrix, thereby augmenting tensile ductility significantly.

Acknowledgements

The authors would like to acknowledge the use of facilities (ARC-LE0237478) within the University of Wollongong (UOW) Electron Microscopy Centre and especially the great assistance of Dr. Gilberto Casillas and Dr. Madeleine Strong Cincotta.

References

[1] D. Miracle, Metal matrix composites – from science to technological significance, Compos. Sci. Technol. 65 (2005) 2526–2540.
[2] S.C. Tjong, Recent progress in the development and properties of novel metal matrix nanocomposites reinforced with carbon nanotubes and graphene nanosheets, Mater. Sci. Eng. R. Rep. 74 (2013) 281–350.
[3] I. El-Mahallawi, H. Abdelkader, L. Yousef, A. Amer, J. Mayer, A. Schwedt, Influence of Al2O3 nano-dispersions on microstructure features and mechanical properties of cast and T6 heat-treated Al Si hypoeutectic alloys, Mater. Sci. Eng. A 556 (2012) 76–87.
[4] S. Naher, D. Brabazon, L. Looney, Computational and experimental analysis of particulate distribution during Al–SiC MMC fabrication, Compos. A: Appl. Sci. Manuf. 38 (2007) 719–729.
[5] M. Mohammadpour, R.A. Khosroshahi, R.T. Mousavian, D. Brabazon, A novel method for incorporation of micron-sized SiC particles into molten pure aluminum utilizing a Co coating, Metall. Mater. Trans. B 46 (2015) 12–19.
[6] S. Tahamtan, A. Halvaee, M. Emamy, Z.Y. Jiang, A. Fadavi Boostani, Exploiting superior tensile properties of a novel network-structure Al/A206 matrix composite by hybridizing micron-sized Al3Ti with Al2O3 nano particulates, Mater. Sci. Eng. A 619 (2014) 190–198.
[7] N. Beigi Khosroshahi, R. Taherzadeh Mousavian, R. Azari Khosroshahi, D. Brabazon, Mechanical properties of rolled A356 based composites reinforced by Cu-coated bimodal ceramic particles, Mater. Des. 83 (2015) 678–688.
[8] N. Beigi Khosroshahi, R. Azari Khosroshahi, R. Taherzadeh Mousavian, D. Brabazon, Effect of electroless coating parameters and ceramic particle size on fabrication of a uniform Ni–P coating on SiC particles, Ceram. Int. 40 (2014) 12149–12159.
[9] A. Fadavi Boostani, S. Tahamtan, Effect of a novel thixoforming process on the microstructure and fracture behavior of A356 aluminum alloy, Mater. Des. 31 (2010) 3769–3776.
[10] A. Fadavi Boostani, S. Tahamtan, Fracture behavior of thixoformed A356 alloy produced by SIMA process, J. Alloys Compd. 481 (2009) 220–227.
[11] A. Fadavi Boostani, S. Tahamtan, Microstructure and mechanical properties of A356 thixoformed alloys in comparison with gravity cast ones using new criterion, Trans. Nonferrous Metals Soc. China 20 (2010) 1608–1614.
[12] I.V. Lightcap, T.H. Kosel, P.V. Kamat, Anchoring semiconductor and metal nanoparticles on a two-dimensional catalyst mat. Storing and shuttling electrons with reduced graphene oxide, Nano Lett. 10 (2010) 577–583.
[13] V.H. Pham, T.T. Dang, S.H. Hur, E.J. Kim, J.S. Chung, Highly conductive poly(methyl methacrylate) (PMMA)-reduced graphene oxide composite prepared by self-assembly of PMMA latex and graphene oxide through electrostatic interaction, ACS Appl. Mater. Interfaces 4 (2012) 2630–2636.
[14] A. Fadavi Boostani, S. Tahamtan, Z.Y. Jiang, D. Wei, S. Yazdani, R. Azari Khosroshahi, et al., Enhanced tensile properties of aluminium matrix composites reinforced with

graphene encapsulated SiC nanoparticles, Compos. A: Appl. Sci. Manuf. 68 (2015) 155–163.
[15] S. Naher, D. Brabazon, L. Looney, Development and assessment of a new quick quench stir caster design for the production of metal matrix composites, J. Mater. Process. Technol. 166 (2005) 430–439.
[16] S. Kandemir, H.V. Atkinson, D.P. Weston, S.V. Hainsworth, Thixoforming of A356/SiC and A356/TiB2 nanocomposites fabricated by a combination of green compact nanoparticle incorporation and ultrasonic treatment of the melted compact, Metall. Mater. Trans. A (2014).
[17] A.S. Isaikin, V.M. Chubarov, B.F. Trefilov, V.A. Silaev, Y.A. Gorelov, Compatibility of carbon filaments with a carbide coating and an aluminum matrix, Met. Sci. Heat Treat. 22 (1980) 815–817.
[18] M.K. Surappa, P.K. Rohatgi, Preparation and properties of cast aluminium–ceramic particle composites, J. Mater. Sci. 16 (1981) 983–993.
[19] G.F. Bolling, J. Cissé, A theory for the interaction of particles with a solidifying front, J. Cryst. Growth 10 (1971) 56–66.
[20] E.M. Agaliotis, M.R. Rosenberger, A.E. Ares, C.E. Schvezov, Influence of the shape of the particles in the solidification of composite materials, Prog. Mater. Sci. 1 (2012) 58–63.
[21] M.K. Surappa, P.K. Rohatgi, Heat diffusivity criterion for the entrapment of particles by a moving solid–liquid interface, J. Mater. Sci. 16 (1981) 562–564.
[22] M.A. Khan, P.K. Rohatgi, A numerical study of thermal interaction of solidification fronts with spherical particles during solidification of metal-matrix composite materials, Compos. Eng. 3 (1993) 995–1006.
[23] C. Faugeras, B. Faugeras, M. Orlita, M. Potemski, R.R. Nair, A.K. Geim, Thermal conductivity of graphene in corbino membrane geometry, ACS Nano 4 (2010) 1889–1892.
[24] R.P. Joshi, P.G. Neudeck, C. Fazi, Analysis of the temperature dependent thermal conductivity of silicon carbide for high temperature applications, J. Appl. Phys. 88 (2000) 265–269.
[25] E. Muñoz, J. Lu, B.I. Yakobson, Ballistic thermal conductance of graphene ribbons, Nano Lett. 10 (2010) 1652–1656.
[26] J.F. Nye, Physical Properties of Crystals: Their Representation by Tensors and Matrices, Oxford University Press, 1985.
[27] H.J. Frost, M.F. Ashby, Deformation Mechanism Maps: The Plasticity and Creep of Metals and Ceramics, 1982.
[28] W. Bao, F. Miao, Z. Chen, H. Zhang, W. Jang, C. Dames, et al., Controlled ripple texturing of suspended graphene and ultrathin graphite membranes, Nat. Nanotechnol. 4 (2009) 562–566.
[29] X. Liu, T.H. Metcalf, J.T. Robinson, B.H. Houston, F. Scarpa, Shear modulus of monolayer graphene prepared by chemical vapor deposition, Nano Lett. 12 (2012) 1013–1017.
[30] C. Lee, X. Wei, J.W. Kysar, J. Hone, Measurement of the elastic properties and intrinsic strength of monolayer graphene, Science (New York, N.Y.) 321 (2008) 385–388.
[31] N. Ramakrishnan, An analytical study on strengthening of particulate reinforced metal matrix composites, Acta Mater. 44 (1996) 69–77.
[32] M.A. M., K. Chawla, Mechanical Metallurgy: Principles and Applications, Prentice-Hall, Englewood Cliffs, New Jersey, 1984.
[33] V.C. Nardone, K.M. Prewo, On the strength of discontinuous silicon carbide reinforced aluminum composites, Scr. Metall. 20 (1986) 43–48.
[34] T. Jiang, R. Huang, Y. Zhu, Interfacial sliding and buckling of monolayer graphene on a stretchable substrate, Adv. Funct. Mater. 24 (2014) 396–402.
[35] A.S. Carrara, F.J. Mcgarry, Matrix and interface stresses in a discontinuous fiber composite model, J. Compos. Mater. 2 (1968) 222–243.
[36] J.F. Nie, Effects of precipitate shape and orientation on dispersion strengthening in magnesium alloys, Scr. Mater. 48 (2003) 1009–1015.
[37] Z. Zhang, D.L. Chen, Contribution of Orowan strengthening effect in particulate-reinforced metal matrix nanocomposites, Mater. Sci. Eng. A 483–484 (2008) 148–152.

Chapter 8 Conclusions and Recommendations

Imparting concurrent enhanced tensile strength and elongation to metal matrix nanocomposites reinforced with nanoparticles is a rigorous task, attributed to the high tendency of nanoparticles for agglomeration in the most solid and liquid processing routes. This PhD study, therefore, represents for the first time the novel concept of the utilization of graphene sheets to diminish the agglomeration of nanoparticles in solid and liquid states manufacturing processes. This is accomplished by exploiting the unique characteristic of graphene sheets to encapsulate the nanoparticles, leading to higher thermal conductivity and tweaking the repelling forces of the SiC nanoparticles, prompting the engulfment of these particles within the solidifying matrix of A356 aluminium alloy rather being agglomerated at the grain boundaries.

Based on this, this study suggests a new solidification model considering the all reported effective parameters, such as drag force, molecular surface forces solid/liquid interfaces to envisage the capacity of graphene sheets in alteration of the solidification mechanism of SiC nanoparticles from particle pushing to particle engulfment. This was accomplished making use of at least 40 % enhancement in thermal conductivity of SiC nanoparticles wrapped by graphene sheets. The model also predicted for the first time that graphene sheets encapsulating SiC nanoparticles can diminish the repelling forces of SiC nanoparticles from advancing solid/liquid interface, prompting engulfment of these particles within solidifying matrix. More interestingly, this study authenticates the aforementioned prediction by demonstrating an exceptional functionality of graphene sheets to manipulate the Hamaker constant of SiC nanoparticles, facilitating a mechanism to tweak the solidification behaviour of different nanoparticles based on the desired applications.

To delineate the actual capability of graphene sheets in strengthening aluminium matrix composites, different manufacturing routes were utilized, including stir casting, pressure-assisted stir casting, thixoforming and semi-solid powder forming processes. To capture the effect of the SiC nanoparticles encapsulated by graphene sheets, based on the aforementioned solidification mechanism and manipulated Hamaker constant, accentuated microstructural

investigation was conducted by FE-SEM and HRTEM on the produced composites, demonstrating the uniform distribution of SiC nanoparticles within the solidified aluminium matrix.

This manipulation of the microstructure can render a significant enhancement in tensile strength and elongation. Results achieved by the tensile tests have shown that the samples manufactured using the SiC nanoparticles encapsulated by graphene sheets demonstrating concurrent enhancement in tensile strength and ductility regardless of the type of the manufacturing process, such as stir casting, pressure-assisted stir casting, thixoforming and semi-solid powder forming processes, which are used. Achieved results have shown that thixoforming process has a profound effect on enhancing the yield strength (about 400%) and tensile ductility (about 600%) compared to composites produced by other processes, attributed to the combination effects of graphene and pressure applied in the semi-solid state, enhancing the dislocation density and diminishing the porosity content of the produced composites, respectively.

Following this characterization of mechanical properties, this PhD study has also represented a novel strengthening model to make a bridge between the effects of graphene sheets and achieved tensile properties of aluminium matrix composites based on Orowan, Hall-Petch, shear lag and thermal enhanced dislocation strengthening mechanisms. More importantly, tensile tests have demonstrated that the devised strengthening model has a good accuracy to envisage the tensile properties of the produced aluminium based composites.

Having considered the results achieved from the strengthening model presented in this study, it is expected that actual capability of graphene sheets in enhancing the mechanical properties of the metal matrix composites is more behind the ones achieved in this study. This can be attributed to the fact that the number of graphene sheets, not agglomerated through Van der Waals interactions, is not as high as to have the strong effect suggested by the model presented. This, therefore, necessitates further studies on the nature of the graphene encapsulating process to control the number of graphene sheets wrapping SiC nanoparticles. This required intensive research on the ball milling parameters such as critical percentage of the graphene sheets in the powder before ball milling process, the weight of ball to

powder, the time of the ball milling. Regarding the solvothermal process used in this study, it is also still in its infancy and should be addressed in detail the correlations between the process parameters such as concentration of nanoparticles in the solution, and the process temperature affecting the evaporation rate and accordingly formation of pores with the number of graphene sheets wrapping SiC nanoparticles.

The strengthening model presented in this study is in its infancy and can be developed more by incorporating the effect of number of graphene sheets on the load transfer from the matrix to these reinforcing sheets. It is also worth to have more studies to develop the strengthening model suggested in this study by considering the effect of interface between the graphene and aluminium matrix, as the quality of interface is crucial in load transfer from matrix to the reinforcement.

Based on the achieved results, it is recommended to have a further study about the quantitative effect of graphene sheets on enhancing the thermal conductivity of SiC nanoparticles to have a better insight into the mechanism that graphene sheets can manipulate the solidification behaviour of nanoparticles, paving a way to manufacture the advanced metal matrix composites with high physical and mechanical properties.

Additionally, according to the some thermal and electrical conductivity done on the composites produced in this study, it is believed that graphene sheets encapsulating SiC nanoparticles can facilitate the easy path for electron movement within the matrix. This low energy path, however, is affected strongly by the nature of the interface between the graphene and surrounding aluminium matrix. So, it is recommended to conduct further studies on the effect of onion-liked graphene sheets on providing the low-resistance electron path within aluminium matrix by consideration the effect of the graphene/aluminium interface on transferring the electrons within the interface between SiC nanoparticles and aluminium matrix.

References

[1] Xu Z, Yan J, Chen W, Yang S. Effect of ultrasonic vibration on the grain refinement and SiC particle distribution in Zn-based composite filler metal. Materials Letters. 2008;62(17–18):2615-2618.

[2] Kai XZ, Li ZQ, Fan GL, Guo Q, Xiong DB, Zhang WL, et al. Enhanced strength and ductility in particulate-reinforced aluminum matrix composites fabricated by flake powder metallurgy. Materials Science and Engineering: A. 2013;587(0):46-53.

[3] Xiong B, Xu Z, Yan Q, Cai C, Zheng Y, Lu B. Fabrication of SiC nanoparticulates reinforced Al matrix composites by combining pressureless infiltration with ball-milling and cold-pressing technology. Journal of Alloys and Compounds. 2010;497(1–2):L1-L4.

[4] Miracle D. Metal matrix composites – From science to technological significance. Composites Science and Technology. 2005;65(15-16):2526-2540.

[5] Esawi AMK, Morsi K, Sayed A, Gawad AA, Borah P. Fabrication and properties of dispersed carbon nanotube–aluminum composites. Materials Science and Engineering: A. 2009;508(1–2):167-173.

[6] Morsi K, Esawi AMK, Borah P, Lanka S, Sayed A, Taher M. Properties of single and dual matrix aluminum–carbon nanotube composites processed via spark plasma extrusion (SPE). Materials Science and Engineering: A. 2010;527(21–22):5686-5690.

[7] Schmidt CW, Knieke C, Maier V, Höppel HW, Peukert W, Göken M. Accelerated grain refinement during accumulative roll bonding by nanoparticle reinforcement. Scripta Materialia. 2011;64(3):245-248.

[8] Bakshi SR, Lahiri D, Agarwal A. Carbon nanotube reinforced metal matrix composites - a review. International Materials Reviews. 2010;55(1):41-64.

[9] Mazahery A, Abdizadeh H, Baharvandi HR. Development of high-performance A356/nano-Al_2O_3 composites. Materials Science and Engineering: A. 2009;518(1–2):61-64.

[10] Karbalaei Akbari M, Mirzaee O, Baharvandi HR. Fabrication and study on mechanical properties and fracture behavior of nanometric Al_2O_3 particle-reinforced A356 composites focusing on the parameters of vortex method. Materials & Design. 2013;46(0):199-205.

[11] El-Mahallawi I, Abdelkader H, Yousef L, Amer A, Mayer J, Schwedt A. Influence of Al_2O_3 nano-dispersions on microstructure features and mechanical properties of cast and T6 heat-treated Al Si hypoeutectic Alloys. Materials Science and Engineering: A. 2012;556(0):76-87.

[12] Mazahery A, Shabani MO. Mechanical properties of A356 matrix composites reinforced with nano-SiC particles. Strength Mater. 2012;44(6):686-692.

[13] Tahamtan S, Halvaee A, Emamy M, Jiang ZY, Fadavi Boostani A. Exploiting superior tensile properties of a novel network-structure AlA206 matrix composite by hybridizing micron-sized Al_3Ti with Al_2O_3 nano particulates. Materials Science and Engineering: A. 2014;619(0):190-198.

[14] Ünlü BS. Investigation of tribological and mechanical properties Al_2O_3–SiC reinforced Al composites manufactured by casting or P/M method. Materials & Design. 2008;29(10):2002-2008.

[15] Rajmohan T, Palanikumar K, Arumugam S. Synthesis and characterization of sintered hybrid aluminium matrix composites reinforced with nanocopper oxide particles and microsilicon carbide particles. Composites Part B: Engineering. 2014;59(0):43-49.

[16] Dao V, Zhao S, Lin W, Zhang C. Effect of process parameters on microstructure and mechanical properties in AlSi9Mg connecting-rod fabricated by semi-solid squeeze casting. Materials Science and Engineering: A. 2012;558(0):95-102.

[17] Tahamtan S, Halvaee A, Emamy M, Zabihi MS. Fabrication of Al/A206–Al_2O_3 nano/micro composite by combining ball milling and stir casting technology. Materials & Design. 2013;49(0):347-359.

[18] El-Mahallawi IS, Shash Y, Eigenfeld K, Mahmoud TS, Ragaie RM, Shash AY, et al. Influence of nanodispersions on strength–ductility properties of semi-solid cast A356 Al alloy. Materials Science and Technology. 2010;26(10):1226-1231.

[19] Karbalaei Akbari M, Baharvandi HR, Shirvanimoghaddam K. Tensile and fracture behavior of nano/micro TiB_2 particle reinforced casting A356 aluminum alloy composites. Materials & Design. 2015;66(0):150-161.

[20] Su H, Gao W, Feng Z, Lu Z. Processing, microstructure and tensile properties of nano-sized Al_2O_3 particle reinforced aluminum matrix composites. Materials & Design. 2012;36(0):590-596.

[21] Bastwros M, Kim G-Y, Zhu C, Zhang K, Wang S, Tang X, et al. Effect of ball milling on graphene reinforced Al6061 composite fabricated by semi-solid sintering. Composites Part B: Engineering. 2014;60(0):111-118.

[22] Wu Y, Kim G-Y. Carbon nanotube reinforced aluminum composite fabricated by semi-solid powder processing. Journal of Materials Processing Technology. 2011;211(8):1341-1347.

[23] Khan MA, Rohatgi PK. A numerical study of thermal interaction of solidification fronts with spherical particles during solidification of metal-matrix composite materials. Composites Engineering. 1993;3(10):995-1006.

[24] Naher S, Brabazon D, Looney L. Development and assessment of a new quick quench stir caster design for the production of metal matrix composites. Journal of Materials Processing Technology. 2005;166(3):430-439.

[25] Mandal D, Viswanathan S. Effect of heat treatment on microstructure and interface of SiC particle reinforced 2124 Al matrix composite. Materials Characterization. 2013;85(0):73-81.

[26] Visser J. On Hamaker constants: A comparison between Hamaker constants and Lifshitz-van der Waals constants. Advances in Colloid and Interface Science. 1972;3(4):331-363.

[27] Bartolucci SF, Paras J, Rafiee MA, Rafiee J, Lee S, Kapoor D, et al. Graphene–aluminum nanocomposites. Materials Science and Engineering: A. 2011;528(27):7933-7937.

[28] Pérez-Bustamante R, Bolaños-Morales D, Bonilla-Martínez J, Estrada-Guel I, Martínez-Sánchez R. Microstructural and hardness behavior of graphene-nanoplatelets/aluminum composites synthesized by mechanical alloying. Journal of Alloys and Compounds. 2014;615, Supplement 1(0):S578-S582.

[29] Chen L-Y, Konishi H, Fehrenbacher A, Ma C, Xu J-Q, Choi H, et al. Novel nanoprocessing route for bulk graphene nanoplatelets reinforced metal matrix nanocomposites. Scripta Materialia. 2012;67(1):29-32.

[30] Rawal SP. Metal-matrix composites for space applications. Journal of Materials Science. 2001;53(4):14-17.

[31] Adebisi AA, Maleque M, Rahman M. Metal matrix composite brake rotor: historical development and product life cycle analysis. International Journal of Automotive and Mechanical Engineering. 2011;4(1):471-480.

[32] Kainer KU. Metal matrix composites: custom-made materials for automotive and aerospace engineering: John Wiley & Sons; 2006.

[33] Camargo PHC, Satyanarayana KG, Wypych F. Nanocomposites: synthesis, structure, properties and new application opportunities. Materials Research. 2009;12(1):1-39.

[34] Chawla KK. Composite materials: science and engineering: Springer Science & Business Media; 2012.

[35] Suresh S. Fundamentals of metal-matrix composites: Elsevier; 2013.

[36] Kang Y-C, Chan SL-I. Tensile properties of nanometric Al_2O_3 particulate-reinforced aluminum matrix composites. Materials Chemistry and Physics. 2004;85(2–3):438-443.

[37] Tjong SC. Novel Nanoparticle-Reinforced Metal Matrix Composites with Enhanced Mechanical Properties. Advanced Engineering Materials. 2007;9(8):639-652.

[38] Ren Z, Chen S. Mechanical properties of nanometric particulates reinforced aluminum composites. School of Material Sience and Engineering. UNSW; 2000.

[39] Ma ZY, Li YL, Liang Y, Zheng F, Bi J, Tjong SC. Nanometric Si_3N_4 particulate-reinforced aluminum composite. Materials Science and Engineering: A. 1996;219(1–2):229-231.

[40] Lan J, Yang Y, Li X. Microstructure and microhardness of SiC nanoparticles reinforced magnesium composites fabricated by ultrasonic method. Materials Science and Engineering: A. 2004;386(1):284-290.

[41] Raming TP, van Zyl WE, Carton EP, Verweij H. Sintering, sinterforging and explosive compaction to densify the dual phase nanocomposite system Y_2O_3-doped ZrO_2 and RuO_2. Ceramics international. 2004;30(5):629-634.

[42] Sahin Y, Acılar M. Production and properties of SiCp-reinforced aluminium alloy composites. Composites Part A: Applied Science and Manufacturing. 2003;34(8):709-718.

[43] Clyne T, Withers P. An introduction to metal matrix composites: Cambridge University Press; 1995.

[44] Arzt E, Dehm G, Gumbsch P, Kraft O, Weiss D. Interface controlled plasticity in metals: dispersion hardening and thin film deformation. Progress in Materials Science. 2001;46(3–4):283-307.

[45] Dao M, Lu L, Asaro RJ, De Hosson JTM, Ma E. Toward a quantitative understanding of mechanical behavior of nanocrystalline metals. Acta Materialia. 2007;55(12):4041-4065.

[46] Clyne TW, Withers PJ. An introduction to metal matrix composites. Cambridge: Cambridge University Press; 1993.

[47] Thostenson ET, Li C, Chou T-W. Nanocomposites in context. Composites Science and Technology. 2005;65(3):491-516.

[48] Dorri Moghadam A, Omrani E, Menezes PL, Rohatgi PK. Mechanical and tribological properties of self-lubricating metal matrix nanocomposites reinforced by carbon nanotubes (CNTs) and graphene – A review. Composites Part B: Engineering. 2015;77(0):402-420.

[49] Esawi AMK, El Borady MA. Carbon nanotube-reinforced aluminium strips. Composites Science and Technology. 2008;68(2):486-492.

[50] Sabirov I, Kolednik O, Valiev RZ, Pippan R. Equal channel angular pressing of metal matrix composites: Effect on particle distribution and fracture toughness. Acta Materialia. 2005;53(18):4919-4930.

[51] Zhang QQ, Wu GQ, Huang Z, Tao Y. Effects of particle/matrix interfaces on the mechanical properties for SiC_p or YAl_{2p} reinforced Mg–Li composites. Journal of Alloys and Compounds. 2014;588(0):1-6.

[52] Hassan SF, Gupta M. Effect of different types of nano-size oxide particulates on microstructural and mechanical properties of elemental Mg. Journal of Materials Science. 2006;41(8):2229-2236.

[53] Kollo L, Bradbury CR, Veinthal R, Jäggi C, Carreño-Morelli E, Leparoux M. Nano-silicon carbide reinforced aluminium produced by high-energy milling and hot consolidation. Materials Science and Engineering: A. 2011;528(21):6606-6615.

[54] Tan MJ, Zhang X. Powder metal matrix composites: selection and processing. Materials Science and Engineering: A. 1998;244(1):80-85.

[55] Tahamtan S, Emamy M, Halvaee A. Effects of reinforcing particle size and interface bonding strength on tensile properties and fracture behavior of Al-A206/alumina micro/nanocomposites. Journal of Composite Materials. 2013;48:3331-3346.

[56] Ip S, Kucharski M, Toguri J. Wetting behaviour of aluminium and aluminium alloys on Al_2O_3 and CaO. Journal of Materials Science Letters. 1993;12(21):1699-1702.

[57] Naidich JV. The wettability of solids by liquid metals. Progress in surface and membrane science. 1981;14:353-484.

[58] Sajjadi SA, Parizi MT, Ezatpour H, Sedghi A. Fabrication of A356 composite reinforced with micro and nano Al_2O_3 particles by a developed compocasting method and study of its properties. Journal of Alloys and Compounds. 2012;511(1):226-231.

[59] Singh V, Joung D, Zhai L, Das S, Khondaker SI, Seal S. Graphene based materials: Past, present and future. Progress in Materials Science. 2011;56(8):1178-1271.

[60] Potts JR, Dreyer DR, Bielawski CW, Ruoff RS. Graphene-based polymer nanocomposites. Polymer. 2011;52(1):5-25.

[61] Wang J, Li Z, Fan G, Pan H, Chen Z, Zhang D. Reinforcement with graphene nanosheets in aluminum matrix composites. Scripta Materialia. 2012;66(8):594-597.

[62] Benjamin J, Bomford M. Dispersion strengthened aluminum made by mechanical alloying. Metallurgical Transactions A. 1977;8(8):1301-1305.

[63] Suryanarayana C, Ivanov E, Boldyrev VV. The science and technology of mechanical alloying. Materials Science and Engineering: A. 2001;304–306(0):151-158.

[64] Hong S-J, Kim H-M, Huh D, Suryanarayana C, Chun BS. Effect of clustering on the mechanical properties of SiC particulate-reinforced aluminum alloy 2024

metal matrix composites. Materials Science and Engineering: A. 2003;347(1–2):198-204.

[65] Hashim J, Looney L, Hashmi MSJ. Metal matrix composites: production by the stir casting method. Journal of Materials Processing Technology. 1999;92–93(0):1-7.

[66] Seo Y-H, Kang C-G. The effect of applied pressure on particle-dispersion characteristics and mechanical properties in melt-stirring squeeze-cast SiCp/Al composites. Journal of Materials Processing Technology. 1995;55(3–4):370-379.

[67] Taha MA, El-Mahallawy NA. Metal–matrix composites fabricated by pressure-assisted infiltration of loose ceramic powder. Journal of Materials Processing Technology. 1998;73(1–3):139-146.

[68] Ibrahim I, Mohamed F, Lavernia E. Particulate reinforced metal matrix composites—a review. Journal of Materials Science. 1991;26(5):1137-1156.

[69] Banerji A, Rohatgi P, Reif W. Role of wettability in the preparation of metal-matrix composites(a review). Metall. 1984;38(7):656-661.

[70] Youssef YM, Dashwood RJ, Lee PD. Effect of clustering on particle pushing and solidification behaviour in TiB2 reinforced aluminium PMMCs. Composites Part A: Applied Science and Manufacturing. 2005;36(6):747-763.

[71] Dhindaw B, Stefanescu D, Singh A, Curreri P. Directional solidification of Cu-Pb and Bi-Ga monotectic alloys under normal gravity and during parabolic flight. Metallurgical Transactions A. 1988;19(11):2839-2846.

[72] Flemings MC. Solidification processing. Metallurgical Transactions. 1974;5(10):2121-2134.

[73] Bronstein V, Itkin Y, Ishkov G. Rejection and capture of cells by ice crystals on freezing aqueous solutions. Journal of Crystal Growth. 1981;52:345-349.

[74] Hashim J, Looney L, Hashmi MSJ. Particle distribution in cast metal matrix composites—Part I. Journal of Materials Processing Technology. 2002;123(2):251-257.

[75] Hadji L. Modelling and asymptotic analysis of particle-interface interaction. Mathematical and Computer Modelling. 2002;36(1–2):147-156.

[76] Gelbstein M, Edry I, Froumin N, Frage N. Interfacial Chemical Interactions in the (Alumina/Graphite/Al Alloys) System: Thermodynamic Modeling and Experimental Results. Metall and Mat Trans A. 2009;40(4):932-936.

[77] Omenyi SN, Neumann AW. Thermodynamic aspects of particle engulfment by solidifying melts. Journal of Applied Physics. 1976;47(9):3956-3962.

[78] Zubko A, Lobanov V, Nikonova VV. Reaction of foreign particles with a crystallization front. Soviet Physics, Crystallography. 1973;18(2):239-241.

[79] Surappa M, Rohatgi P. Preparation and properties of cast aluminium-ceramic particle composites. Journal of Materials Science. 1981;16(4):983-993.

[80] Uhlmann DR, Chalmers B, Jackson K. Interaction Between Particles and a Solid-Liquid Interface. Journal of Applied Physics. 1964;35(10):2986-2993.

[81] Surappa MK, Rohatgi PK. Heat diffusivity criterion for the entrapment of particles by a moving solid-liquid interface. Journal of Materials Science. 1981;16(2):562-564.

[82] Habibnejad-Korayem M, Mahmudi R, Poole WJ. Enhanced properties of Mg-based nano-composites reinforced with Al_2O_3 nano-particles. Materials Science and Engineering: A. 2009;519(1–2):198-203.

[83] Paek S-M, Yoo E, Honma I. Enhanced cyclic performance and lithium storage capacity of SnO_2/graphene nanoporous electrodes with three-dimensionally delaminated flexible structure. Nano letters. 2008;9(1):72-75.

[84] Zhang L-S, Jiang L-Y, Yan H-J, Wang WD, Wang W, Song W-G, et al. Mono dispersed SnO_2 nanoparticles on both sides of single layer graphene sheets as anode materials in Li-ion batteries. Journal of Materials Chemistry. 2010;20(26):5462-5467.

[85] Lightcap IV, Kosel TH, Kamat PV. Anchoring Semiconductor and Metal Nanoparticles on a Two-Dimensional Catalyst Mat. Storing and Shuttling Electrons with Reduced Graphene Oxide. Nano Letters. 2010;10(2):577-583.

[86] Kok M. Production and mechanical properties of Al_2O_3 particle-reinforced 2024 aluminium alloy composites. Journal of Materials Processing Technology. 2005;161(3):381-387.

[87] Gu D, Wang H, Dai D, Yuan P, Meiners W, Poprawe R. Rapid fabrication of Al-based bulk-form nanocomposites with novel reinforcement and enhanced performance by selective laser melting. Scripta Materialia. 2015;96:25-28.

[88] Karbalaei Akbari M, Baharvandi HR, Mirzaee O. Nano-sized aluminum oxide reinforced commercial casting A356 alloy matrix: Evaluation of hardness, wear resistance and compressive strength focusing on particle distribution in aluminum matrix. Composites Part B: Engineering. 2013;52(0):262-268.

[89] Barekar NS, Tzamtzis S, Hari Babu N, Fan Z, Dhindaw BK. Processing of Ultrafine-Size Particulate Metal Matrix Composites by Advanced Shear Technology. Metall and Mat Trans A. 2009;40(3):691-701.

[90] Wang XJ, Wang NZ, Wang LY, Hu XS, Wu K, Wang YQ, et al. Processing, microstructure and mechanical properties of micro-SiC particles reinforced magnesium matrix composites fabricated by stir casting assisted by ultrasonic treatment processing. Materials & Design. 2014;57(0):638-645.

[91] Koli DK, Agnihotri G, Purohit R. A Review on Properties, Behaviour and Processing Methods for Al- Nano Al_2O_3 Composites. Procedia Materials Science. 2014;6:567-589.

[92] Ahamed H, Senthilkumar V. Role of nano-size reinforcement and milling on the synthesis of nano-crystalline aluminium alloy composites by mechanical alloying. Journal of Alloys and Compounds. 2010;505(2):772-782.

[93] Yang Y, Lan J, Li X. Study on bulk aluminum matrix nano-composite fabricated by ultrasonic dispersion of nano-sized SiC particles in molten aluminum alloy. Materials Science and Engineering: A. 2004;380(1–2):378-383.

[94] Shayan M, Niroumand B. Synthesis of A356–MWCNT nanocomposites through a novel two stage casting process. Materials Science and Engineering: A. 2013;582(0):262-269.

[95] Montanari R, Tagliaferri V, Donnini R. Metal matrix composite: structure and technologies. 2009.

[96] Montanari R, Tagliaferri V, Donnini R. Metal matrix composite: structure and technologies. Germany: VDM Verlag Dr. Muller; 2009.

[97] Morsi K, Esawi A. Effect of mechanical alloying time and carbon nanotube (CNT) content on the evolution of aluminum (Al)–CNT composite powders. Journal of Materials Science. 2007;42(13):4954-4959.

[98] Cao HQ, Luo J, Yang WW. Preparation of Dispersion Strengthened Aluminum Alloy by High Energy Ball Milling. Advanced Materials Research, vol. 602: Trans Tech Publ; 2013. p. 598-601.

[99] Koch C. Materials synthesis by mechanical alloying. Annual Review of Materials Science. 1989;19(1):121-143.

[100] Fogagnolo JB, Robert MH, Torralba JM. Mechanically alloyed AlN particle-reinforced Al-6061 matrix composites: Powder processing, consolidation and mechanical strength and hardness of the as-extruded materials. Materials Science and Engineering: A. 2006;426(1–2):85-94.

[101] El-Eskandarany MS. Mechanical solid state mixing for synthesizing of SiC_p/Al nanocomposites. Journal of Alloys and Compounds. 1998;279(2):263-271.

[102] Tang F, Hagiwara M, Schoenung JM. Microstructure and tensile properties of bulk nanostructured Al-5083/SiC p composites prepared by cryomilling. Materials Science and Engineering: A. 2005;407(1):306-314.

[103] Schultz BF, Ferguson JB, Rohatgi PK. Microstructure and hardness of Al_2O_3 nanoparticle reinforced Al–Mg composites fabricated by reactive wetting and stir mixing. Materials Science and Engineering: A. 2011;530(0):87-97.

[104] León CA, Mendoza-Suarez G, Drew RL. Wettability and spreading kinetics of molten aluminum on copper-coated ceramics. J Mater Sci. 2006;41(16):5081-5087.

[105] Akbari MK, Baharvandi H, Mirzaee O. Fabrication of nano-sized Al_2O_3 reinforced casting aluminum composite focusing on preparation process of reinforcement powders and evaluation of its properties. Composites Part B: Engineering. 2013;55:426-432.

[106] Poovazhagan L, Kalaichelvan K, Rajadurai A, Senthilvelan V. Characterization of Hybrid Silicon Carbide and Boron Carbide Nanoparticles-Reinforced Aluminum Alloy Composites. Procedia Engineering. 2013;64:681-689.

[107] Zhang H, Geng L, Guan L, Huang L. Effects of SiC particle pretreatment and stirring parameters on the microstructure and mechanical properties of SiCp/Al–6.8Mg composites fabricated by semi-solid stirring technique. Materials Science and Engineering: A. 2010;528(1):513-518.

[108] Alhawari KS, Omar MZ, Ghazali MJ, Salleh MS, Mohammed MN. Wear Properties of A356/Al_2O_3 Metal Matrix Composites Produced by Semi-solid Processing. Procedia Engineering. 2013;68:186-192.

[109] Qin XH, Jiang DL, Dong SM. Nanometer, submicron and micron sized aluminum powder prepared by semi-solid mechanical stirring method with addition of ceramic particles. Materials Science and Engineering: A. 2004;385(1–2):31-37.

[110] Weiss D, Black M. Using Semi-Solid Extrusion for the Production of Aluminum-Nanocomposite Master Alloys. Solid State Phenomena, vol. 217: Trans Tech Publ; 2015. p. 426-430.

[111] Ralph B, Yuen HC, Lee WB. The processing of metal matrix composites — an overview. Journal of Materials Processing Technology. 1997;63(1–3):339-353.

[112] Curle U, Ivanchev L. Wear of semi-solid rheocast SiC_p/Al metal matrix composites. Transactions of Nonferrous Metals Society of China. 2010;20:s852-s856.

[113] Jiang J, Wang Y. Microstructure and mechanical properties of the rheoformed cylindrical part of 7075 aluminum matrix composite reinforced with nano-sized SiC particles. Materials & Design. 2015;79:32-41.

[114] Goh CS, Wei J, Lee LC, Gupta M. Properties and deformation behaviour of Mg–Y_2O_3 nanocomposites. Acta Materialia. 2007;55(15):5115-5121.

[115] Nardone VC, Prewo KM. On the strength of discontinuous silicon carbide reinforced aluminum composites. Scripta Metallurgica. 1986;20(1):43-48.

[116] Zhang Z, Chen DL. Contribution of Orowan strengthening effect in particulate-reinforced metal matrix nanocomposites. Materials Science and Engineering: A. 2008;483–484(0):148-152.

[117] Hull D, Bacon DJ. Introduction to dislocations: Pergamon Press Oxford; 1984.

[118] Kamrani S, Simchi A, Riedel R, Seyed Reihani S. Effect of reinforcement volume fraction on mechanical alloying of Al–SiC nanocomposite powders. Powder Metallurgy. 2007;50(3):276-282.

[119] Sanaty-Zadeh A. Comparison between current models for the strength of particulate-reinforced metal matrix nanocomposites with emphasis on consideration of Hall–Petch effect. Materials Science and Engineering: A. 2012;531:112-118.

[120] Miller W, Humphreys F. Strengthening mechanisms in particulate metal matrix composites. Scripta Metallurgica et Materialia. 1991;25(1):33-38.

[121] Redsten A, Klier E, Brown A, Dunand D. Mechanical properties and microstructure of cast oxide-dispersion-strengthened aluminum. Materials Science and Engineering: A. 1995;201(1):88-102.

[122] Nie JF. Effects of precipitate shape and orientation on dispersion strengthening in magnesium alloys. Scripta Materialia. 2003;48(8):1009-1015.

[123] Hung Y-P. Microstructures and Mechanical Strengthening Mechanisms of Nanoparticle Reinforced Mg Based Composites, 2006.

[124] Smallman RE, Ngan A. Physical metallurgy and advanced materials: Butterworth-Heinemann; 2011.

[125] Hull D, Clyne T. An introduction to composite materials: Cambridge university press; 1996.

[126] Zhang Z, Chen DL. Consideration of Orowan strengthening effect in particulate-reinforced metal matrix nanocomposites: A model for predicting their yield strength. Scripta Materialia. 2006;54(7):1321-1326.

[127] Tham LM, Gupta M, Cheng L. Effect of limited matrix–reinforcement interfacial reaction on enhancing the mechanical properties of aluminium–silicon carbide composites. Acta Materialia. 2001;49(16):3243-3253.

[128] Ci L, Ryu Z, Jin-Phillipp NY, Rühle M. Investigation of the interfacial reaction between multi-walled carbon nanotubes and aluminum. Acta Materialia. 2006;54(20):5367-5375.

[129] Casati R, Amadio M, Biffi CA, Dellasega D, Tuissi A, Vedani M. Al/Al_2O_3 Nanocomposite Produced by ECAP. Materials Science Forum, vol. 762: Trans Tech Publ; 2013. p. 457-464.